

CHAPTER 1

1.1 Introduction

Insects are a major cause of discomfort and disease worldwide, which can impede the economic and social development of nations [1]. In particular, in warm and humid tropical and subtropical regions, they pose a great risk of human disease by spreading viruses, worms, and protozoa. For example, *Aedes aegypti* and *Aedes albopictus* mosquitoes are responsible for the transmission of yellow fever, dengue and dengue hemorrhagic fever, and chikungunya [2]. In addition, *Culex* mosquitoes can spread filariasis and Japanese encephalitis. Bites of infective female *Anopheles* spp. transmit malaria, a major communicable disease affecting mankind due to *Plasmodium* parasites, such as *P. vivax* (Pv), *P. falciparum* (Pf), *P. malariae* (Pm), and *P. ovale* (Po).

1.1.1. Burden of mosquito-borne diseases

1.1.1.1 Global burden of malaria

Malaria is an entirely preventable and treatable mosquito-borne illness. In 2013, 97 countries exhibited ongoing malaria transmission. Among an estimated 3.4 billion people risking malaria, 1.2 billion were at high risk. These high-risk areas present over one malaria case per 1,000 population [2].

About 207 million malaria cases (uncertainty range: 135–287 million) leading to approximately 627,000 deaths (uncertainty range: 473,000–789,000) were estimated in 2012. Typically, 90% of all malaria-related deaths occur in Sub-Saharan Africa [3].

In 2012, malaria killed an estimated 482,000 children under five years of age. According to recent assessments, it causes 300–500 million clinical cases and 1.5–2.7 million deaths every year worldwide because of the Pf parasite. [3, 4]

The World Health Organization (WHO) estimates that India accounts for 75% of all malaria cases in South-East Asia. In India, about 95% of the population resides in malaria-endemic areas, and 80% of reported malaria cases are confined to tribal, hilly, hard-to-reach, or inaccessible areas where 20% of the population resides. Currently, more than two billion people risk contracting

malaria, and the estimated global annual incidence of clinical malaria exceeds 300 million cases [4]. More than one million people die every year from direct causes of malaria, with children being at highest risk [5].

1.1.1.2 Global burden of dengue

Dengue is a mosquito-borne infection found in tropical and sub-tropical regions around the world. In recent years, its transmission has increased significantly in urban and semi-urban areas to become a major international public health concern.

The worldwide incidence of dengue has grown dramatically in recent decades. Over 2.5 billion people—over 40% of the world population—are now at risk from dengue. WHO currently estimates potential 50–100 million dengue infections worldwide every year [6].

In 2013, 2.35 million dengue cases were reported in the Americas alone, of which 37,687 cases were severe. In addition to explosive outbreaks, these numbers have been increasing with the spreading of the disease to new areas.

1.1.2 Evolution of mosquito control measures

On August 20, 1897, Sir Ronald Ross made the groundbreaking discovery of the malarial parasite in the female *Anopheles* mosquito [7], for which he was awarded the Nobel Prize in medicine in 1902 [8]. Because no effective vaccines or drugs were available to prevent or treat malaria, its transmission was mainly managed by controlling the vector [9].

In the first half of the twentieth century, vector control technology was relatively straightforward and relied on source reduction, larvivorous fish [10,11], petroleum hydrocarbon oils, and some simple synthetic and botanical materials [12,13,14]. The discovery of the insecticide dichlorodiphenyltrichloroethane (DDT, Figure 1.1) in 1940's was a major breakthrough in the control of vector-borne diseases [15]. DDT and its high efficiency as a contact poison against several arthropods were discovered by Sir Paul Müller who received the Nobel Prize in physiology and medicine in 1948. This insecticide very effectively killed indoor resting mosquitoes when sprayed on the walls of houses. Moreover, it was cheap to produce and remained active for several months [16, 17].

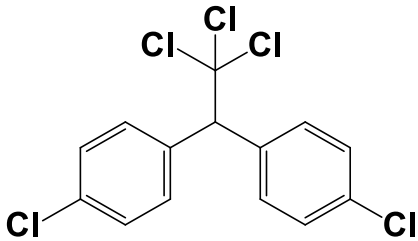


Figure 1.1: Molecular structure of DDT.

In their work entitled “The Excellent Powder, DDT’s Political and Scientific History [17],” Don Roberts, Richard Tren, Roger Bate, and Jennifer Zambone have conducted the most comprehensive assessment of the science, history, and public policy of this widely used chemical. DDT has been banned in the United States since 1972 because it was instrumental in the near extinction of birds, such as the bald eagle and the peregrine falcon [17]. This persistent chemical accumulates in animal tissues and presents rising concentration in animals that are higher in the food chain. It is particularly toxic to fish, aquatic invertebrates, and insects (including some that are beneficial). In spite of concerns over its persistence and toxicity, its public health benefits outweigh any potential harm by far, explaining its continued utilization in many parts of the world. It has been banned in most other developed countries but is still used in many developing countries. In 2006, the WHO issued a position statement promoting indoor residual spraying (IRS) with DDT for malaria vector control in epidemic and endemic areas [18]. Other international organizations concurred because of the great burden of malaria and the relative ineffectiveness of current treatment and control strategies [19]. Although the Stockholm Convention of 2001 targeted DDT as one of the twelve persistent organic pollutants for phase-out and eventual elimination, it allowed a provision for its continued indoor use for disease vector control [20]. Several studies have addressed DDT’s efficacy [19] and its repellent effects at sub lethal amounts in comparison with synthetic pyrethroids [21, 22].

In India, DDT has been banned for agricultural use but remains used as an indoor residual spray for malaria control under the WHO specifications and precautions for its safe production, use, and disposal [22].

During the second half of the twentieth century, various synthetic organic chemicals, improved petroleum oil formulations, insect growth regulators, synthetic pyrethroids, and microbial control

agents were developed and employed to control mosquitoes and other disease-vectoring insects. Among these control agents, petroleum oil formulations remained under use through the entire century. [23, 24]

1.1.3 Current status

While the twentieth century mainly relied on DDT and few other options, current mosquito control approaches are more structured and present several safe options.

Existing available vector control options include IRS, biological control, larvicide, environmental management such as source reduction, space spraying, and personal protection measures. In India, two principal measures used for mosquito control involve mass or public control methods as part of Public Health programs as well as personal protection measures.

1.1.3.1 Public mosquito control programs

Public mosquito control programs are community oriented and usually implemented on a large scale. They target adult mosquitoes and larval growth, prevent breeding, and reduce mosquito–man contacts using various chemical and biological products.

1.1.3.1.1 Chemical control measures

Chemical control products include larvicidal oils, wettable powders, and suspension concentrates and granules based on organophosphorus compounds such as chlorpyrifos, fenitrothion, fenthion, and malathion [14]. In addition, insecticide impregnated nets, screens, and fabric may be utilized generally using synthetic pyrethroids such as deltamethrin, cypermethrin, permethrin, and cyfluthrin [25,26]. High-potency products are applied by insecticide sprays and fogging on roofs, walls, and lower furniture surfaces where the vector species rest, providing protection for up to three months [14]. Though these products are effective for mosquito control, there is a growing concern on their serious adverse effects on other insects, fish, and other aquatic animals [14].

1.1.3.1.2 Biological control measures

The biological control of mosquitoes and other pests involve introducing into their environment their enemies such as parasites, disease causing organisms, and predatory animals. These enemies may also include other insects, viruses, bacteria, protozoa, fungi, plants, nematodes, worms, and fish.

Among these methods, larvivorous fish belonging to the tooth carp family (Cyprinodontidae) [27, 28] have been employed. In addition, *Bacillus thuringiensis*, especially *Bt israelensis*, which are bacterial larvicides present in natural soil [29], have been used to interfere with the digestive systems of larvae. These bacteria can be dispersed by hand or dropped by helicopter in large areas but, unfortunately, lose their effectiveness after the larvae turn into pupae because pupae do not eat.

1.1.3.1.3 Personal protection measures

Personal protection measures are used by individuals or small groups to shield themselves from insect bites and subsequent diseases caused by contact between the human body and the insects.

One of the main nontoxic ways to prevent mosquito bites is the mosquito net. If properly used and maintained (no holes), it provides maximum personal protection against biting insects. In many areas of the world, mosquitoes are a nuisance that pose a serious health threat. The WHO and the U.S. Center for Disease Control highly recommend that people staying in mosquito-infested areas [30,31] sleep under an active ingredient impregnated bed net [32,33].

Another very popular mode of protection consists in applying products on the skin as personal repellants. The most effective ingredient in these products is N,N-diethyl-meta-toluamide (DEET) [34,35]. It inhibits the detection of human odor cues in insects, making it the most popular mosquito-repelling skin treatment since its invention by the U.S. Department of Agriculture in 1945 [36,37]. Despite their widespread use over many years, DEET-based products have occasionally been associated with some minor to moderate adverse reactions. DEET concentrations in repellents range from 5% to 100% [38].

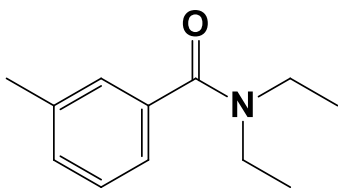


Figure 1.2: Molecular structure of DEET.

Studies have shown the effectiveness of DEET in reducing mosquito attacks on a human subject by combining wind and vapor-phase DEET repellent [37]. Controlled release formulations comprising DEET and N, N diethyl phenylacetamide have been investigated to deliver long-lasting repellency effects [39, 40, and 41].

Permethrin-based soaps [42, 43] have also been widely evaluated for anti-mosquito protection and have proven efficient for more than 8 h [44, 45]. DEET and permethrin have also been used to treat clothing, especially military uniforms, against mosquitoes [46–50].

Less common mosquito repellents include catnip oil extract, nepetalactone, citronella, and eucalyptus oil extract. [51, 52, 53]. Many studies have been conducted to evaluate the efficacy of their essential oils. Hao *et al.*, have studied the host-seeking and blood-feeding behavior of *Aedes albopictus*, exposed to vapors of geraniol, citral, citronellal, eugenol, or anisaldehyde [54]. Their initial laboratory results showed that anisaldehyde and geraniol were promising spatial repellents against *Ae. albopictus* and may play a major role in new repellent technology. Citronella patches, bands, and candles are also very popular in areas with low to moderate infestation [55–58]

Recently, extensive scientific work has addressed mosquito attractants as a safe alternative to mosquito control. Constantini *et al.* [59] have attempted to understand the role of body odors in the relative attractiveness of different men to malarial vectors. The study suggested that the attractiveness differed between people and CO₂ acts as surrogate bait for malarial vectors. Lindsay *et al.* evaluated variations in the attractiveness of human subjects to malaria mosquitoes in Gambia. Their findings supported the view that some individuals within a community were at greater risk from mosquito-borne pathogens than others [60].

Mukabana *et al.* assessed host-specific cues that cause the differential attractiveness of Kenyan men to the African malaria vector *Anopheles gambiae*. They demonstrated that in the vicinity of humans when exposed to a blend of physical and olfactory signals from more than one host, *An. gambiae* effectively and consistently expressed host selection behavior that results in nonrandom biting [61]. Specific trials were also conducted to understand other attractant chemicals in addition to CO₂.

New mosquito traps have been developed using this understanding of attraction [62, 63]. In these traps, mosquito attractants emit a plume of CO₂ along with other mosquito attractants such as sugary scents, lactic acid, octenol, heat, water vapor, and sounds. Because of these mammal scent and output mimics, female mosquitoes are drawn toward the trap before being typically sucked by an electric fan into a net or a holder, in which they are collected [64].

Other products such as Bug zappers have been used. However, these products kill a wide range of flying insects, including many beneficial insects that eat mosquitoes. Despite their availability in many markets including India, they have not proven effective at controlling the overall mosquito population.

Although all these personal protection products, such as DEET, citronella-based personal repellants [65, 66], mosquito traps, and bug zappers [67], are being used, they are neither adequate nor very effective for household use [68]. Moreover, the community program cannot provide a long-term complete protection [69]. Hence, safe and effective products that can be used at home for protecting the entire family are needed.

1.1.4 Household insecticides

The term “household insecticide products” refers to ready-to-use products that are effective against specific target insects and are readily accessible to the general population through supermarkets, shops, pharmacies, and other retail outlets in cities and in the countryside. These products have been developed for safe and effective consumer use. Household insecticide products are most effective when combined with physical control measures that aim at eliminating and reducing vector and pest breeding sites or keeping them away from human habitation [70]. This combination of different control measures is called “integrated control.” The most important common

household insecticide products will be described in the following sections. In addition to mosquito coils, insecticide baits for cockroaches, ants, and flies; glue traps for cockroaches and flies; and dustable powders, they exist as aerosols for oil- and water-based spatial applications (flying insect killers (FIKs)), residual application, and crawling insect control (crawling insect killers (CIKs)). In addition, oil sprays and water-based liquids may be applied using manual pump systems. Electric vaporizer systems, such as mat and liquid and gel-type vaporizers, have been developed along with strips, from which active substances evaporate without electrical energy, and moth protection products such as moth cellulose, moth bags, and balls. The biological efficacy and safety of these product formats depend on active ingredient being used.

1.1.4.1 Active ingredients used in household insecticides

Active ingredients commonly used in household insecticide products are grouped into five classes [71].

- **Chlorinated hydrocarbons** have been widely used in the past. However, they have been completely abandoned for household use because their persistence in the environment and bioaccumulation represent risks to non-target organisms, such as humans.
- **Organophosphates** are derived from phosphorus-based acids. They are generally active against a broad spectrum of insects, do not persist in the environment, and do not bio-accumulate. In the majority of cases, they are used for residual activity targeting crawling pests.
- **Carbamates** are derived from carbamic acid and exhibit similar properties to organophosphates.
- **Pyrethroids** are synthetic chemical analogs of chrysanthemum-extracted natural pyrethrins characterized by their generally low mammalian toxicity when in an appropriate formulation [72]. They consist of active ingredients with high knockdown activity, such as allethrins, and those mostly known for their high residual activity, such as permethrin.
- **Synergists** are not active ingredients, but they enhance the insecticidal activity of certain groups such as pyrethroids. The most commonly used synergist is piperonyl butoxide.

1.1.5 Use of synthetic pyrethroids as household insecticides

Active ingredients used in household insecticide products are expected to display powerful biological and toxicological activity. Amongst the various classes of insecticides, synthetic

pyrethroids have been found to be most suitable for the formats like mosquito sprays, aerosols, coils and liquid vaporizers.

Usually, plants and wood containing repellent or insecticidal substances have been burnt. The first naturally occurring insecticide discovered was natural pyrethrum (Figure 1.3) from the pyrethrum daisy *Tanacetum cinerariifolium* grown in Kenya.

1.1.6 Evolution of synthetic pyrethroids

Pyrethroids were introduced in the late 1900s by UK based Rothamsted Research scientists following the structural elucidation of pyrethrin I and II by Hermann Staudinger and Leopold Ružička in the 1920s. The synthesis of pyrethroid analogs of the natural product pyrethrum represented a major advancement in chemistry [73].

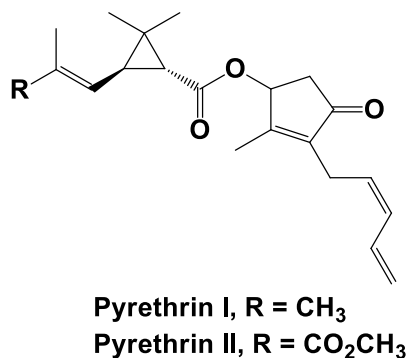


Figure 1.3: Natural pyrethrum structures.

These insecticides exhibit relatively low mammalian toxicity and an unusually fast biodegradation. Their development coincided with the identification of DDT-related problems. Initial investigations consisted in identifying the most active components of pyrethrum, which was known for its insecticidal properties and was extracted from East African chrysanthemum flowers. Pyrethrum rapidly knocks down flying insects but exhibits negligible persistence, which is environmentally friendly but results in poor efficacy [74] when applied in the field. Pyrethroids are essentially chemically stabilized forms of natural pyrethrum [75].

1.1.6.1 Altering the chemistry of natural pyrethrum

The earliest pyrethroids were related to pyrethrin I and II by changing the alcohol group involved in the chrysanthemic acid ester. This relatively modest change can lead to substantially altered activities. For example, the 5-benzyl-3-furanyl ester called resmethrin is weakly toxic to mammals (LD_{50} (rat, oral) * = 2,000 mg/kg) but 20- to 50-fold more effective than natural pyrethrum and is also readily biodegraded.

Note: * LD_{50} is the dose required to kill half of a tested population after a specified test duration.

Developed in the 1960s, first generation pyrethroids, such as bioallethrin, tetramethrin, resmethrin, and bioresmethrin, showed higher activity than natural pyrethrum but were unstable in sunlight.

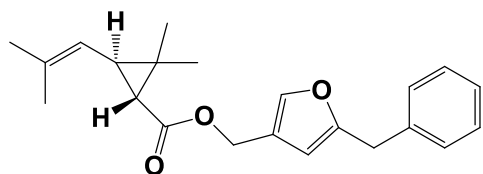


Figure 1.4: Molecular structure of bioresmethrin.

By 1974, the Rothamsted team discovered a second generation of more persistent compounds, such as permethrin. In this family of pyrethroids, acid and alcohol components were both altered, requiring more elaborate organic synthesis. Cypermethrin and deltamethrin incorporated dichlorovinyl and dibromovinyl derivatives, respectively.

These compounds were substantially more resistant to light- and air-induced degradation, making them suitable for agricultural use, but presented significantly higher mammalian toxicities. Over the subsequent decades, these derivatives were followed with other proprietary substances, such as fenvalerate, lambda-cyhalothrin, and beta-cyfluthrin [33].

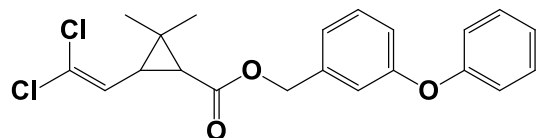


Figure 1.5: Molecular structure of permethrin.

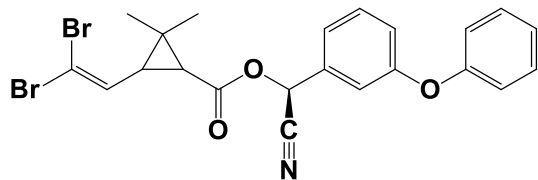


Figure 1.6: Molecular structure of deltamethrin.

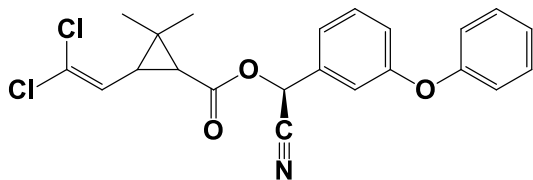


Figure 1.7: Molecular structure of cypermethrin.

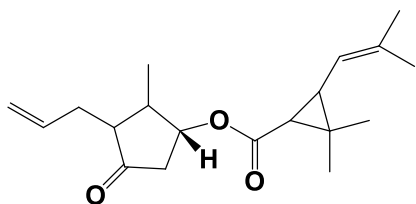


Figure 1.8: Molecular structure of d-allethrin

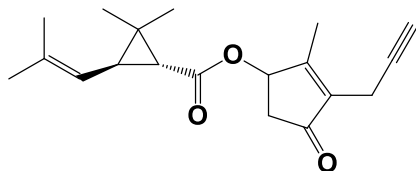


Figure 1.9: Molecular structure of prallethrin

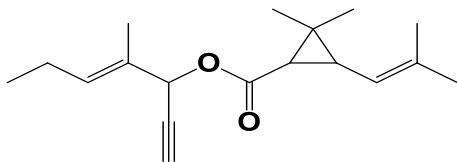


Figure 1.10: Molecular structures of empenthrin

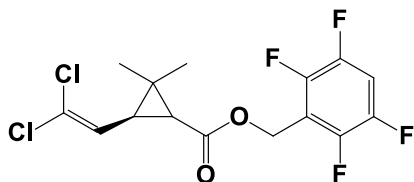


Figure 1.11: Molecular structures of transfluthrin

1.1.7 Mode of action of pyrethroids

Pyrethroids are popular insecticides because of their ability to penetrate insect exoskeletons. These axonic poisons paralyze organisms by keeping sodium channels in their neuronal membranes open. Sodium channels are membrane proteins with a hydrophilic interior. This tiny hole is shaped precisely to strip away the partially charged water molecules from a sodium ion, creating a favorable path that allows sodium ions to pass through the membrane, enter the axon, and propagate an action potential. When a toxin keeps the channels in their open state, the nerves cannot de-excite, causing organism paralysis [79].

In the 1970s, two major companies, i.e., Sumitomo Chemicals, Japan and Bayer Life Sciences, Germany, got breakthroughs that resulted in the commercialization of photostable synthetic pyrethroids for use in the field in the form of d-allethrin (Figure 1.9) [76].

1.1.8 Bio-efficacy of synthetic pyrethroids

Photostable synthetic pyrethroids were tested using specially designed bioassays targeting houseflies and mosquitoes. They showed high insecticidal action and low mammalian toxicity, leading to their widespread use as household insecticides. Common pyrethroid-based household insecticides in India are natural pyrethrum (Figure 1.3), bioresmethrin (Figure 1.4), permethrin (Figure 1.5), cypermethrin (Figure 1.6), deltamethrin (Figure 1.7), empenthrin (Figure 1.8), and transfluthrin (Figure 1.9). These insecticides are implemented as mosquito coils, aerosols, electric mosquito mats, and liquid vaporizers [77,78]

1.2 Background on household insecticides

Many devices, such as mosquito coils, aerosols, electric mosquito mats, and electric vaporizers, have been developed for protection from mosquito bites. These devices utilize pyrethroids as main active ingredients, which are vaporized by combustion, atomization into fine droplets, or electrical heating to kill or repel these insects.

1.2.1 Existing household insecticide formats

1.2.1.1 Aerosols

Spatial spray products are pressurized aerosol cans [80] containing a liquid formulation and a propellant, such as liquid petroleum gas, designed to release small droplet suspensions in the air to control flying insects.

When applied in a room, these FIK aerosols act immediately on mosquitoes and flies. Usually, no residual effect is sought from this application. Active ingredients of FIKs mainly belong to the pyrethroid family.

1.2.1.2 Mosquito coils

Smoke and mosquito coils were the first mosquito protection methods developed by humans and remain widely used worldwide. They are of particular importance in areas without reliable electricity.

Coils consist of a base made of wood powder, starch, coconut shell powder, dyestuff, glue, and burning regulators. In addition, insecticides are formulated at a relatively low dosage [80, 81, and 82]. This limits the impact of simple smoke particles and significantly improves the biological effect of the repellent-based coils, which produce a potential knockdown or killing after prolonged exposure [83–86]. Smoke generation during use increases the efficacy of this format [87–90]. The most common active ingredients belong to non persistent quick knockdown pyrethroids [91, 92], in particular esbiothrin, which has proven very effective [93, 94]. New active ingredients, such as prallethrin, transfluthrin, and metofluthrin, are also used.

1.2.1.3 Electric vaporizer systems

Electric vaporizer systems (e.g., mat, liquid, and membrane vaporizers) encompass all products that require an electrical heating device to evaporate insecticide from a base, or refill, which may consist of any suitable material. Heater and refill form a unit and must be used together for optimum effect because, in many cases, they have been designed together by the manufacturer. Active ingredients used in these systems belong to the natural pyrethrins and quick knockdown pyrethroids exhibiting a relatively high vapor pressure.

The modes of insecticide delivery have evolved from mosquito coils to liquid vaporizers with varying features [93]. Moreover, considerable efforts have been deployed to synthesize new pyrethroids with enhanced vapor activity.

1.2.2 Search for new active insecticides

In 2005, Sumitomo Chemicals registered metofluthrin (Figure 1.10), a new and novel pyrethroid showing high ambient concentration by virtue of its relatively high vapor pressure upon heating or combustion [94]. When vaporized at room temperature, metofluthrin achieved mosquito control [95].

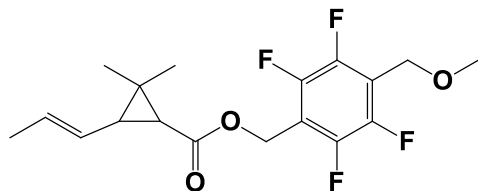


Figure 1.12: Molecular structure of Metofluthrin.

1. 2.2.1 Literature review on metofluthrin

Developed in 2005, Metofluthrin displays a 100-fold higher vapor activity (vapor pressure: 1.96×10^{-3} Pa at 25 °C) than most common synthetic pyrethroids (1.33×10^{-5} Pa at 25 °C for Prallethrin) [94]. Therefore, it may be implemented in various devices involving a polymer matrix or a cellulosic substrate that do not require electrical power or heating. In these formats, metofluthrin has exhibited satisfactory release and extremely good performance in controlling mosquito threat [95].

Following this study, several investigations have addressed the efficacy, toxicity, and safety across various geographies, of various metofluthrin based formats. Laboratory and field trials of metofluthrin-based paper fan emanators were performed by measuring landing rates, which correspond to number of mosquitos landing for blood meal on a host over a known period. These measurements indicated that these emanators reduced mosquito bites on human volunteers [96]. Field efficacy studies conducted using a Denguri-type paper delivery device demonstrated that metofluthrin effectively repelled mosquitoes in this format [97]. A field evaluation of spatial repellency of metofluthrin-impregnated plastic strips against mosquitoes indicated a rapid decrease in mosquito population lasting up to six weeks [98]. Similar to the old Japanese Denguri toy [99], another format, in which paper is folded to form various shapes, has been tested for the sustained release of metofluthrin. This format showed a consistent release of active ingredient over time.

In other approaches, the active ingredient has been vaporized by air flow from a fan at room temperature. In addition, the fan required less power than heating, making the use of batteries possible [94]. Hence, a nonelectric solution for the emanation of metofluthrin from impregnated papers is achievable and may offer a mobile device option for consumers on the go.

In addition, several bio efficacy studies have been performed on metofluthrin-based formats. A comparative evaluation of the insecticidal efficacy of metofluthrin and other pyrethroids against colonies of Asian *Culex quinquefasciatus* originating from Indonesia, Thailand, Vietnam, and Malaysia was conducted employing topical application. Metofluthrin was found to be the most effective against all four *Culex quinquefasciatus* colonies. The LD₅₀-based relative effective ratio of metofluthrin against d-allethrin was higher in *Culex quinquefasciatus* (33.3–78.8) than in *Culex pipiens pallens* (27.8). The Vietnam colony exhibited the highest susceptibility in the study [100]. Kawada and Hitoshi [101] studied the spatial repellency of metofluthrin-impregnated paper strips against *Anopheles* and *Culex* strains in wall-free shelters in Indonesia. They observed more than 80% reduction in mosquito collections during the first four weeks but a decrease in efficacy after about six weeks. Moreover, they assessed the performance of metofluthrin-impregnated plastic strips against *Aedes* in Vietnam and environmental factors affecting their efficacy [102]. The study showed that one strip containing 600 mg in a 2.6–5.52 m² area reduced the mosquito collection for eight weeks. In addition, an increase in temperature and a decrease in room opening area positively affected spatial repellency.

Argueta *et al.*, investigated the spatial repellency of metofluthrin-impregnated multilayered paper strips against *Aedes albopictus* under outdoor conditions and found high spatial repellency (>80%) with the metofluthrin-impregnated (200 mg) device for more than 6 weeks, [101]. A field evaluation of the spatial repellency of metofluthrin-impregnated plastic strips against *Anopheles gambiae* complex in Bagamoyo, Coastal Tanzania, demonstrated the efficacy of metofluthrin [102].

Lucas [103] has reported US laboratory and field trials involving metofluthrin to reduce mosquito biting outdoors, and, results demonstrate that metofluthrin-treated emanators are highly effective at repelling mosquitoes.

Rapley and Luke [104] have studied the effect of sustained release of metofluthrin on the biting, movement, and mortality of *Aedes* mosquitoes in a domestic setting. The comparison of a metofluthrin emanator with allethrin-based coils showed that the metofluthrin-based product was

more efficient than the coils and displayed a spillover effect that significantly reduced biting counts in neighboring rooms.

Lee [105] compared the repellent effects and zones of action of metofluthrin and transfluthrin using portable blowers for personal protection. Each battery-powered blower contained 0.6% transfluthrin or metofluthrin. The mosquitoes were highly susceptible to both pyrethroids. Mortality rates ranged from 95% to 100% at a distance of 10 cm and decreased at 70 cm. Lukwa and Chiwade [106] investigated the efficacy of mosquito coils containing metofluthrin or esbiothrin in experimental huts in Zimbabwe. They discovered that both formulations resulted in Anopheles mortality of less than 95%, indicating their lack of insecticidal effect. Achee *et al.* [107] identified the effective concentration of spatial repellency of dengue vectors using metofluthrin-based coils and DDT-impregnated fabrics. The study utilized air sampling methods to detect and quantify volatile active ingredients under field conditions and correlated the measurements to the knockdown values. The findings show that, man-vector contact and disease transmission are routinely interrupted by spatial repellent and contact irritant actions of common public health insecticides.

To evaluate next-generation mosquito repellents, Schmidt [108] investigated odorant-binding proteins (OBPs) located on the insect's antennae. These OBPs bind odorant molecules and transport them toward receptors located on the olfactory neuron surfaces. The resulting odorant-receptor linkage activates a cue in the mosquito's nervous system, alerting the insect of the human presence. This study suggested that OBPs may become one attractive target for next-generation repellents.

Ujihara *et al.* [109] reviewed the recent development of synthetic pyrethroids for household use and their synthesis. They revealed that norchrysanthemetic acid displayed a significant vapor activity at room temperature when esterified with fluorobenzyl alcohols. In particular, metofluthrin exhibited the highest potency in mosquito coil formulations as well as the best vapor activity at room temperature against various mosquitoes.

Morre *et al.* [110] assessed the behavior of mosquitoes in sub-Saharan zones for subjects using DEET, permethrin-impregnated bed nets [111,112], and lemon grass oils and nonusers. They discovered that with incomplete community repellent usage, nonusers may be exposed to an increased risk of malaria. These results also have implications on repellent-efficacy assay design

because protection appears magnified when mosquitoes are given a choice between repellent-users and nonusers.

In addition to evaluate different formats and their efficacy, Deguchi *et al.* determined the toxicity of metofluthrin [113]. A two-year treatment with high doses of metofluthrin produced hepatocellular tumors in male and female Wistar rats. The study also attempted to understand the mode of action of these metofluthrin-induced rat liver tumors.

Detailed information on the chronic, sub-chronic, and other toxicity profiles of metofluthrin has been compiled and documented by the Environmental Protection Agency (EPA) [100]. Data on its environmental fate and effects are also documented in the EPA Fact sheet. [100]

1.2.2.2 Current uses of metofluthrin as a household insecticide

Metofluthrin may be used as an effective active ingredient in devices without the need for electricity or heat because of its relatively high vapor pressure. The factors affecting its release differ from those of existing pyrethroids, such as d-allethrin and prallethrin. Consequently, its delivery formats are no longer restricted to electrical vaporizing mats, liquid vaporizers, aerosol sprays, and coils. In addition to conventional delivery mechanisms, two types of formulations have been tested for metofluthrin.

- a. Fan-type formulation: The active ingredient is vaporized by air flow from a fan at room temperature. The power required to operate the fan is much lower than that for heating, making the use of batteries as a power source possible [94].
- b. Ambient vaporization formulation: The active ingredient impregnated in paper or resin is allowed to vaporize without heating or power use. This approach is easy to use and can be used even in places where electricity is not available.

In these non-heated delivery devices, the substrate consists of

1. Paper, similar to Denguri toy (Figure 1.11) [94]. This substrate achieved a sustained release of metofluthrin over time [100].

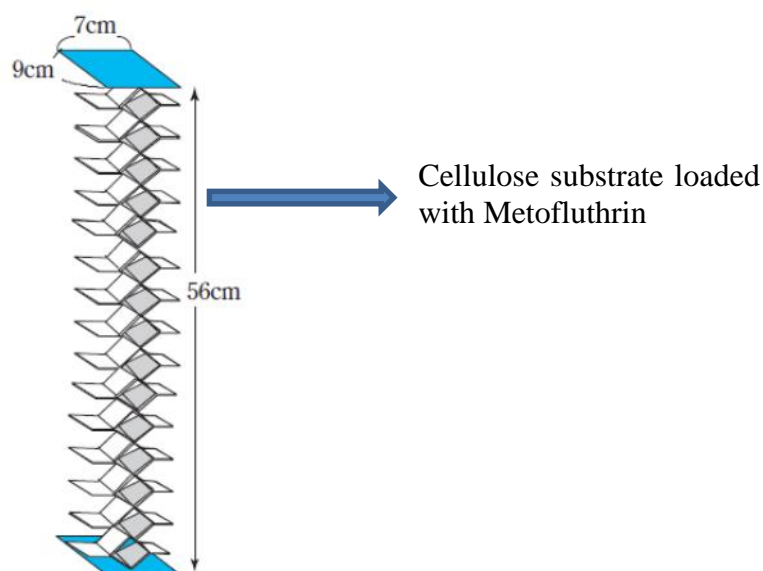


Figure 1.13: Paper emanatory *.

*from Discovery and Development of a Novel Pyrethroid Insecticide 'Metofluthrin (SumiOne®,Eminence®)' by Noritada MATSUO, Kazuya UJIHARA, Yoshinori SHONO, Tomonori IWASAKI & Masayo SUGANO

2. Polyolefin resin (Figure 1.12). This substrate was tested for residual characteristics and exhibited stable efficacy for at least eight weeks when used daily for 10 h [100].



Figure 1.14: Clip-on polymer-based device.

The paper delivery device [94] acting as a stable flying insect control item consisted of a cellulosic substrate with a surface area ranging between 50×10^{-4} and $5000 \times 10^{-4} \text{ m}^2$, 20–3000 mg/m^2 of Metofluthrin.

1. 3. Research gaps

Several household insecticide products available in the global market contain metofluthrin as the active ingredient against mosquitoes. These commercial products include mosquito coils, paper emanators, and plastic or resin-based battery operated small portable devices. Laboratory and field trials of these products have provided sufficient evidence for the in-use efficacy of metofluthrin. Scientists have investigated suitable formats for its implementation in household insect control as well as its efficacy against different species of mosquitoes in various formats in field trials.

However, because metofluthrin is a relatively new molecule, existing studies have focused on its performance given normal in use atmospheric and substrate conditions. To our knowledge there have been no studies on investigating dependence of its release on various external parameters, such as wind velocity, temperatures, humidity, nature, and type of different substrates onto which it is impregnated.

Furthermore, the absence of a suitable end of life indicator is a major issue for metofluthrin-impregnated based paper and polymeric substrates because it makes the depletion of activity difficult to monitor. The variability of external factors, such as relative humidity (RH), wind velocity, and temperature, also precludes reasonably the accurate prediction of a reasonable product end-of-life.

Existing reports address formats and field trials in various countries, such as Japan, US, Vietnam, Indonesia, Tanzania, and Zimbabwe. However, few studies have dealt with metofluthrin-based product performance and efficacy in Indian households. India is unique in terms of its diversity in geography, variety of mosquito species, atmospheric conditions (such as temperature), and house designs. A wide range of external variables, such as temperature and RH, are observed across the length and breadth of the country in addition to seasonal variations, which may influence the extent of metofluthrin release from substrates. For instance, atmospheric temperatures can reach sub-zero temperatures in winter and exceed 40 °C in summer. Although mosquitoes are known to thrive from 15 °C to 35 °C, they have been reported to survive harsh weather. Moreover, the design of Indian houses is mostly characterized by the presence of ceiling fans, large windows, and doors. These features influence the performance and efficacy of studied formats.

There have been no modeling studies have been reported to provide some insight into the release kinetics of this active ingredient from cellulose emanators. Consequently, rationalizing and

predicting end-of-life using volatility of metofluthrin-based products under various atmospheric conditions are difficult. Therefore, the formulation of a transport model accounting for the diffusional release of metofluthrin from various substrates to the atmosphere is highly desirable. Moreover, a proper set of boundary conditions expressing the continuity of mass fluxes at matrix/air interfaces may facilitate the evaluation of actual transport rates without resorting to any empirical correlation. Such a model is expected to predict the controlled release of metofluthrin from different polymer matrices under a wide range of operating and fluid dynamic conditions. The present thesis aims to bridge this gap by modelling the release kinetics of this active ingredient from a polymer matrix.

1. 4 Research motivations

The limited understanding of the factors influencing the release of metofluthrin currently hampers the prediction of end-of-life of metofluthrin-based product. This necessitates, therefore, development of a model that predetermines this release via experimentation and computation.

Our study primarily aims to determine the diffusion release pattern of various metofluthrin-based devices as a function of variable temperature conditions, wind velocity, and initial loading concentration. It is expected to provide a much deeper understanding of the impact of these parameters on the active ingredient release from the substrate. In addition, the influence of the metofluthrin release rates from various substrates at identical loading concentrations will indicate the nature of metofluthrin–substrate interactions, which could be studied through spectroscopic investigations.

The ideal goal of this study, under ideal conditions, is to formulate an accurate mathematical model to analyze and extrapolate the controlled release of metofluthrin from a polymer matrix in a room where air flows in a turbulent fashion from a source (ceiling fan) and around the polymer matrix. In addition, the model may be used to investigate the time evolution of some characteristic parameters, such as the metofluthrin content of the matrix, expressed as a function of the operating conditions, i.e., initial metofluthrin concentration, wind velocity, temperature, and RH of the air. Once validated using experimental data, the newly developed model can be exploited to optimize parameters, including the extremely important initial loading, required to maintain an effective metofluthrin concentration in the surrounding media over an extended time period.

Controlled release theories have been consistently used to understand the delivery of pesticides, fertilizers, drugs, herbicides, and related substances for polymer carriers [115]. Moreover, numerous potential products relying on controlled release have been described previously. The slow migration of these substances from polymer matrices is quite well known and has been implemented in several products, such as the slow release of mosquito larvicides from polyvinyl chloride [116] and natural rubber [117] to control mosquito larvae for up to six months.

The study of factors influencing metofluthrin release, is expected to lead to a predictive model for metofluthrin release and life in a set of atmospheric conditions and substrate characteristics.

1. 5 Scope and limitations

The scope of the present study is to

1. Evaluate the effect of external variables, such as
 - a) Initial concentration b) atmospheric temperature c) wind velocity, and d) nature of substrates, on the release profile of metofluthrin from impregnated substrates.
2. Measure metofluthrin release from various polymeric substrates to understand and investigate the role of metofluthrin–substrate interactions. Attempts are made to address the correlation between metofluthrin release and its interaction with various substrates through spectroscopic investigations.
3. Develop a diffusion model which reasonably explains the release profile of metofluthrin as observed experimentally.

This study only focuses on the release profiles of metofluthrin because of its implications in insecticidal activity under ambient conditions. In addition, our substrates are restricted to temperatures below 37 °C because of its relevance to normal human usage conditions. The study is conducted for a 1200 cm² area polymeric sheet and does not address resin emanators. It considers a few variable external factors, thereby limiting the development of a generalized experimental model to predict end of life of metofluthrin-based product.

CHAPTER 2

Diffusion

This study focuses on developing an understanding of external factors influencing metofluthrin release from substrates. To this end, experiments were planned to measure release rates from various substrates impregnated with known amounts of the active ingredients.

Diffusion is the net action of matter (i.e., particles or molecules), heat, momentum, or light to minimize a concentration gradient. Although it is not a chemical reaction, its process minimizes the thermodynamic Gibbs free energy. Therefore, it is a spontaneous, “passive” rather than an “active” form of transport phenomenon occurring in nature. Its distinguishing feature is its ability to produce mixing or mass transport without requiring bulk motion. Diffusion should not be confused with other transport mechanisms, such as convection and advection, which utilize bulk motion to displace particles from one location to another.

Diffusion results from random molecular motions that lead to complete mixing and can be a slow process. It typically progresses at rates of about 5 and 0.05 cm/min, respectively, in gases and liquids but at only about 0.00001 cm/min in solids. In general, these rates depend on temperature to a smaller extent than other phenomena. Low rates are responsible for the importance of diffusion. In many cases, diffusion occurs sequentially with other phenomena. When it is the slowest step of a sequence, it reduces the overall rate of this process. For example, it often limits the efficiency of commercial distillations and the rate of industrial reactions using porous catalysts. It slows down acid/base reaction and nutrient absorptions by the human. It controls the growth of penicillin producing microorganisms, steel corrosion rate, and flavor release from food.

In gases and liquids, diffusion processes can often be accelerated by agitation. For example, copper sulfate in a tall bottle dissolves completely in a few minutes if the solution is stirred. This accelerated mixing results from the combination of diffusion and stirring but not diffusion alone. Diffusion depends on random molecular motions occurring over small distances. Agitation and stirring are not molecular but macroscopic processes that move portions of the fluid over large distances. After this macroscopic process, diffusion mixes newly adjacent portions of the fluid. In other cases, such as pollutant dispersal, the agitation of wind or water produces dispersion, which qualitatively resembles diffusion.

As might be expected, dispersion is related to diffusion on two different levels. First, dispersion is a form of mixing and, thus, involves diffusion at the molecular level. Although not understood in detail, molecular dispersion occurs so rapidly that it is rarely the most important feature of the process. Second, dispersion and diffusion are mathematically described using similar equations, meaning that analyses developed for diffusion can often correlate dispersion results. Consequently, diffusion models were used to describe and understand the metofluthrin release process in this thesis.

The description of diffusion involves a mathematical model based on a fundamental hypothesis or law. Interestingly, two common choices exist for this law. The more fundamental and commonly cited Fick's law of diffusion relies on a diffusion coefficient. The second law involves a mass transfer coefficient, which is a type of reversible rate constant. The notion of diffusion is typically induced by a phenomenological approach, which starts with Fick's laws of diffusion and their mathematical consequences, or a physical and atomistic one, which considers the random walk of the diffusing particles. According to Fick's laws, the diffusion flux is proportional to the negative gradient of concentrations. Movement occurs from higher to lower concentration regions [118].

2.1 Fick's first law of diffusion

Adolf Fick—a 26-year old anatomy demonstrator from Zurich—proposed his law of diffusion in 1855. Using Graham's research, he stated his goal as “the development of a fundamental law for the operation of diffusion in a single element of space” [118]. He highlighted a deep analogy between diffusion and heat or electrical conduction, creating a formalism analogous to Fourier's law for heat conduction (1822) and Ohm's law for electrical current (1827).

Fick's first law relates the diffusive flux to the concentration under the assumption of steady state. It postulates that the flux moves from high to low concentration regions with a magnitude that is proportional to the concentration gradient (spatial derivative). In one (spatial) dimension, the law is written as follows:

$$J = -D \frac{\partial \phi}{\partial x} \quad \text{Equation 2.1}$$

Where J is the “diffusion flux” (e.g., in mol /($\text{m}^2 \cdot \text{s}$)) and represents the amount of substance that flows through a small area during a small time interval, D is the diffusion coefficient or diffusivity [$\text{length}^2 \text{ time}^{-1}$] (e.g., in m^2/s), ϕ (for ideal mixtures) is the concentration in dimensions of [amount of substance per unit volume] (e.g., in mol/m^3), and χ is the position [length] (e.g., m).

The diffusivity is proportional to the squared velocity of the diffusing particles, which depends on temperature, fluid viscosity, and particle size according to the Stokes–Einstein relation. In dilute aqueous solutions, the diffusion coefficients are similar and range from 0.6×10^{-9} to $2 \times 10^{-9} \text{ m}^2/\text{s}$ at room temperature for most ions. For biological molecules, they typically range from 1×10^{-11} to $1 \times 10^{-10} \text{ m}^2/\text{s}$.

In two or more dimensions, the delta or gradient operator ∇ , which generalizes the first derivative, gives,

$$J = -D\nabla\phi. \quad \text{Equation 2.2}$$

The driving force for the one-dimensional diffusion is the quantity $-\frac{\partial\phi}{\partial x}$, Which corresponds to the concentration gradient for ideal mixtures. In non-ideal solutions or mixtures, the driving force for diffusion of individual species is the gradient of their chemical potential. Consequently, for the one-dimensional case, Fick’s first law is written as follows:

$$J_i = -\frac{Dc_i}{RT} \frac{\partial\mu_i}{\partial x} \quad \text{Equation 2.3}$$

where the index i denotes the i^{th} species, c is the concentration (mol/m^3), R is the universal gas constant ($\text{J}/(\text{K mol})$), T is the absolute temperature (K), and μ is the chemical potential (J/mol).

If the primary variable is the mass fraction y_i (e.g., in kg/kg), Eq. (2.3) becomes

$$J_i = -\rho D \nabla y_i \quad \text{Equation 2.4}$$

Where ρ is the fluid density (e.g., in kg/m^3) and ∇ is outside the gradient operator.

2.2 Fick's second law of diffusion

Fick's second law predicts how diffusion causes the concentration to change with time.

$$\frac{\partial \phi}{\partial t} = D \frac{\partial^2 \phi}{\partial x^2} \quad \text{Equation 2.5}$$

Where ϕ is the concentration in dimensions of [(amount of substance) length⁻³] (e.g., in mol/m³) and t is the time (e.g., in s).

It is derived from Fick's first law and the mass conservation in the absence of any chemical reactions as

$$\frac{\partial \phi}{\partial t} + \frac{\partial J}{\partial x} = 0 \rightarrow \frac{\partial \phi}{\partial t} - \frac{\partial}{\partial x} \left(D \frac{\partial \phi}{\partial x} \right) = 0 \quad \text{Equation 2.6}$$

Assuming that the diffusion coefficient D is constant, the orders of the differentiation are exchanged and multiplied by the constant to produce the form shown in Eq. (2.5).

$$\frac{\partial}{\partial x} \left(D \frac{\partial \phi}{\partial x} \right) = D \frac{\partial}{\partial x} \frac{\partial \phi}{\partial x} = D \frac{\partial^2 \phi}{\partial x^2} \quad \text{Equation 2.7}$$

For diffusion in two or more dimensions, Fick's second law becomes

$$\frac{\partial \phi}{\partial t} = D \nabla^2 \phi \quad \text{Equation 2.8}$$

Which is analogous to the heat equation.

If the diffusion coefficient is not a constant but depends on the coordinate and/or concentration, Fick's second law yields

$$\frac{\partial \phi}{\partial t} = \nabla(D \nabla \phi) \quad \text{Equation 2.9}$$

An important example is the case where ϕ is at a steady state, i.e., the concentration remains constant over time so that the left part of Eq. (2.9) equals zero. In one dimension with constant D , the concentration will be a linear function of x . In two or more dimensions,

$$\nabla^2 \phi = 0 \qquad \text{Equation 2.16}$$

In fundamental studies, diffusion coefficients can be used to determine the concentration as a function of position and time. Practical problems, in which one experiment is used to predict the behavior of a similar one, rely on mass transfer coefficients.

The diffusion coefficient is the proportionality constant, the unknown parameter appearing in Fick's law. Calculations of the flux and the concentration profile using the Fick's law require the knowledge of D values in these particular situations. It has been observed that these coefficients depend largely on experimental measurements in the absence of a universal theory for their accurate calculation. Unfortunately, measurements are unusually difficult to realize and their results exhibit variable quality. Accordingly, the quality of these measurements needs to be assessable.

First, let us list the characteristics that tend to stick in everyone's mind. In gases, diffusion coefficients can be estimated theoretically and are approximately $0.1 \text{ cm}^2/\text{s}$. In liquids, they cannot be as reliably estimated and cluster around $10^{-5} \text{ cm}^2/\text{s}$. In solids, they are lower ($10^{-30} \text{ cm}^2/\text{s}$) and vary strongly with temperature. In polymers and glasses, they lie between liquid- and solid-state values (about $10^{-8} \text{ cm}^2/\text{s}$) and highly depend on solute concentration.

In the investigation of metofluthrin release, the diffusion constant needs to be calculated before applying Fick's laws of diffusion. This calculation is achieved using the Arrhenius equation [120].

2.3 Arrhenius equation

The Arrhenius equation is a simple but remarkably accurate formula for the temperature dependence of reaction rates. It was first proposed by Svante Arrhenius in 1889 from earlier physical justification and interpretation by Dutch chemist J. H. Van't Hoff. Currently, best considered as an empirical relationship, it has proven useful for modeling the temperature variance of diffusion coefficients, population of crystal vacancies, creep rates, and many other thermally induced processes/reactions. Developed in 1935, the Eyring equation also relates rate and energy.

A historically useful generalization supported by the Arrhenius equation is that, for many common chemical reactions at room temperature, the reaction rate doubles for every 10 °C increase in temperature.

The Arrhenius equation (Eq. (2.11)) gives the relationship between the rate constant k of a chemical reaction and the absolute temperature T (in K), where A is the pre-exponential factor (or simply the prefactor), E_a is the activation energy, and R is the universal gas constant.

$$k = Ae^{-E_a/RT} \quad \text{Equation 2.11}$$

Alternatively, the equation is also written as follows:

$$k = Ae^{-E_a/(k_B T)} \quad \text{Equation 2.12}$$

Where k_B is the Boltzmann constant.

Equations 2.11 and 2.12 only differ by the energy units of E_a . In Eq. 2.11, E_a is given in energy per mole, which is common in chemistry, while it is expressed in energy per molecule directly in Eq. 2.12, which is common in physics. These units are accounted for using R or k_B as the multiplier of T .

The unit of the pre-exponential factor A is identical to that of the rate constant and changes depending on the order of the reaction. For a first-order reaction, the unit is s^{-1} and, for that reason, the prefactor is often called the frequency factor or attempt frequency of the reaction. Most simply, k is the number of collisions during a reaction per second, A is the total number of collisions leading to a reaction or not per second, and $e^{-E_a/RT}$ is the probability that any given collision results in a reaction. Increasing the temperature or decreasing the activation energy augments the reaction rate.

Given the small temperature range of kinetic studies, it is reasonable to assume the activation energy as being independent of temperature. Similarly, under a wide range of practical conditions, the weak temperature dependence of A is negligible compared to that of $\exp(-E_a/RT)$, except for

“barrier less” diffusion-limited reactions, in which the pre-exponential factor is dominant and directly observable.

2.4 Modified Arrhenius equation

The modified Arrhenius equation makes the temperature dependence of the pre-exponential factor explicit. An arbitrary temperature dependence of the pre-factor produces an over complete Arrhenius description and a singular inverse problem (i.e., determining the pre-factor and activation energy from experimental data). The modified equation is usually written as follows:

$$k = A(T/T_0)^n e^{-(E_a/RT)} \quad \text{Equation 2.13}$$

Where T_0 is the reference temperature and n is the dimensionless power. Evidently, the original Arrhenius expression corresponds to $n = 0$. Fitted rate constants typically range between -1 and 1 . Theoretical analyses yield various predictions for n . As previously indicated, “it is not feasible to establish, on the basis of temperature studies of the rate constant, whether the predicted $T^{1/2}$ dependence of the pre-exponential factor is observed experimentally.” However, if additional evidence, such as density dependence, is available from theory and/or experiment, incisive tests of the Arrhenius law are possible.

Another common modification is the stretched exponential form.

$$k = A \exp \left[- \left(\frac{E_a}{RT} \right)^\beta \right] \quad \text{Equation 2.14}$$

Where β is a unit less number of order 1. This number is typically regarded as a fudge factor to make the model fit the data but can have theoretical meaning. For example, it reveals the presence of a range of activation energies in special cases, such as the Mott variable-range hopping.

The natural logarithm of the Arrhenius equation yields

$$\ln(k) = \frac{-E_a}{R} \frac{1}{T} + \ln(A) \quad \text{Equation 2.15}$$

Which has the same form for the linear equation

$$y = mx + b \quad \text{Equation 2.16}$$

Consequently, when a reaction rate constant obeys the Arrhenius equation, a plot of $\ln(k)$ with respect to (T^{-1}) gives a straight line, whose slope and intercept provide E_a and A . This procedure has become so common in experimental chemical kinetics that practitioners exploit it to calculate the activation energy of a reaction. The activation energy is defined as $-R$ times the slope of a plot of $\ln(k)$ vs (T^{-1}) .

$$E_a = -R \left[\frac{\partial \ln k}{\partial (1/T)} \right]_p \quad \text{Equation 2.17}$$

Fick's law of diffusion has been applied by Collins and Doglia to determine real-time concentrations of pesticides released by diffusion [120]. It has also been utilized to study the migration of volatile compounds present in polypropylene/polyethylene/ Tenax composite polymer laminates serving as multilayer packaging in food [121]. The diffusion of fumigant in soil and in air has been also investigated using Fick's second law by the Department of Pesticide regulation [122]. Zhang and Niu have evaluated the diffusion of volatile organics from painting material in standard field and cell using Fick's law and Arrhenius equation [123].

CHAPTER 3

Active ingredient—Metofluthrin

3.1 Physical and chemical properties of metofluthrin

Metofluthrin (Figure 3.1) [2,3,5,6-tetrafluoro-4-(methoxymethyl)benzyl (EZ)-(1RS,3RS;1RS,3SR)-2,2-dimethyl-3-prop-1-enylcyclopropanecarboxylate] is a pale yellow transparent oily liquid. Its physical and chemical properties are listed in Table 3.1 [94,124]. It dissolves in almost all organic solvents but is insoluble in water. Its vapor pressure at 25 °C is 1.96×10^{-3} Pa. This value substantially exceeds those of other known pyrethroid insecticides, which typically exhibit maximum vapor pressures of about 10^{-5} Pa (1.33×10^{-5} Pa at 25 °C for prallethrin).

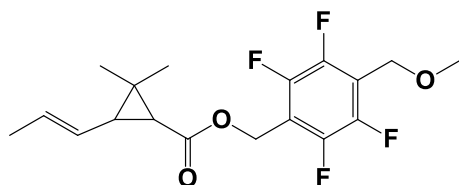


Figure 3.1: Structure of metofluthrin.

Table 3.1: Physical and chemical properties of metofluthrin.

Sr. No.	Property	Observation
1	Molecular formula	$C_{18}H_{20}F_4O_3$
2	Molecular weight	360.34
3	Appearance	Pale yellow transparent liquid
4	Odor	Slightly characteristic odor
5	Vapor pressure (Gas saturation method) (25 °C)	1.96×10^{-3} Pa
6	Specific gravity	1.21
7	Kinetic viscosity (20 °C)	19.3 mm ² /s
8	Flash point (Cleveland open method)	178 ° C
9	Distribution coefficient (Ambient shake flask method)	Log P = 5.64

10	Solubility in water (20 °C saturated solution method)	0.73 mg/L
11	Solubility in organic solvents	Completely soluble in Acetonitrile, Dimethyl sulfoxide, Methanol, Ethanol, Acetone, and Hexane

3.1.1 Thermal analysis

Differential thermogravimetric analysis (TGA) [94] showed vaporization-induced weight loss from 98 °C and decomposition-related weight fluctuations at 202.7 °C. This suggests that metofluthrin is stable up to 95 °C, and the onset of decomposition occurs above 202.7 °C.

3.1.2 Stability

Metofluthrin is stable for six months at 50 °C and is not affected by humidity [94]. It remains intact for three years when stored at room temperature. In addition, 1% (w/v) solution in various general purpose solvents, such as methanol, ethanol, 2-propanol, kerosene (Isopar® M), isopropyl myristate, and propylene glycol, do not change when stored at 60 °C for one month. Metofluthrin presents higher stability than d-allethrin and prallethrin, which are used in heated and ambient vaporization formulations as well as in the sun, demonstrating its suitability for outdoor applications. Its photostability also exceeds those of prallethrin and d-trans allethrin [94].

3.2 Biological efficacy of metofluthrin

Bio-efficacy studies on mosquitoes have shown the lethal efficacy of metofluthrin [94]. These results are compiled in Table 3.2 for medically important pests.

Table 3.2: Comparative bio-efficacy data for synthetic pyrethroids.

Compound	<i>Culex pipiens</i>	<i>Aedes albopictus</i>	<i>Musca domestica</i>	<i>Blattella germanica</i>
LD ₅₀ *				
Metofluthrin	0.0015	0.00047	0.24	1.3
d-allethrin	0.038	0.023	0.21	2.9

Prallethrin	0.0056	0.0050	0.13	0.59
d-tetramethrin	0.0096	0.0036	0.28	7.8
Permethrin	0.0028	0.0012	0.013	1.5
*LD ₅₀ (µg/female adult) by topical application method. The median lethal dose (LD ₅₀) is a dose of a toxin, radiation, or pathogen that is required to kill half the members of a tested population after a specified test duration.				

The LD₅₀ of topically applied metofluthrin equals 0.0015 µg/female adult for *Culex pipiens* adults. This value represents approximately twenty-five and four times lesser concentration than those of d-allethrin and prallethrin, respectively, which are the most widely used pyrethroids presently [94], indicating its high efficacy.

3.2.1 Biological efficacy of metofluthrin in products formats

In addition to high efficiency in controlling various mosquito species, metofluthrin exhibits suitable physical properties for various vaporization formulations. Detailed investigations in leveraging these properties in typical heated vaporization formulations, such as mosquito coils and liquid vaporizers, also have indicated its high relative efficacy as an insecticidal active ingredient compared to d-allethrin and prallethrin [94].

In addition to existing delivery devices, such as aerosols, coils, and liquid vaporizers, two types of formulations not employing heat, including fan type and ambient vaporization formulations exist for metofluthrin. For a country like India, which exhibits a large rural population experiencing electric power supply issues and challenging socioeconomic conditions, a device working at ambient temperature is very relevant. This thesis, therefore, attempts to develop a deeper understanding of factors influencing metofluthrin release under ambient conditions.

3.2.2 Gas chromatography analysis of metofluthrin release from substrates

Metofluthrin can be analyzed by multiple techniques depending on the purpose and range of determinations. In general, technical active substances are determined by capillary gas chromatography-flame ionization detector (GC-FID) using a DB-5 column having 5% phenyl and 95% dimethylpolysiloxane as stationery phase and di butyl phthalate was used as an internal standard [114,125,126]. Impurities in the technical material are analyzed using chiral high-

performance liquid chromatography coupled with a UV spectrophotometer at 270 nm. Trace residues in soils and air are quantified by GC with an electron capture detector using a DB-5 column and an internal standard. Mass spectrometry (MS), nuclear magnetic resonance (NMR), and Fourier transform infrared spectroscopy (FTIR) can be used to identify to materials.

The objective of this present analysis consisted in determining the residual metofluthrin content in impregnated cellulose substrates. Therefore, the pyrethroid was analyzed by capillary GC-FID. The adsorbed metofluthrin (provided by Sumitomo Chemicals, Japan) was completely extracted from the substrates and directly injected in the GC instrument for residual content analysis [137].

Instruments and conditions

Gas chromatograph Agilent 6820A, fitted with a flame ionization detector.

Column: Capillary HP-5, 30 m × 320 μm × 0.25 μm

Oven temperature program: 220 °C for 15 min and 1 °C/min to 300 °C

Injector temperature: 275 °C

Detector temperature: 300 °C

3.2.2.1 Sample preparation procedures

The typical experimental procedure for metofluthrin quantification is described below. The substrate consisted in a multi-layer, foldable cellulose or polymer structure (10 × 60 cm²).

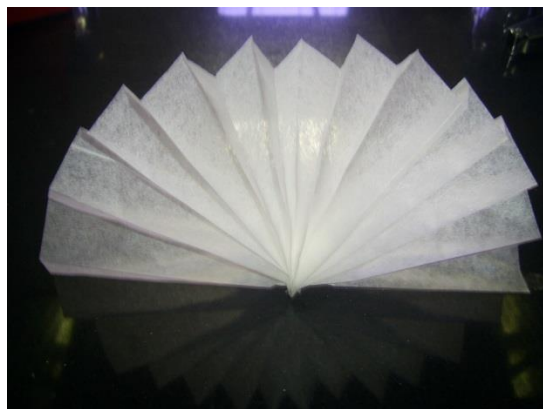


Figure 3.2: Cellulose or polymer substrate loaded with metofluthrin.

Metofluthrin (66 mg) was diluted in isopropyl alcohol (20 mL) and uniformly applied to the cellulose or polymer surface. The solvent was then allowed to evaporate at ambient temperature

before refolding. Blank emanators treated with acetone served as controls. The total surface area of the unfolded cellulose matrix was approximately 1200 cm².

To avoid any losses during storage, the prepared samples were sealed in aluminum foil-based laminates using a band heat sealer and stored at ambient laboratory temperature until use [94].

Standard solution

In a 100-mL volumetric flask, metofluthrin Technical grade 0.30 ± 0.05 g, was accurately weighed and diluted to the volume with chloroform. This solution (10 mL) was transferred by a pipette into a second 100-mL volumetric flask before adding 5% (w/v) diisobutyl phthalate in chloroform (1 mL) used as an internal standard solution and chloroform dilution to 100 mL. The solution was homogenized and transferred in the injection vial. The prepared stock solution was stored in a refrigerator at 5 ± 1 °C, as per stability and storage information on metofluthrin (Section 3.1.3).

Sample solution

The substrate was carefully detached from the holder and weighed on a precision balance. All glue-containing parts were removed and discarded. The remainder was cut into little pieces and put in a 250 mL Erlenmeyer flask. Chloroform (45 mL) was added to the flask and stirred on magnetic stirrer for 5 min. The extracts were transferred quantitatively to a 100-mL volumetric flask. This extraction was repeated once, and all the extracts were transferred to the same flask. The 5% (w/v) di-isobutyl phthalate solution in chloroform (5 mL) was added to the collected extracts and diluted to 100 mL with chloroform. The sample solution was filtered with a 0.45 µm nylon millipore filter before injection in the GC instrument.

Sample analysis before the release study

The metofluthrin content of the prepared samples were evaluated before initiating the release study to confirm the uniform dosing and spreading of the pyrethroid on the substrate. The prepared samples were sealed in aluminum foil laminates and allowed to equilibrate for 24 h under ambient storage conditions. Samples were then tested, as described above.

To check the uniform distribution of metofluthrin, the impregnated cellulose strip was cut into previously marked four identical pieces. The active ingredient content of these individual pieces was determined, as described above.

3.2.2.2 Results and calculations

The standard solution was injected until internal standard ratios remained below 2% for three successive injections. Next, the sample solution was injected, and the metofluthrin content was calculated by the internal standard method. Di-isobutyl phthalate and metofluthrin exhibited retention times of 3.83 and 4.63 min, respectively.

The metofluthrin content (in mg/sample) *was calculated using*

$$C = \frac{M_1 \times A_1 \times A_3 \times P_1}{A_2 \times A_4},$$

Where M_1 is the mass in grams of the metofluthrin reference standard, A_1 is the internal standard peak area for the injected metofluthrin reference standard solution, A_3 is the metofluthrin peak area for the injected sample solution, A_2 is the metofluthrin peak area for the injected metofluthrin reference standard solution, A_4 is the internal standard peak area for the injected sample solution, and P_1 is the percent purity of the metofluthrin reference standard.

Analytical method validation

The analytical method was validated over the expected data range. The linear correlation coefficient and the standard deviation were found to be 1.0001 and 0.15, respectively, while the average recovery equaled 99.98%.

Representative data collected

Theoretical loading: 66.0033 mg

(Basis strength of stock solution and loading per sample)

Experimental determination

$$\begin{aligned} \text{Metofluthrin content (mg/sample)} &= \frac{M_1 \times A_1 \times A_3 \times P_1}{A_2 \times A_4} \\ &= \frac{66.0033 \times 91583.99 \times 123115.56 \times 100}{116696.68 \times 96669.12} \\ &= 65.97 \text{ mg} \end{aligned}$$

Representative sampling during the uniformity check

The dosed sample was cut into four parts (A, B, C, and D), which were individually analyzed for metofluthrin content.

The determined active ingredient in mg in 4 cut parts of substrate was as shown below:

Metofluthrin content in mg in four parts of substrate	
A = 16.49 mg	B = 16.49 mg
C = 16.50 mg	D = 16.49 mg

Total metofluthrin content in mg =65.97 mg

The results showed that metofluthrin spread uniformly on the substrate and displayed very good recovery. This procedure was followed for all four substrates under evaluation

3. 2.3 Bio-efficacy determination method

The GC method described in the previous section helps in metofluthrin characterization. Bio-efficacy measurements are equally important to confirm the adequacy of this active ingredient [102]. Bio-efficacy test provides outcome that consist a) KT_{50} in minutes which is the time taken to knockdown 50% of the test population and b) the mortality after 24 h of the test [127,128], which corresponds to the number of deaths to the knockdown test population after 24 h [129].

Description

The efficacies of cellulose strip impregnated with 66 mg of Metofluthrin and Standards and Industrial Research Institute of Malaysia (SIRIM) standard coil formulation (d-trans allethrin 0.1% m/m) are compared by a bioassay [130]. The tests assess the knockdown speed and resultant mortality of exposed insects 1 h after device activation.

Test conditions

All tests were performed in an unventilated empty 24 m³ room illuminated by an external 150 W incandescent lamp placed above a glass window on the roof. Tests are conducted at 27 ± 1 °C and 35%–55% RH on a population of three- to seven-day-old female *Culex quinquefasciatus* mosquitoes.

Setup and measurement procedure

Control tests were conducted prior to any measurement, to ensure that test chambers were devoid of any insecticide contamination. The test sample is placed 70 cm above the floor near a chamber wall. A fan rotating at very low speed (i.e., 300 rpm) is positioned at the same height at the opposite wall chamber and is switched on. Subsequently, about 100 female mosquitoes are released in the chamber and the mosquito knockdown time is recorded.

First, the initial bio-efficacy measurement is conducted for a freshly opened sample. A similar open sample is placed in another room and allowed to age for 60, 120, 180, 240, and 300 h. The aged sample is placed in the test chamber for bio-efficacy measurements, and the KT_{50} value is measured for each aging interval. The knocked down mosquitoes are collected and examined after 24 h for mortality.

During the counting period, knocked down mosquitoes are counted every 2.5 min for 60 min and the median KT_{50} is calculated by the Bliss Probit method [131]. One hour subsequent to the beginning of the test, knocked down insects are picked up using an aspirator and transferred in a clean container with sugar solution. The number of mosquitoes that are not revived after 24 h is used as a measure to determine the mortality.

Observations

Table 3.3: KT_{50} and mortality after 24 h obtained using a metofluthrin-impregnated cellulose emanator against *Culex quinquefasciatus*.

a) Knockdown time

Hours of use	Replicates					Average KT_{50} (min)
	KT_{50} (min)					
	1	2	3	4	5	
Initial	34	29	37	39	39	32
60	39	35	31	42	30	35
120	47	44	34	46	35	41
180	38	39	52	45	49	45
240	55	47	44	41	54	48
300	54	56	55	54	56	55

b) Mortality

Hours of use	Replicates					Average Mortality in %
	Mortality after 24 h (%)					
	1	2	3	4	5	
Initial	100	100	100	100	100	100
60	99	100	100	100	100	100
120	100	100	100	99	100	100
180	100	100	98	100	100	100
240	100	99	100	100	98	99
300	98	99	99	98	98	98

Table 3.4: KT_{50} and mortality after 24 h obtained using a SIRIM standard coil formulation against *Culex quinquefasciatus*.

a) Knockdown time

Mosquito species	Replicates					Average KT_{50} min
	KT_{50} min					
	1	2	3	4	5	
<i>Culex quinquefasciatus</i>	49	45	53	46	58	50

b) Mortality

Mosquito species	% Mortality after 24 h					Average Mortality in %
	1	2	3	4	5	
<i>Culex quinquefasciatus</i>	99	100	100	100	100	100

Conclusion

The results of the comparative bio-efficacy study of the metofluthrin-based cellulose emanator and commercially available SIRIM standard mosquito coils (0.2% d-Allethrin mosquito coils (m/m)) demonstrates the efficacy of the cellulose emanator for protecting household indoor areas against *Culex quinquefasciatus* mosquitoes. The test product also maintains a good knockdown and killing effect during 300 h of usage as evidenced by the data.

3.2.4 Accelerated storage stability of Metofluthrin based product

The relatively high vapor pressure of metofluthrin has been mentioned in earlier section. This physical property imparts metofluthrin the ability to get partitioned into the atmosphere from its original state. From a product development viewpoint this has important implications with respect to the longevity of the product, as well as, the attendant claims on bio efficacy which are being made.

Hence, it is critical to establish through relevant measurements that the amount of metofluthrin incorporated in the product is retained till the point of usage by the consumer. It is also evident therefore that given metofluthrin's propensity to get partitioned into the atmosphere in a facile manner, the packaging element would play a key role in ensuring product longevity. The following paragraph describes the analytical methodology adopted to conduct measurements on samples of our interest.

As a representative example the samples for measurement were prepared using cellulose substrates dosed with 66 mg of Metofluthrin. These samples were then packed within thermo formed PET based external packaging, sealed externally in a plastic laminate, and, stored at temperature of 40°C. These samples were then analyzed for their metofluthrin content at time intervals of 1, 3 and 6 months respectively using GC (Refer Section 3.2.2 for experimental details) and the results obtained at these times compared with those obtained before sample storage.

Conclusion:

The samples containing metofluthrin incorporated within cellulose remained stable throughout the test period as evidenced by absence of any substantial losses during the time periods. It is therefore reasonably estimated that such products would be expected to have a predicted shelf life under normal ambient temperature conditions of at least 3 years.

CHAPTER 4

Influence of external variable factors on metofluthrin release

Metofluthrin is a relatively newer synthetic compound within the pyrethroid class of compounds. This molecule was discovered and registered by Sumitomo Chemical Corporation, Japan in 2005 and has been shown to be highly efficacious against mosquitoes. What distinguishes metofluthrin from its earlier congeners is its relatively high vapour pressure at 25°C of 1.96×10^{-3} Pa which confers upon itself the ability to volatilize under ambient conditions. This ability of getting partitioned into the vapour phase under normal conditions opens up the possibility of exploring creative household insecticidal formats which do not need either electricity or combustion, unlike, its predecessor compounds. In addition, metofluthrin has been found to be extremely safe, as well as, is capable of expressing its efficacies at far lower concentrations.

Hence, it is plausible to think of insecticidal formats containing metofluthrin as the active ingredient, but, which functions independently of heat or electricity by virtue of its high vapour pressure coefficient. It is important to note that external factors like temperature, wind velocity, humidity (RH), as well as, substrate properties like exposed surface areas, pore characteristics and inherent porosities might strongly influence the diffusion led release profile of metofluthrin from its formats (132,133). This therefore introduces an element of uncertainty in correctly predicting the products end-of-life given the fact that external variable factors are at play. Therefore, it is critical to understand the relationship between the release of this active ingredient and factors influencing it. To the best of our knowledge investigating links between the release rate of metofluthrin and external ambient conditions has not been studied, hitherto. This necessitates focusing on the development of a generalized predictive model which would capture the influences of external variable factors on metofluthrin release and thereby allow a far better handle on predictability of a format's end of life.

4.1 Temperature effect on metofluthrin release

4.1.1 Background on dosage selection

The release profile of metofluthrin is investigated under various temperature conditions. Studies have been conducted using nonheated fan and ambient Denguri paper formulations involving 100 to 200 mg metofluthrin dosages for 8 to 12 h of daily use lasting between 30 to 60 days. The amount of Metofluthrin chosen for impregnation onto various substrates is in accordance with the regulatory compliances as recommended by Central Insecticide Board, Govt. Of India.

4.1.2 Methodology

A Known amount of metofluthrin is dosed in cellulose substrates, which are placed in three test rooms kept at controlled temperatures to facilitate release. At regular time intervals, the residual metofluthrin is extracted from the cellulose sample and analyzed by GC, as mentioned in Section 3.2.

Materials and equipment

Metofluthrin

Isopropyl alcohol

Cellulose substrates ($10 \times 60 \text{ cm}^2$)

Gas chromatograph Agilent 6820A, fitted with a flame ionization detector.

Column: Capillary HP-5, $30 \text{ m} \times 320 \mu\text{m} \times 0.25 \mu\text{m}$

Oven temperature program: $220 \text{ }^\circ\text{C}$ for 150 min and heating at $1 \text{ }^\circ\text{C}/\text{min}$ to $300 \text{ }^\circ\text{C}$

Injector temperature: $275 \text{ }^\circ\text{C}$

Detector temperature: $300 \text{ }^\circ\text{C}$

Method

A stock solution of Metofluthrin in isopropyl alcohol is prepared to dose cellulose substrates with $66 \pm 1 \text{ mg}$ of metofluthrin. The prepared samples are kept open and unfolded to enable solvent evaporation. Next, they are placed in three 30 m^3 standard test rooms equipped with a fan in the middle of the ceiling. These rooms are maintained at 17 ± 1 , 27 ± 1 , and $37 \pm 1 \text{ }^\circ\text{C}$ and $65 \pm 5\%$ RH, respectively. The wind velocity at different locations in the room is measured using an anemometer and set to 0.2 m/s at test locations by adjusting the fan speed. After wind velocity measurements, these locations are marked for sample placement. Samples are placed and allowed to equilibrate at specified temperatures for 60, 120, 180, 240, and 300 h.

At these scheduled exposure times, samples are collected, and residual metofluthrin content is analyzed by GC, producing the released metofluthrin quantity. All measurements are conducted in triplicates, and standard deviation and average values calculated and reported.

4.1.3 Results

Table 4.1: Cumulative metofluthrin % release from cellulosic substrate at controlled temperatures at a wind velocity of 0.2 m/s.

Cumulative release of Metofluthrin in % as a function of time													
		Cumulative release of Metofluthrin in %											
Duration of use in hours		At 37 °C	Mean	Std. Dev	% RSD	At 27 °C	Mean	Std. Dev	% RSD	At 17 °C	Mean	Std. Dev	% RSD
60	Rep 1	31.8	31.7	0.2624	0.8287	23.6	23.789	0.4008	1.685	16.4	16.667	0.303	1.8182
	Rep 2	31.8				23.5				17.0			
	Rep 3	31.4				24.2				16.7			
120	Rep 1	49.5	48.8	0.6604	1.3537	38.8	38.182	0.6061	1.5873	29.5	29.747	0.4871	1.63723
	Rep 2	48.3				37.6				30.3			
	Rep 3	48.5				38.2				29.4			
180	Rep 1	62.9	62.9	0.75757	1.2048	53.3	53.636	1.0926	2.0370	43.3	42.424	0.8436	1.9885
	Rep 2	63.6				54.8				42.3			
	Rep 3	62.1				52.7				41.7			
240	Rep 1	72.0	72.2	1.1572	1.6023	66.4	65.151	1.0606	1.6279	52.0	53.030	0.9935	1.87355
	Rep 2	71.2				64.4				53.9			
	Rep 3	73.5				64.7				53.2			
300	Rep 1	82.6	81.8	0.66044	0.80720	75.8	75.757	0.60602	0.8	62.4	63.687	1.21523	1.90820
	Rep 2	81.4				75.2				64.8			
	Rep 3	81.5				76.4				63.8			

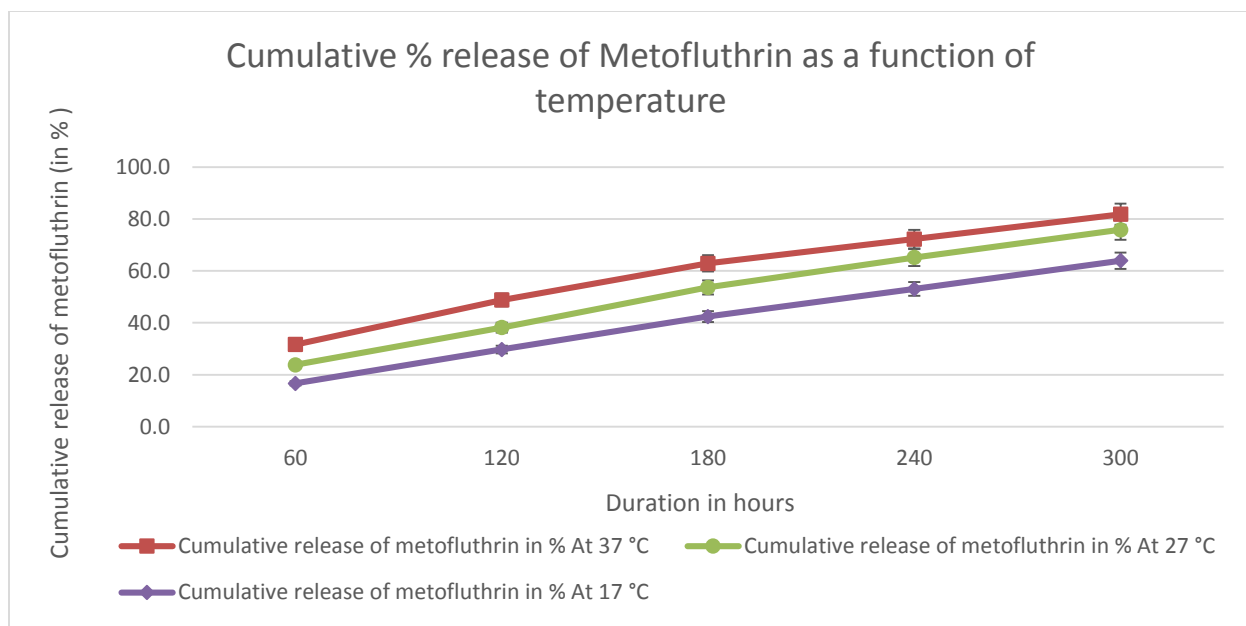


Figure 4.1: Cumulative metofluthrin release rates at different controlled temperatures.

4.1.4 Conclusion

These measurements show that metofluthrin release increases with increasing temperature.

4.2 Concentration dependence of metofluthrin release

One aspect worthy of investigation in our release studies is to understand the dependence of initial metofluthrin concentrations present on substrates to their release profiles. From a practical viewpoint, this assumes importance because of the implications this might have on a) attaining and b) maintaining threshold aerial metofluthrin concentrations responsible for expressing insecticidal efficacy. Studies were therefore designed to measure release profiles of metofluthrin when incorporated on substrates at varying initial concentrations.

4.2.1 Background

The household insecticide industry is extremely tightly regulated globally. Hence, the type as well as permissible amounts of active ingredients to be used, are fundamentally dictated by the rules and regulations of the Central Insecticide Board within our country. The basis for usage of 66 mg of metofluthrin impregnated onto cellulose strips in our experimental studies is in accordance with CIB rules and regulations governing their use. Additionally, our independent scientific

measurements and assessment of format longevity for an intended 30day period, as far as, bio-efficacy is concerned, was another mandatory guideline to be adhered to. However, in order to understand the role of initial loading concentrations of metofluthrin on release , variations within the permitted loading limits could be studied legitimately

4.2.2 Sample preparation and measurement methods

Known metofluthrin amounts are dosed in cellulose substrates and placed in test rooms under standard conditions to facilitate release. At regular time intervals, residual metofluthrin is extracted from the cellulose samples and characterized by GC, as described in section 3.2.

Materials and equipment

Metofluthrin

Isopropyl alcohol

Cellulose substrates ($10 \times 60 \text{ cm}^2$)

Gas chromatograph: Agilent 6820A, fitted with a flame ionization detector.

Column: Capillary HP-5, $30 \text{ m} \times 320 \mu\text{m} \times 0.25 \mu\text{m}$

Oven temperature program: $220 \text{ }^\circ\text{C}$ for 150 min and heating at $1 \text{ }^\circ\text{C}/\text{min}$ to $300 \text{ }^\circ\text{C}$

Injector temperature: $275 \text{ }^\circ\text{C}$

Detector temperature: $300 \text{ }^\circ\text{C}$

Method

Metofluthrin solutions having three different concentrations are prepared in isopropyl alcohol to prepare cellulose samples containing 33, 66, and 132 mg of metofluthrin. The obtained samples are kept open and unfolded to facilitate solvent evaporation. The samples are then placed in a standard test room ($3 \times 3 \times 3.33 \text{ m}^3$, total volume: 30 m^3) fitted with a fan in the middle of the ceiling. The temperature is maintained at $27 \pm 1 \text{ }^\circ\text{C}$ and $65 \pm 5\% \text{ RH}$. The fan speed is adjusted to achieve a wind velocity of $0.5\text{--}0.6 \text{ m/s}$ at test locations, which is monitored using an anemometer. Once these locations are marked, samples are positioned and allowed to equilibrate under ambient conditions for 60, 120, 180, 240, and 300 h. At these scheduled intervals, samples are collected and their residual metofluthrin content is determined by GC. The active ingredient release is quantified using this measurement. All tests are conducted in triplicates. Average values and standard deviations were calculated and shown in the graphs.

4.2.3 Results and discussion

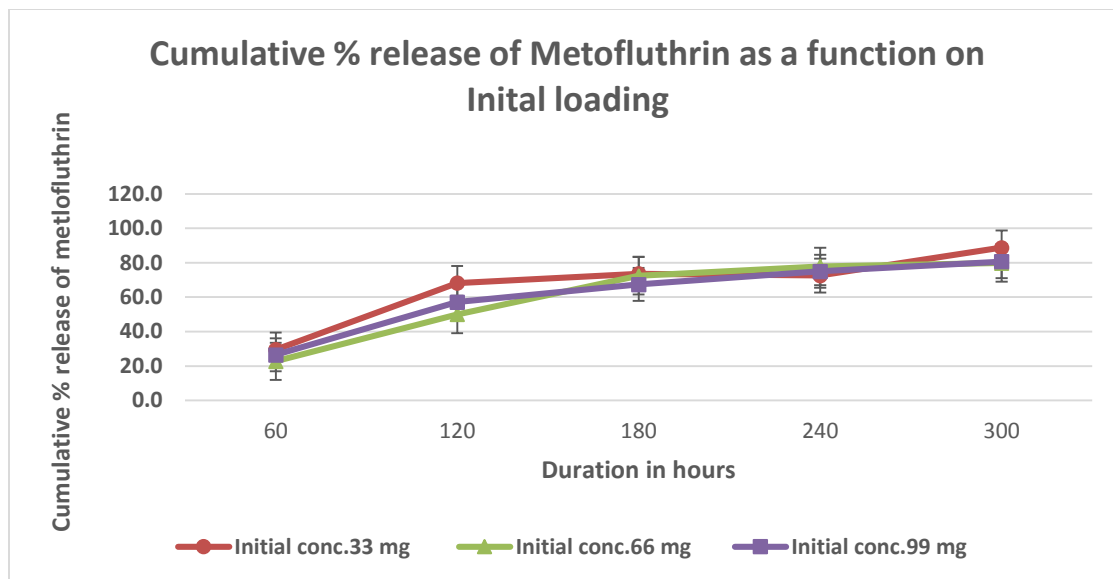


Figure 4.2: Cumulative metofluthrin release rate as a function of initial loading.

Conclusion

The metofluthrin release were found to be converge beyond 120 h for sample containing varying initial concentrations of Metofluthrin indicating the non-dependence of Metofluthrin release on initial loading.

4.3 Wind velocity effect on metofluthrin release

4.3.1 Principles

The release profile of metofluthrin was determined at various wind velocities. Known amounts of active ingredient are dosed in cellulose substrates and placed in three test rooms under the identical temperature and humidity conditions at different wind velocities to promote release. The metofluthrin remaining after specified time intervals is extracted from the cellulose sample and quantified by GC, as shown in Section 3.2.

4.3.2 Experimental details

Materials and equipment

Metofluthrin

Isopropyl alcohol

Cellulose substrates (10×60) cm²

Gas chromatograph: Agilent 6820A, fitted with a flame ionization detector.

Column: Capillary HP-5, 30 m \times 320 μ m \times 0.25 μ m

Oven temperature program: 220 °C for 150 min and heated at 1°C/min to 300 °C

Injector temperature: 275 °C

Detector temperature: 300 °C

Digital Anemometer, Aktakom make, Model ATE -1019

Method

A stock solution of metofluthrin in isopropyl alcohol is prepared to impregnate cellulose samples with 66 ± 1 mg of metofluthrin. The prepared samples are kept open and unfolded to facilitate solvent evaporation before being transferred in two 30 m³ standard test rooms equipped with a fan in the middle of the ceiling. Rooms are maintained at 27 °C and $65 \pm 5\%$ RH.

In one room, the ceiling fan was switched OFF to prevent any wind draft, but a small opening was provided as an outlet for the released active ingredient. Once the measured wind velocity was found to be null, the locations are marked for sample placement. Samples are then set in marked positions and allowed to release the active ingredient under ambient conditions.

In the second room, the ceiling fan was switched ON, and the wind velocity is measured at different locations using an anemometer. The fan speed is adjusted to obtain wind velocities of 0.25, 0.5, and 1 m/s at the test locations. A small opening is also provided as an outlet for the released active ingredient. After scheduled exposures of 60, 120, 180, 240, and 300 h, samples were collected and their residual metofluthrin content is quantified by GC, providing the released active ingredient. All measurements are conducted in triplicates. Average values and standard deviations were calculated and reported.

4.3.3 Results and discussion

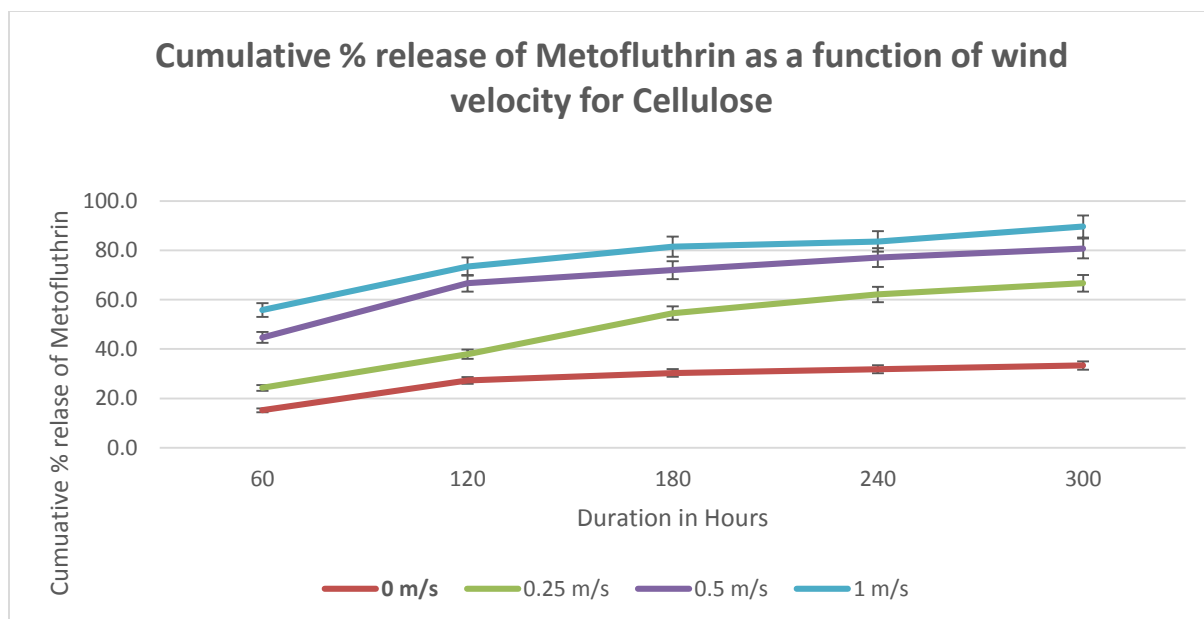


Figure 4.3: Cumulative metofluthrin release rate as a function of wind velocity.

The cumulative release at a wind velocity of zero correspond to a steady state release case and reflects the self-release tendency of metofluthrin to get volatilized in air in the absence of any convective draft.

4.3.4 Conclusion

In general, an increase in wind velocity enhances metofluthrin release. Interestingly, a static wind velocity results in 30% metofluthrin release, indicating that self-diffusion proceeds, even in the absence of external wind draft. In addition, the release tends to converge with in the 0.5–1.0 m/s wind velocity range.

4.4 Surface area dependence of metofluthrin

The release profile of metofluthrin is determined on substrates presenting different surface areas.

4.4.1 Principles

Known amounts of metofluthrin are dosed in cellulose substrates exhibiting three different sizes and placed in test rooms under identical standard temperature, humidity, and wind velocity conditions to enable release. After regular time intervals, residual metofluthrin is extracted from the cellulose sample and measured by GC, as mentioned in Section 3.2.

4.4.2 Experimental details

Materials and equipment

Metofluthrin

Isopropyl alcohol

Cellulose substrates with a total exposed surface area of 600 cm² (2 sides of 10 cm × 30 cm)

Cellulose substrates with a total exposed surface area of 1200 cm² (2 sides of 10 cm × 60 cm)

Cellulose substrates with a total exposed surface area of 2400 cm² (2 sides of 10 cm × 120 cm)

Gas chromatograph Agilent 6820A, fitted with a flame ionization detector.

Column: Capillary HP-5, 30 m × 320 μm × 0.25 mm

Oven temperature program: 220 °C for 150 min and heating at 1 °C/min to 300 °C

Injector temperature: 275 °C

Detector temperature: 300 °C

Method

Cellulose samples containing 66 mg of metofluthrin are prepared using an active ingredient solution in isopropyl alcohol. These samples are kept open and unfolded to enable solvent evaporation before being placed in three 30 m³ standard test rooms fitted with a ceiling fan. Rooms are maintained at 27 ± 1 °C and 65 ± 5% RH.

The wind velocity is measured at different locations in the rooms using an anemometer and set to 0.5–0.6 m/s at marked test locations by adjusting the fan speed. Samples are positioned at the marked positions and allowed to release active ingredient at ambient conditions for 60, 120, 180, 240, and 300 h. At these scheduled exposure times, samples were collected and analyzed by GC. The resulting residual content provided the quantity of released active ingredient. All measurements were conducted in triplicates. Average values and standard deviations were calculated and shown in the graphs.

4.4.3 Results and discussion

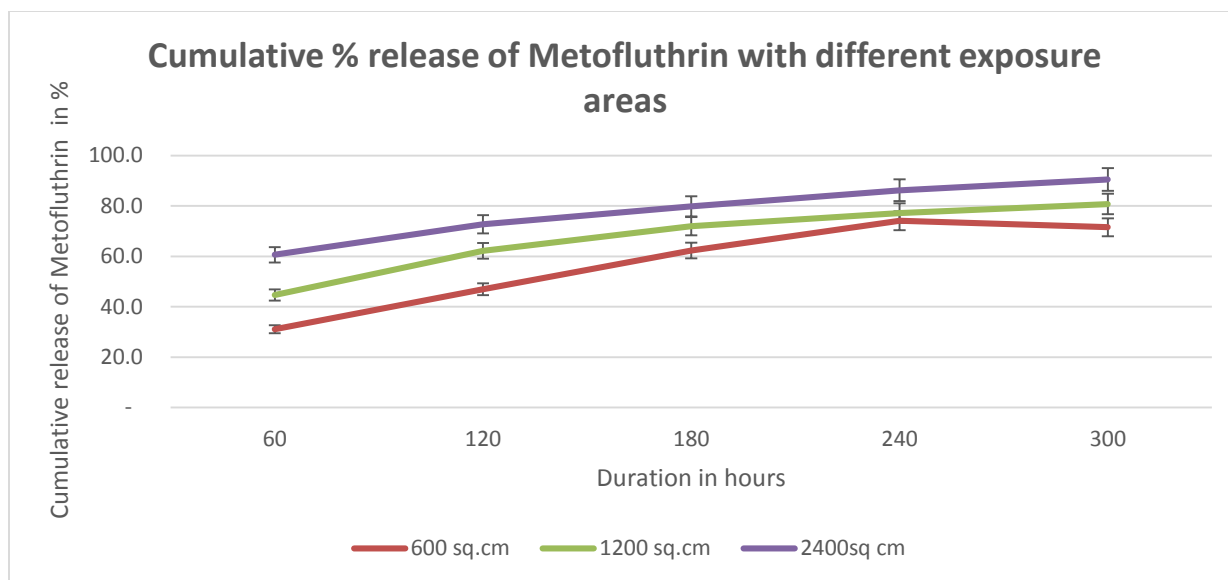


Figure 4.4: Cumulative metofluthrin release rate as a function of substrate exposed area.

4.4.4 Conclusion

The release rate as a function of exposed area accounts for both sides of the emanator. In Chapter 1, metofluthrin was suggested to exhibit higher diffusion when exposed over larger surface areas because of its high vapor pressure. We find that, an increase in surface area from 600 to 2400 cm² substantially enhances metofluthrin release, validating the hypothesis mentioned in chapter 1.

CHAPTER 5

Influence of substrate characteristics

The primary objective of this study is to develop an understanding of the factors influencing metofluthrin release from various substrates. Chapter 4 focused on determining the impact of external parameters, such as ambient temperature, wind velocity, and initial loading on the substrate, on this release. All these studies used cellulose as the substrate for the purpose of representation.

In addition to external factors, substrate characteristics play an important role in controlling the release of the impregnated active ingredients. This has been documented in a Virex Inc. patent entitled “Polymeric substrates containing povidone-iodine as a control release biologically active agent” [134]. In particular, the nature of the substrate and its inherent physical and chemical properties would play a key role on the release of active ingredient [133]. The same would apply to understanding of Metofluthrin release from various substrates.

In addition, the rate of diffusion is expected to depend on the physical and chemical properties of metofluthrin and the nature of its interactions with the various substrates. This chapter describes the investigations of metofluthrin release from various substrates and attempts to rationalize the resulting spectral data and substrate physical and chemical characteristics.

5.1 Substrate nature

Various cellulosic and polymeric substrates have served as supports for different types of allethrin and metofluthrin compositions [94]. A nonwoven fabric containing an impregnated insecticide has also been utilized for sustained release [135]. However, no study has recommended optimal types of substrates and their suitability for metofluthrin release in household insecticidal formats yet.

This study attempts to understand factors governing metofluthrin release from several polymeric substrates. The nature of these individual substrates is evaluated by various spectroscopic and imaging methods to deeply understand the extent of their interactions with metofluthrin, and consequently their influence on release. The behavior of pesticides in woven and nonwoven

substrates has been studied extensively. Specifically, fibers have proven to quickly reach saturation in woven fabrics because of their wicking action, whereas molecules penetrate nonwoven substrates more slowly [136]. Therefore, nonwoven fabrics may be more suitable for sustained release. Here, the assessed polymeric substrates consisted of cellulosic substrates, nonwoven polypropylene, nonwoven nylon, and nonwoven polyethylene terephthalate (PET) sheets.

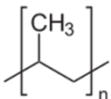
5.1.1 Characteristics of polymeric substrates

Nonwoven fabrics are fabric-like materials made from long fibers bonded together by chemical, mechanical, heat, or solvent treatment. They are broadly defined as sheet or web structures assembled by entangling fibers or filaments and by perforating films mechanically, thermally, or chemically. These flat, porous sheets directly derive from separate fibers, molten plastic, or plastic film. They are not made by weaving or knitting and do not require converting the fibers to yarn.

These engineered fabrics may be a limited life, single-use fabric or a very durable fabric. They provide specific functions, such as absorbency, liquid repellence, resilience, strength, wash ability, cushioning, filtration, antibacterial properties, and sterility. These properties are often combined to create fabrics suited for well-defined applications while achieving a good balance between product use/life and cost. Nonwoven fabrics mimic the appearance, texture, and strength of their woven counterparts and can be as bulky as the thickest paddings. When combined with other materials, they provide a spectrum of products with diverse properties. These materials may be used alone or as components of apparel, home furnishings, health care, engineering, industrial, and consumer goods. Their numerous applications include surgical masks, gowns, and caps for medical purposes as well as various consumer products, such as high efficiency particulate air filters, tea and coffee bags, geo-textiles, and diaper stock [137].

5.1.2 Nonwoven polypropylene

Table 5.1: Typical physical and chemical data of polypropylene.

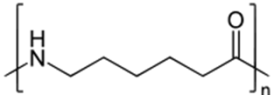
Parameter	Information
Molecular structure	 $\left[\text{CH}_2 - \underset{\text{CH}_3}{\text{CH}} - \text{CH}_2 \right]_n$

IUPAC name	Poly(propene)
Molecular formula	(C ₃ H ₆) _n
Density @20°C Amorphous	0.855 g/cm ³
Melting point	130–171 °C

Polypropylene is generally available as granules for injection and extrusion molding applications before conversion into useful items. It is also used for manufacturing of spun-bond nonwoven fabric manufacturing, where, the granules are melt spun through jets into thousands of fibers with a diameter of about 20 μm. These very fine filaments are uniformly laid down into random three-dimensional structures, which are transferred on a calendar and thermally bond into consolidated spun bond fabrics [138,139].

5.1.3 Nonwoven nylon

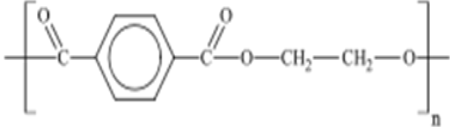
Table 5.2: Typical physical and chemical data of nylon.

Parameter	Information
Molecular structure	
IUPAC name	Poly(hexamethylenediamine-6-yl) lactam
Molecular formula	(C ₆ H ₁₁ NO) _n
Density @ 20 °C Amorphous	1.084 g/cm ³
Melting point	220 °C

Nylon 6 finds application in a broad range of products requiring high-strength materials such as gears, fittings, and bearings for under-the-hood parts in the automotive industry. It is also used in the manufacture of numerous threads, ropes, filaments, nets, tire cords, and nylon fabrics. Nonwoven fabrics are obtained by spinning and autogenously bonding continuous nylon filaments into flat, smooth, strong, and crisp materials [139].

5.1.4 Nonwoven PET

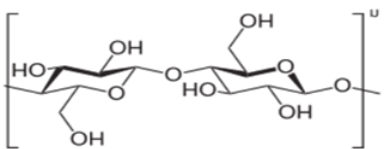
Table 5.3: Typical physical and chemical data of PET.

Parameter	Information
Molecular structure	
IUPAC name	poly(ethylene terephthalate)
Molecular formula	(C ₁₀ H ₈ O ₄) _n
Density @ 20 °C	1.38 g/cm ³
Melting point	>250 °C,

PET is a thermoplastic polyester resin used in synthetic fibers; containers for beverage, food, and other liquids; thermoforming applications, and engineering resins often in combination with glass fiber. PET fabric consists of a continuous filament, nonwoven needle punched polyester.

5.1.5 Cellulosic substrates

Table 5.4: Typical physical and chemical data on cellulose.

Parameter	Information
Molecular structure	
IUPAC name	It is a mixture.
Molecular formula	(C ₆ H ₁₀ O ₅) _n
Density @ 20 °C	1.5 g/cm ³

Melting point	Decomposes
---------------	------------

Cellulose is the major constituent of paperboard, card stock, and textiles made from cotton, linen, and other plant fibers [140].

5.2 Influence of substrate properties on metofluthrin release

5.2.1 Principle

Various substrates impregnated with known metofluthrin amounts are placed in test rooms under controlled temperature conditions and a regulated wind velocity of 0.5 m/s to facilitate release. At regular time intervals, residual metofluthrin is extracted from the samples using an appropriate solvent and quantified by GC, as described in Section 3.2.

5.2.2 Experimental details

Materials

Metofluthrin (purity 98 %)

Isopropyl alcohol

Gas Chromatograph Agilent 6820A, fitted with a flame ionization detector.

Column: Capillary HP-5, 30 m × 320 m × 0.25 m

Oven temperature program: 220 °C for 150 min and heated at 1 °C/min to 300 °C

Injector temperature: 275 °C

Detector temperature: 300 °C

Evaluated substrates

Substrates used for the study are cellulosic and specialty treated papers as well as nonwoven PET, polypropylene, and nylon sheets. Nonwoven polypropylene and PET sheets (30 g/m², 10 × 60 cm²) are supplied by KT exports (Mumbai). Nonwoven nylon sheets (30 g/m², 10 × 60 cm²) are purchased from Cerex International (USA). Specialty cellulose papers (13 g/m², 10 × 60 cm²) are provided by MP specialty (Spain).

Method

Substrates impregnated with 66 mg of metofluthrin are prepared from an active ingredient solution in isopropyl alcohol. These samples were kept open and unfolded to enable solvent evaporation

before being placed in standard test rooms (approximately 30 m³) equipped with a ceiling fan. The rooms are maintained at 27 °C and 65 ± 5% RH.

The wind velocity was measured at different locations in the rooms using an anemometer and set to an average of 0.5 m/s by adjusting the fan speed. Next, these locations were marked for sample placement. The samples are positioned and allowed to release the active ingredient under ambient conditions for 60, 120, 180, 240, and 300 h. At these scheduled exposure times, samples are collected and analyzed by GC. Using the obtained residual content, the released metofluthrin is calculated. All measurements are conducted in triplicates. Average values and standard deviations were calculated and shown in the graphs.

5.2.3 Observations

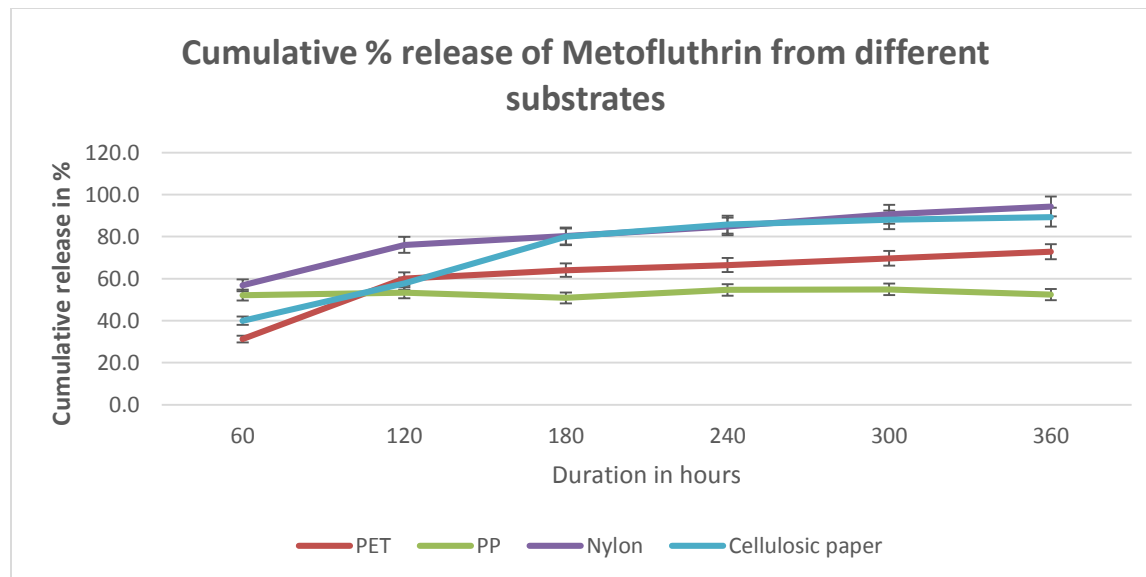


Figure 5.1: Cumulative release of metofluthrin from different substrates.

5.2.4 Conclusion

The cellulose substrate displays a relatively sustained release. Nylon initially exhibits the highest release for 120 h before reaching a plateau at a similar range to cellulose. The other substrates, synthetic polypropylene and PET materials show comparatively lower release.

The kinetics of metofluthrin release is the highest for nylon, very closely followed by cellulose, and decreases in the order nylon ~ cellulose > PET > polypropylene. This observed pattern can be rationalized from an improved understanding of surface properties and interactions with

metofluthrin. Factors, such as surface area, average pore size, tortuosity, and chemical interactions of substrates with metofluthrin, may play a crucial role in this release. Subsequent chapters will be addressing factors key to metofluthrin release.

5.3 Thermal analysis of physical interactions

Metofluthrin shows different release rates from various impregnated substrates. One reason for these dissimilarities may be the extent of interactions between metofluthrin and these substrates. Section 5.1 suggests that the desorption temperature of metofluthrin from a weakly interacting substrate is lower than that of a strongly interacting one. Thermo-analytical tools have been employed to study interactions between materials, such as inert materials and hydrocarbons to identify effective adsorbents from sand, cotton, and organo-clays for diesel spill cleanup [141, 154]. Therefore, these methods can be utilized to gain valuable insight into such metofluthrin–substrate interactions.

5.3.1 Thermal study

Thermal analysis encompasses physical property measurements of a substance as a function of temperature. Thermo analytical tools, such as thermo-gravimetry, thermo-volumetry, and differential thermal analysis, have been employed increasingly to investigate chemical reactions in liquid and solid states at elevated temperatures. They involve continuously measuring physical property changes, such as weight, volume, and heat capacity variation, while the sample temperature increases at a predetermined rate.

Conventional thermal techniques used to investigate such intermolecular interactions are differential scanning calorimetry (DSC), differential thermo-gravimetry (DTG), temperature programmed desorption (TPD), and headspace gas chromatography (HS-GC) [142,143]. These thermal techniques are utilized to probe the extent of interaction between metofluthrin and various surfaces.

DSC measures thermally induced changes in physical property against time or temperature. The DSC instrument determines temperature and heat flow associated with material transitions as a function of time and temperature. During a temperature change, it measures heat quantity, which

is radiated or absorbed excessively by the sample, based on the temperature difference between sample and reference materials.

TGA determines the temporal variation of a given sample mass according to a specified temperature profile. These changes in sample weight may result from evaporation in an inert gas environment or chemical reaction, such as oxidation and degradation.

5.3.1.1 Differential scanning calorimetry

DSC measures the difference in heat required to increase sample and reference temperatures as a function of temperature. Sample and reference are maintained at nearly the same temperature throughout the experiment. This technique is used to measure many sample properties and identify fusion, crystallization, and glass transition temperatures (T_g). It is also suitable for the study of oxidation and other chemical reactions.

Experimental details

The polymeric substrates involved in this study, exhibit melting points ranging between 140 and 250°C. Therefore, the samples were heated from 30 to 150 °C at a heating rate of 5°C/min and maintained at 150 °C. Cellulose samples used in earlier studies were impregnated with 66 mg of metofluthrin for a substrate surface area of 600 cm². However, this concentration did not elicit an adequate response during thermal studies. Consequently, the thermo-analytical samples are prepared by impregnating a cellulose substrate (13 g/m², 10 × 10 cm²) with a metofluthrin (purity 98.5%) solution in isopropyl alcohol (A.R) to achieve a higher concentration of 30 mg per 100 cm². The prepared samples are kept open and unfolded to promote solvent evaporation.

Table 5.5: DSC operating conditions.

Sr. No.	Details	
1	Name of the equipment	Differential scanning calorimeter
2	Manufacturer	Shimadzu
3	Model No.	DSC 60
4	Sampling procedure	Cellulose sample dosed with metofluthrin in a sheet form was rolled as a sample
5	Operating conditions such as carrier gas, flow rates, and temperatures	Nitrogen Temp Prog from 30 to 150 °C at 5 °C/min Hold time 1 min at 150 °C

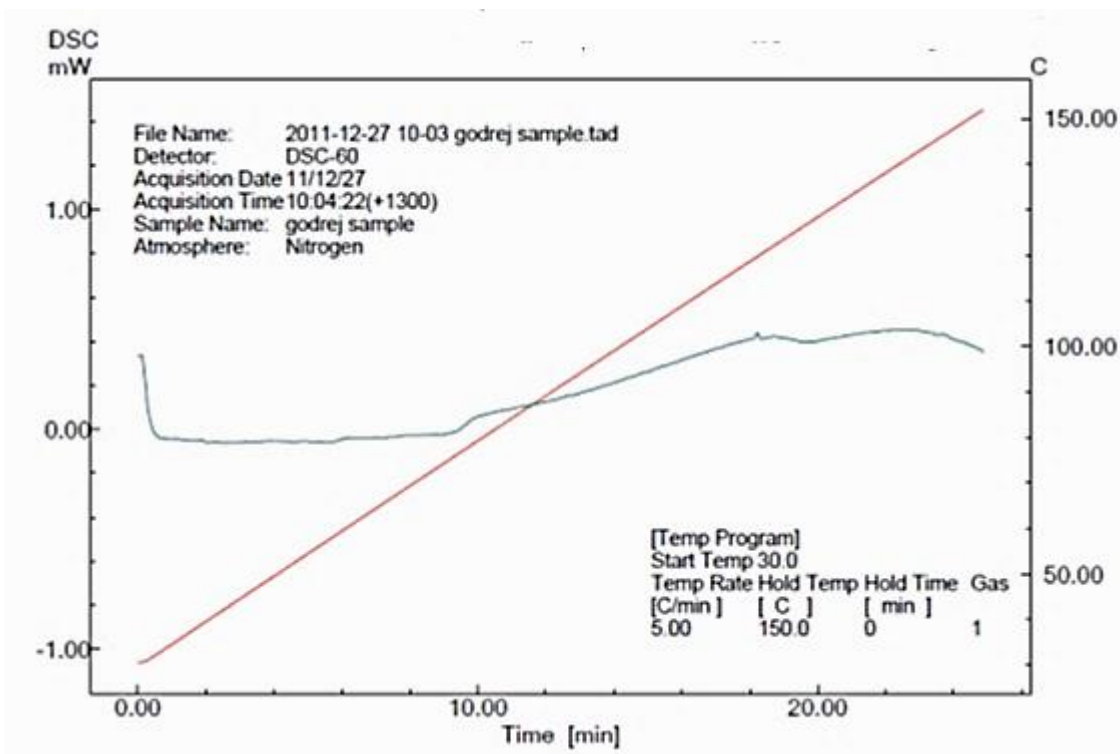


Figure 5.2: DSC plot of metofluthrin-impregnated cellulose.

Conclusion

The DSC curve of metofluthrin-impregnated cellulose in the temperature range of 30 to 150 °C does not show any endothermic or exothermic events. This indicates the absence of material transitions when metofluthrin is loaded on cellulose substrates. Thermogravimetry is hence employed to get a better understanding of this phenomenon.

5.3.1.2 Thermogravimetry

Thermogravimetry is a technique of physical chemistry, materials research, and thermal analysis based on the continuous recording of specimen mass changes as a function of a combination of temperature with time, and additionally of pressure and gas composition. Changes in weight originate from the breaking and/or formation of various bonds at elevated temperatures, which lead to the evolution of volatile products or the formation of heavier reaction products. For example, DTG has widely been used to study the controlled release of drugs such as simvastatin

[143] and ciprofloxacin [144]. Here, TGA is employed to study and measure the release of metofluthrin impregnated in different substrates by measuring the corresponding weight loss, rate of weight loss, and residue content in different substrates under similar test conditions.

Principles

The weight loss of different metofluthrin-impregnated substrates is evaluated by thermogravimetry. A sample weighing from 1 to 100 mg, but sometimes as large as 100 g, is placed on one arm of a recording microbalance or thermobalance. Arm and sample are positioned in a furnace, which is temperature controlled using a preprogrammed temperature/time profile. Next, the sample is heated from 30 °C to 150 °C at a heating rate of 5 °C/min. The temperature is maintained at 150 °C because some polymeric substrates display melting point around 140 °C and tend to decompose at higher temperatures.

Experimental details

Materials

Metofluthrin (purity 98.5%)

Isopropyl alcohol A.R

Cellulose, Nonwoven PET, Nonwoven polypropylene and Nonwoven nylon dosed with Metofluthrin 32 mg/100 cm²

Method:

Substrates are impregnated with a metofluthrin solution in isopropyl alcohol such that loading of 66 mg was attained. The prepared samples are kept open and unfolded to facilitate solvent evaporation.

Table 5.6: DTG experimental conditions

Sr. No	Details	
1	Name of equipment	Differential thermo gravimeter
2	Manufacturer	Shimadzu
3	Model No.	DTG 60 H
4	Sampling procedure	Cut into small discs

- | | | |
|---|--|---|
| 5 | Accessories used | Platinum pans |
| 6 | Operating conditions such as carrier gas, flow rates, and temperatures | Nitrogen
Temp program from 30 °C to 100 °C at 2 °C/min. Hold time 30 min at 100 °C |

Observations

DTG plots of various substrates impregnated with identical amounts of metofluthrin are shown in Figures 5.3–5.7. All thermal studies are conducted under identical operating conditions.

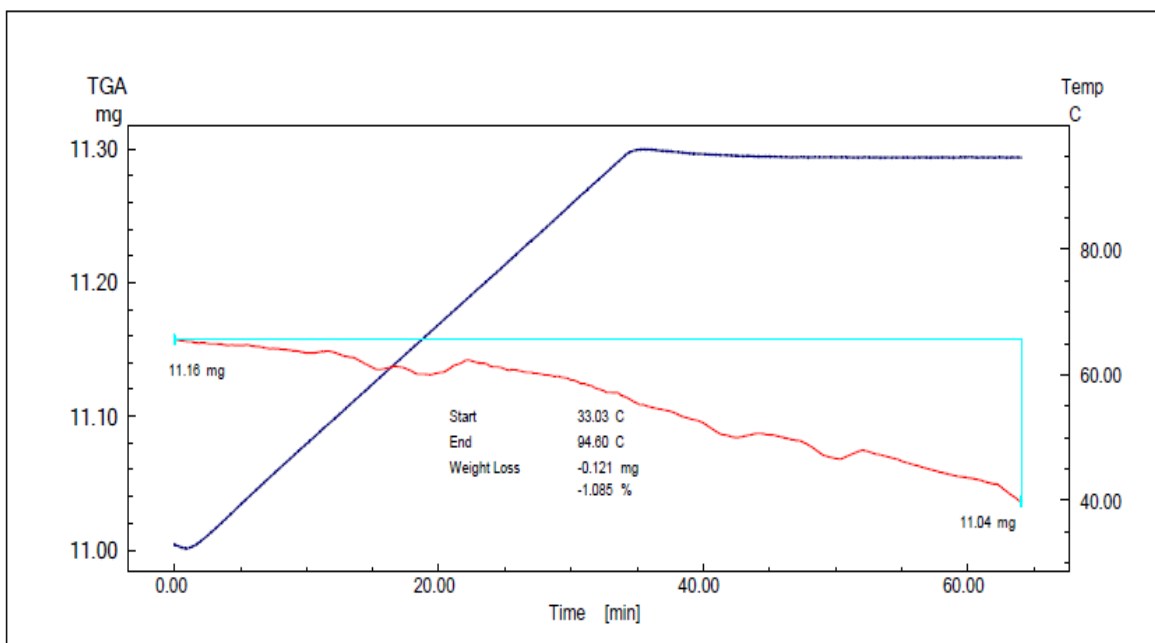


Figure 5.3: DTG plot of Metofluthrin (neat liquid ~ 98 % Purity).

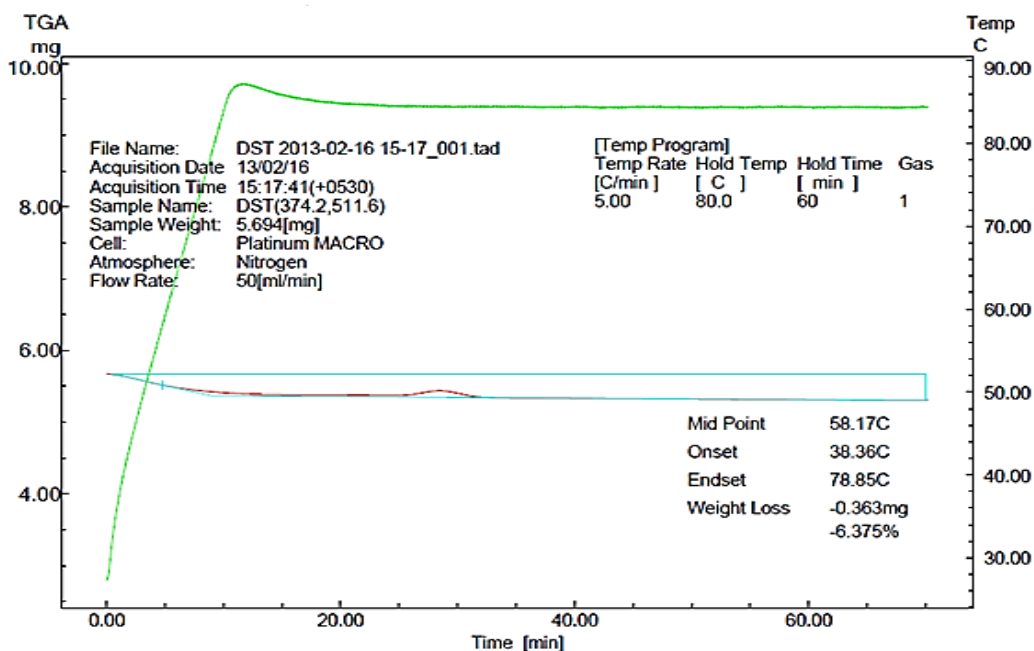


Figure 5.4: DTG plot of metofluthrin-impregnated cellulose.

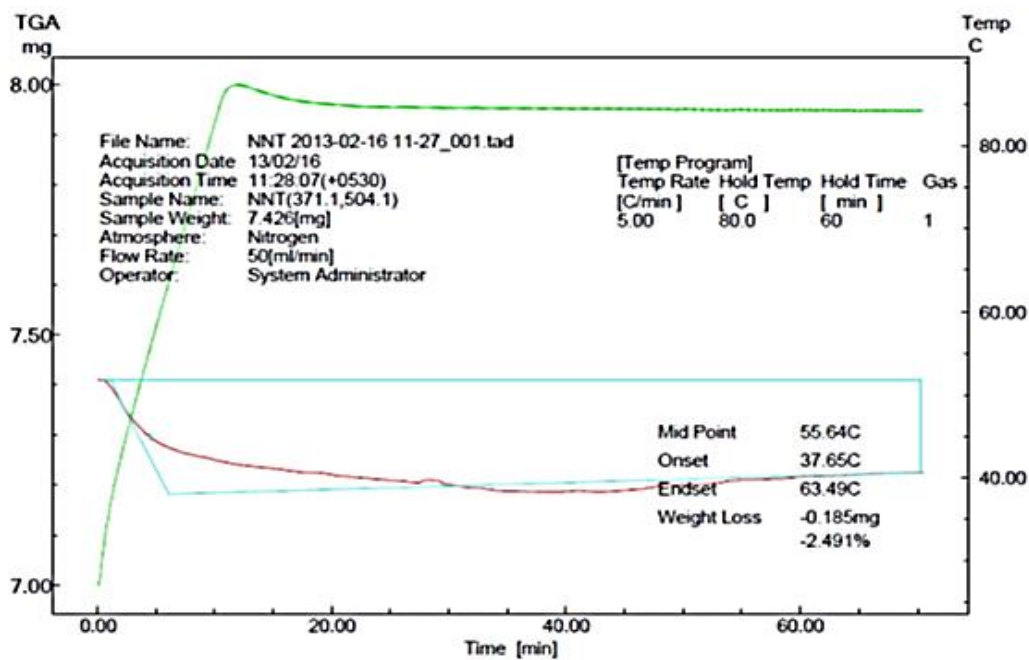


Figure 5.5: DTG pot of metofluthrin-impregnated nonwoven nylon.

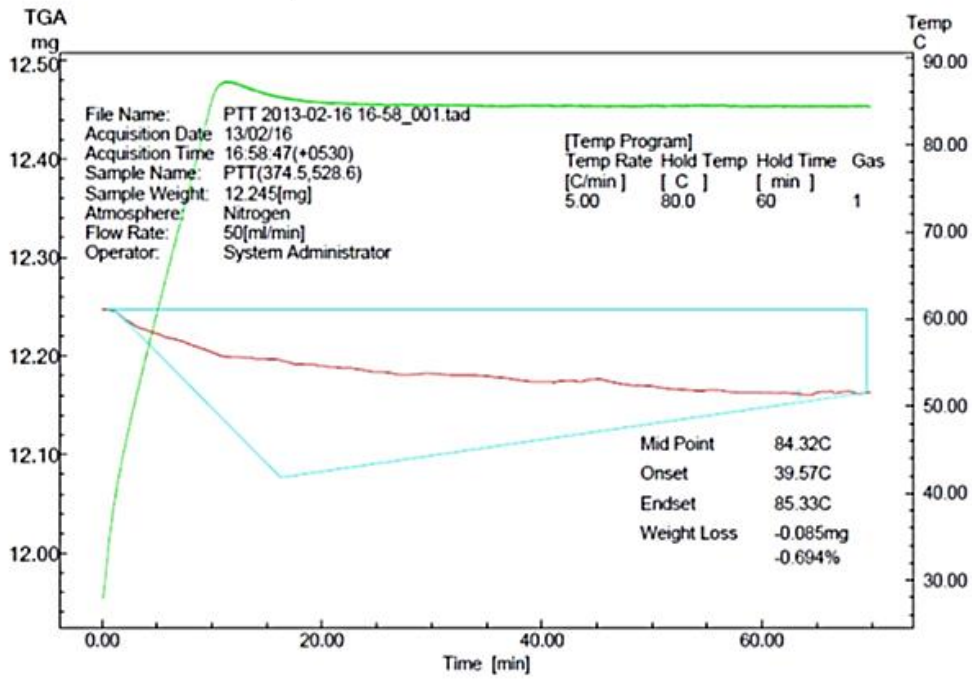


Figure 5.6: DTG plot of metofluthrin-impregnated nonwoven PET.

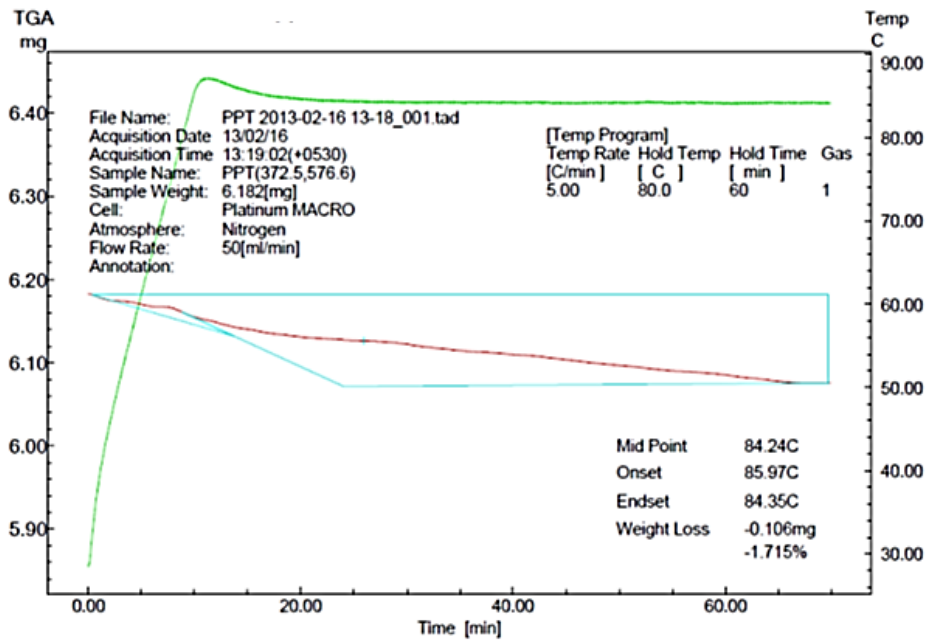


Figure 5.7: DTG plot of metofluthrin-impregnated nonwoven polypropylene.

Observation

Table 5.7 lists the weight losses of various metofluthrin-impregnated substrates measured by DTG under identical experimental conditions.

Table 5.7: DTG weight losses of various metofluthrin-impregnated substrates.

	Metofluthrin	MFT impregnated with Cellulose	MFT impregnated with PET	MFT impregnated with Nylon	MFT impregnated with Polypropylene
% weight loss*	1.085	6.375	0.694	2.491	1.715

*Corresponding to metofluthrin release between 25 °C and 80 °C

Conclusion

Weight changes obtained by TGA experiments differ considerably across substrates. Among these substrates, cellulose exhibits the weakest interaction with metofluthrin, as evidenced by its highest release. Interestingly, this study also suggests that TGA weight losses are directionally similar and in line with the release rates for cellulose and nylon. However, the order of release rates is different for PET and polypropylene. Based on this study, the release rate from polypropylene is higher than PET, which needs further investigation. Therefore, substrate porosities and surface interactions within substrates may play an important role in metofluthrin release. These results also indicate that chemical interactions between metofluthrin and functional groups could be determinant of this release.

5.4 Headspace gas chromatography analysis

HS-GC is the study of the gas space above a sample placed in an airtight chromatography vial. Volatile sample components diffuse in the gas phase, forming the headspace.

This headspace gas is subsequently injected in a gas chromatograph for compositional analysis. HS-GC is most suited for the analysis of very light volatiles in samples that can be efficiently

partitioned from the liquid or solid matrix into headspace gas volume. It is used to determine the concentration of volatile organics present in a nonvolatile matrix. It is recommended for the evaluation of volatile components from herbs needed to estimate their essential oil content [145]. This technique is particularly useful because of its nondestructive nature and its straightforward sample preparation procedures. Due to minimal sampling protocols, there is minimum disturbance to sensitive products such as essential oils.

This technique has recently grown to gain worldwide acceptance for the analyses of alcohol in blood and residual solvents in pharmaceutical products. Its common applications also include industrial analyses of monomers in polymers and plastic, flavor compounds in beverages and food products, and fragrances in perfumes and cosmetics.

Because of its relatively high vapor pressure, metofluthrin tends to quickly undergo partition in its gaseous phase. Consequently, HS-GC is the method of choice to measure metofluthrin release from various products.

5.4.1 Experimental conditions

Table 5.8: Gas chromatograph.

Sr. No	Details	
1	Name of the equipment	Headspace gas chromatography
2	Manufacturer	Shimadzu
3	Model No.	GC 2010 plus
4	Accessories used such as specific column	RTX-5 MS, 30 m × 0.25 mm
5	Operating conditions such as carrier gas, flow rates, and temperatures	Injector temp: 160 °C, oven temp: 40 °C to 220 °C hold time: 10 min, Ramp rate: 10 °C/min, detector temp: 230 °C Total flow: 10.2 mL/min

Table 5.9: Headspace sampler.

Sr. No.	Details	
1	Name of the equipment	Headspace
2	Manufacturer	Shimadzu

3	Model No.	Versa Plus
4	Sampling procedure	With pressure loop sampling system
5	Operating conditions such as carrier gas, flow rates, and temperatures	Sample temp: 90 °C, Transfer line temp: 120 °C, Sample equilibrium time: 30 min

Sampling

A 10 mg/mL metofluthrin solution in methanol is directly injected in the column to check for response and retention time. Subsequently, liquid metofluthrin is placed in headspace vials. Similarly, metofluthrin-impregnated substrates are transferred in headspace vials and subjected to the conditions mentioned above for analysis.

5.4.2 Observations

Figures 5.8–5.13 show GC and HS-GC results obtained for various metofluthrin-impregnated substrates.

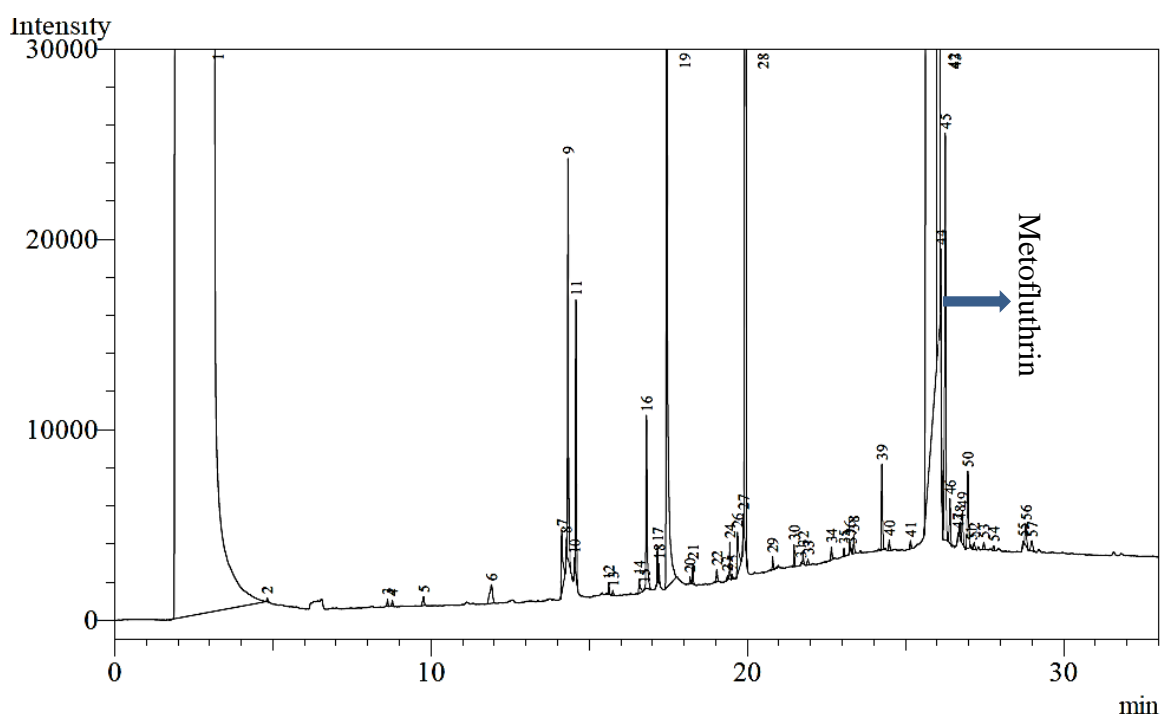


Figure 5.8: Gas chromatogram of 10 mg/mL metofluthrin in methanol obtained by direct column injection.

The direct column injection is performed to observe GC, note the retention time of meofluthrin, and determine the comprehensive composition of metofluthrin-derived volatiles and nonvolatiles.

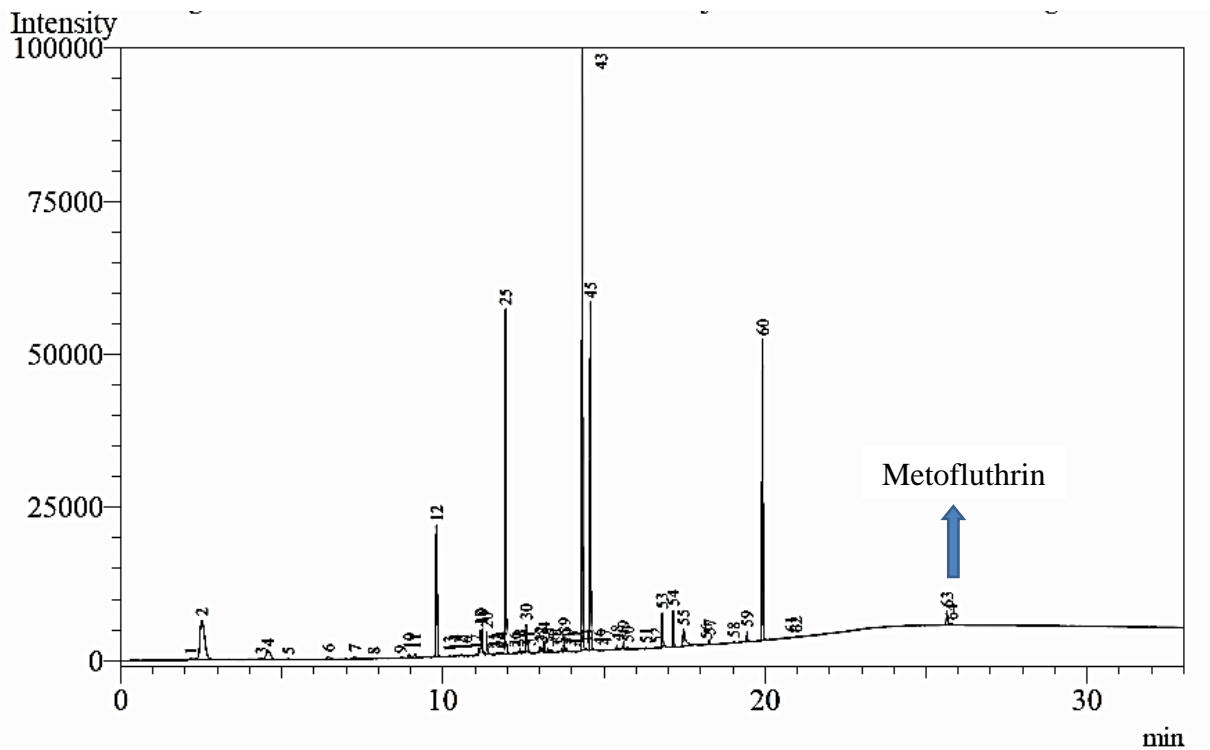


Figure 5.9: HS-GC profile of metofluthrin.

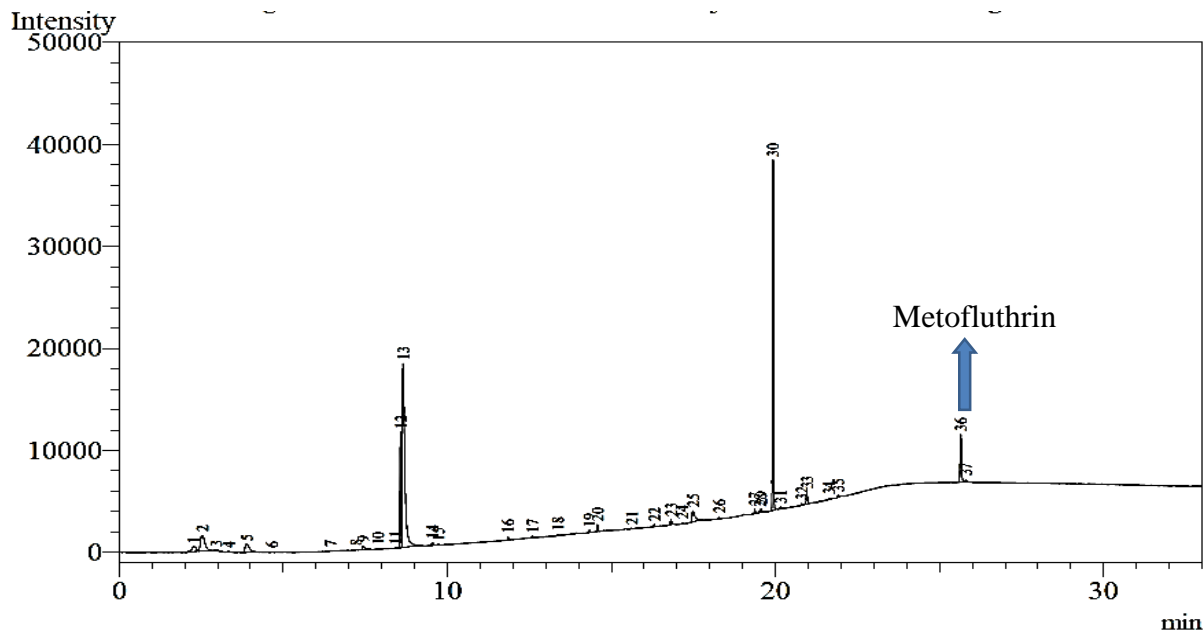


Figure 5.10: HS-GC profile of the metofluthrin-impregnated cellulose substrate.

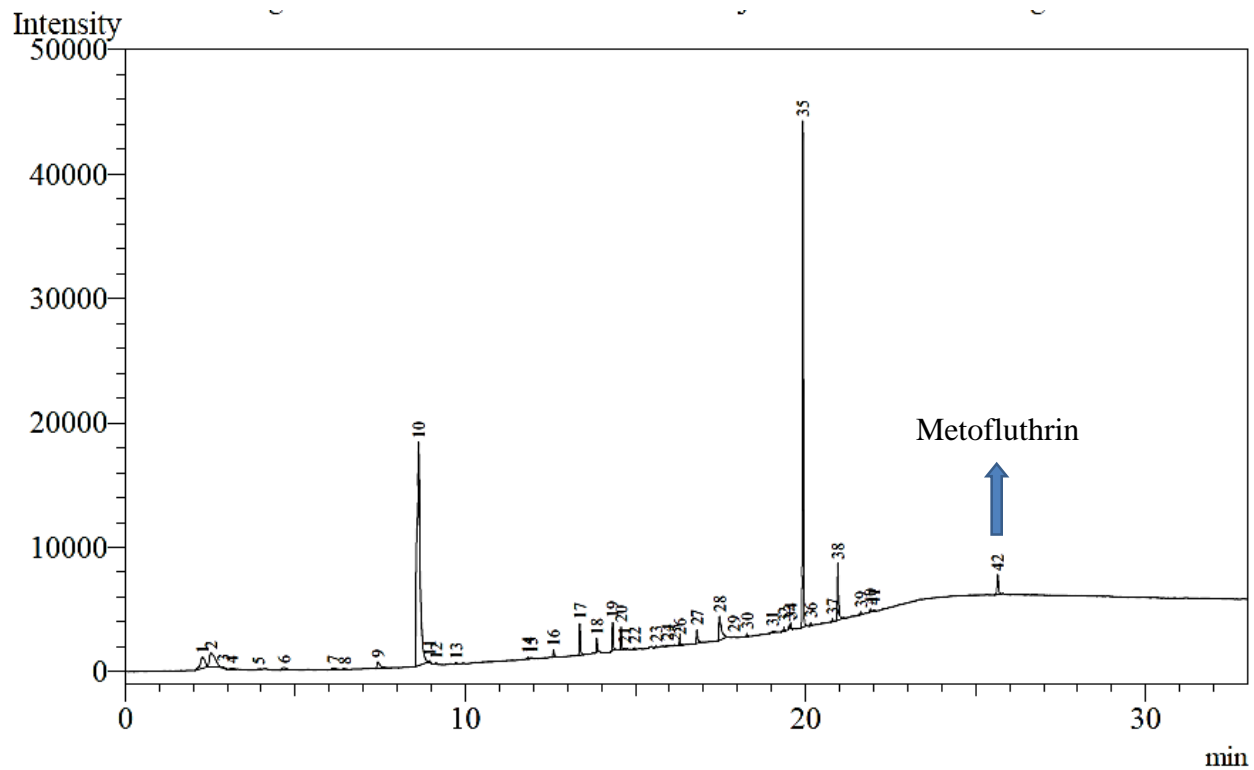


Figure 5.11: HS-GC profile of the metofluthrin-impregnated nonwoven nylon substrate.

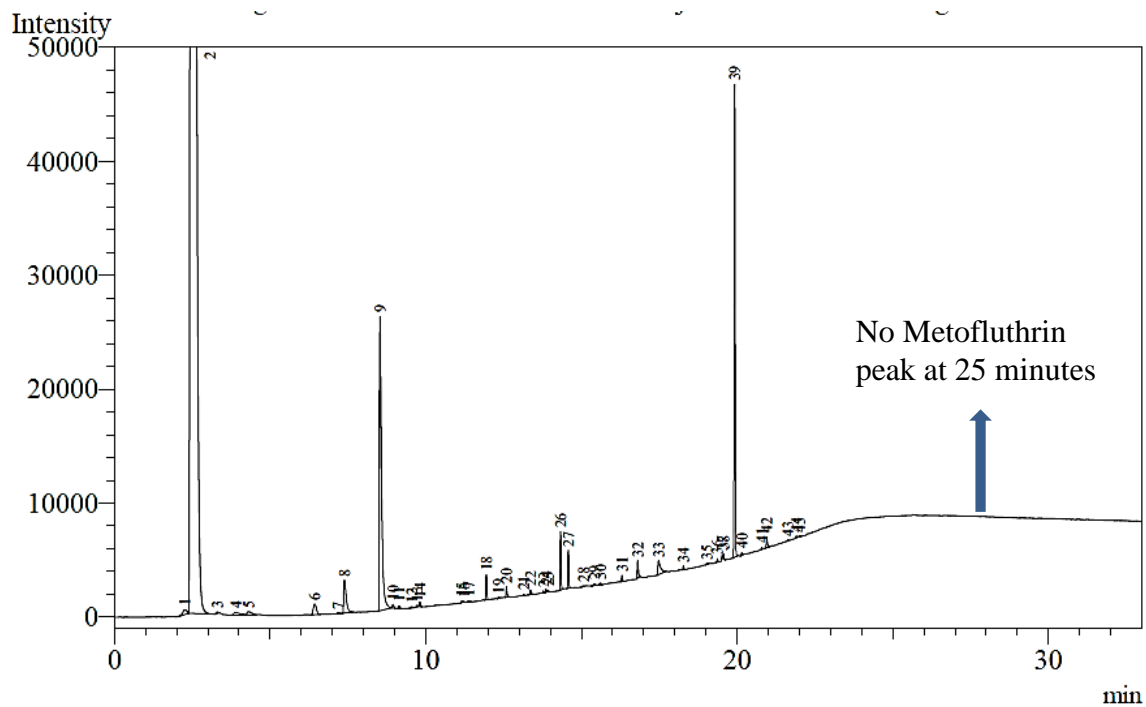


Figure 5.12: HS-GC profile of the metofluthrin-impregnated nonwoven PET substrate.

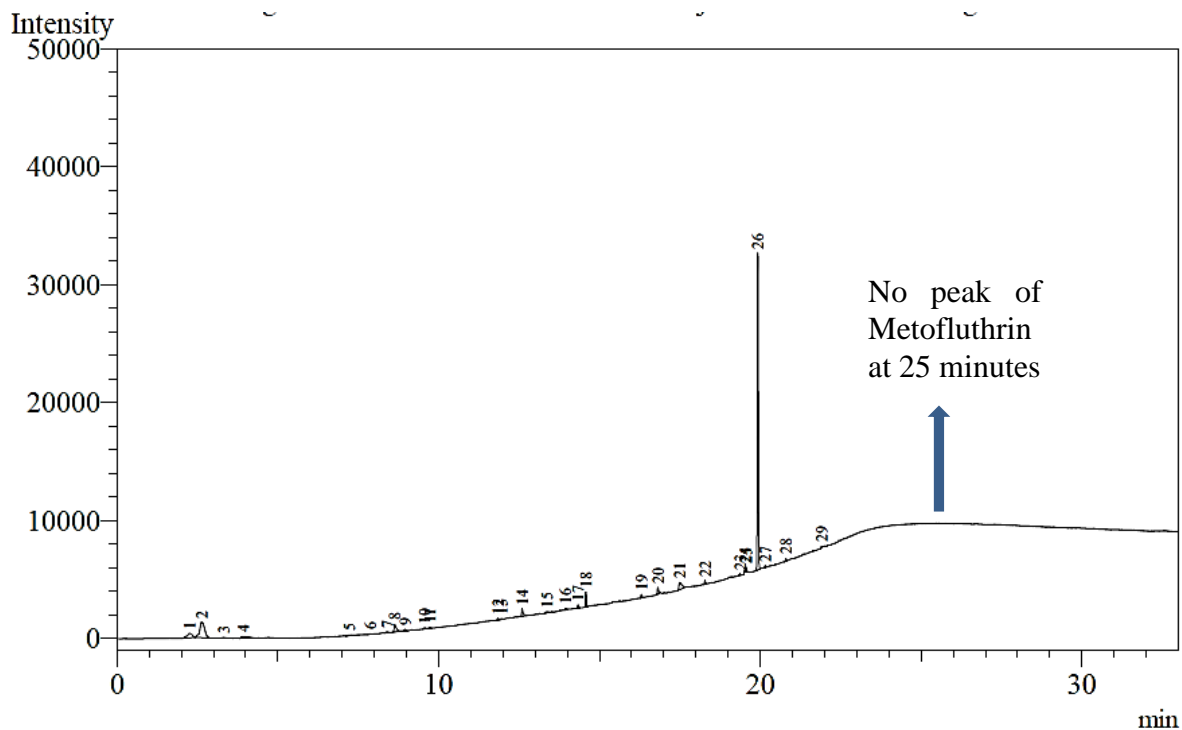


Figure 5.13: HS-GC profile of the metofluthrin-impregnated nonwoven polypropylene substrate.

Table 5.10: HS-GC metofluthrin peak areas obtained for different substrates.

	Metofluthrin (On the columns)	Metofluthrin via headspace	Cellulose via headspace	Nylon via headspace	PET via headspace	Polypropylene via headspace
	Peak areas of the peak retention time at 25.6 min					
Sample amount	1 micro l of 10 mg/ml Metofluthrin solution	50 micro l of liquid Metofluthrin	Solid substrates impregnated with Metofluthrin			
Response in area	26218983	6663	12908	4849	0	0

5.4.3 Conclusion

The HS-GC analysis detects the active ingredient in the headspace component for the liquid sample as well as metofluthrin-impregnated cellulose and nylon. The remaining metofluthrin-impregnated

PET and polypropylene substrates have shown lower release rates and weight losses by DTG but no metofluthrin in the headspace. It must be noted while TGA is dynamic experimental tool with steady purge of Nitrogen, measurements of volatiles in HS-GC involves equilibrating of substrate at high temperatures. These factors could explain difference in rates between these techniques and results obtained there from.

5.5 Temperature programmed desorption

TPD—also known as thermal desorption spectroscopy—enables the observation of desorbed molecules from surfaces when surface temperatures are increased. It is based on the principle that molecules or atoms adsorb a surface upon contact, minimizing their energy by forming a chemical bond with the surface. The binding energy varies with the combination of the adsorbate and surface. When the surface is heated, the energy transferred to the adsorbed species causes it to desorb. The temperature of this phenomenon is known as the desorption temperature. Therefore, TPD provides information on the binding energy. [146]

5.5.1 Principles

TPD measures the mass of desorbed molecules, showing which molecules adsorb on the surface. Moreover, TPD recognizes the different adsorption conditions of the same molecule from the desorption temperature variations because of the different desorption sites on the surface, e.g., terraces vs. steps. In addition, TPD peak intensities also provide the amounts of individual adsorbed molecules on the surface and the integral of the spectrum represents the total amount of adsorbed species.

This technique employs thermal conductivity detector responding to the desorbed molecules and gives a quantitative signal that differs from the TGA weight loss. It has been used for determining dimethyl and trimethylamine in gaseous samples extracted from the breath of renal patients [147]. TPD is expected to be more suitable to study metofluthrin–substrate interactions and confirm the TGA results. An attempt is made here to evaluate the desorption pattern of metofluthrin from different substrates using TPD.

5.5.2 Experimental conditions

Table 5.11: TPD operating conditions

Sr. No.	Details
1	Name of the equipment
2	Manufacturer THERMO scientific TPD RO
3	Model No. 1100 series
4	Sampling procedure, if any 100.1 mg sample (substrates loaded with 5% m/m Metofluthrin)
5	Accessories used such as specific column Argon, 20 mL/min, 25 °C to 120 °C, 20 °C/min ramp.
6	Operating conditions such as carrier gas, flow rates, and temperatures Argon, 20 mL/min, 25 °C to 120 °C, 20 °C/min ramp.

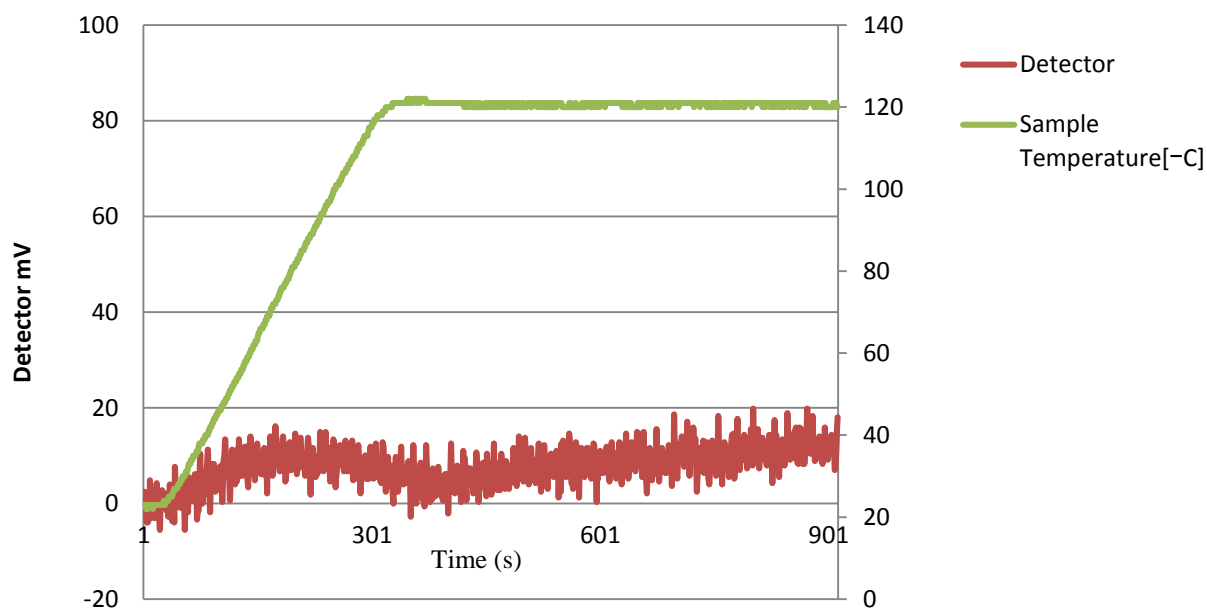


Figure 5.14: TPD plot of metofluthrin-impregnated cellulose.

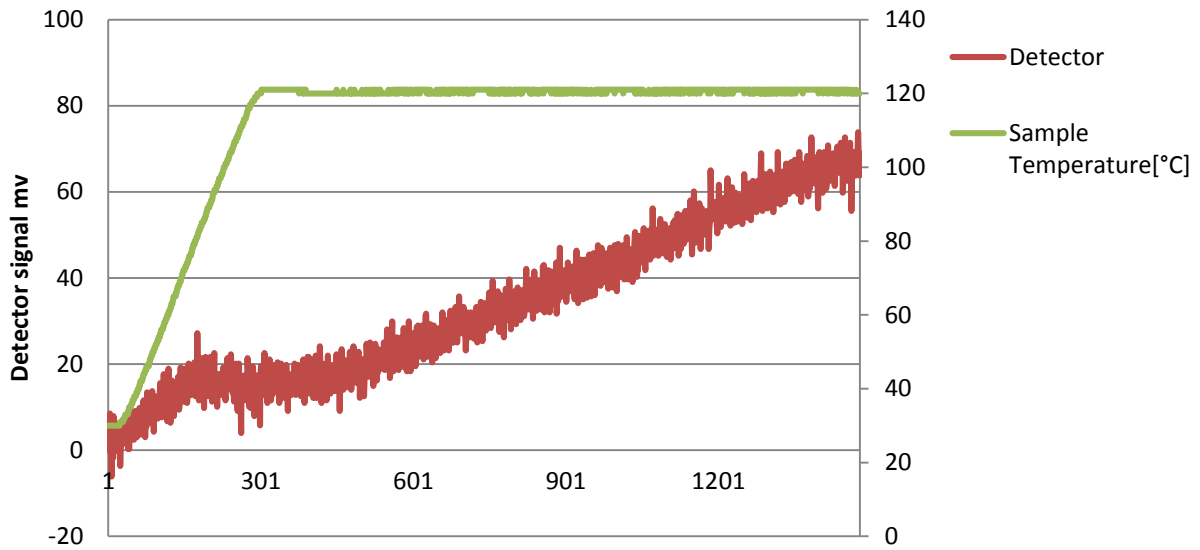


Figure 5.15: TPD plot of metofluthrin-impregnated nonwoven nylon.

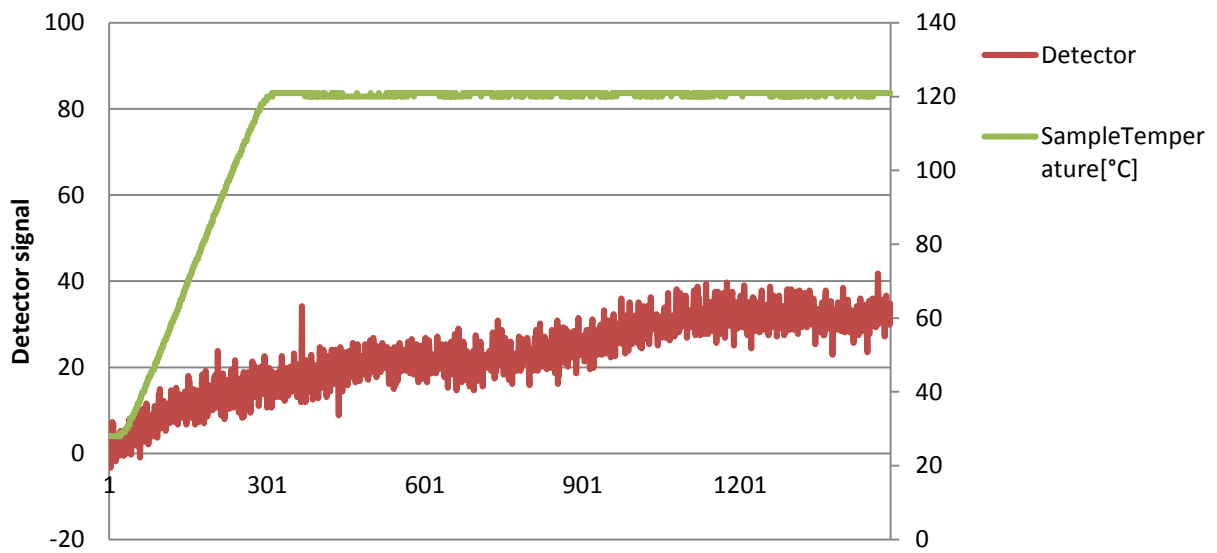


Figure 5.16: TPD plot of metofluthrin-impregnated nonwoven polypropylene.

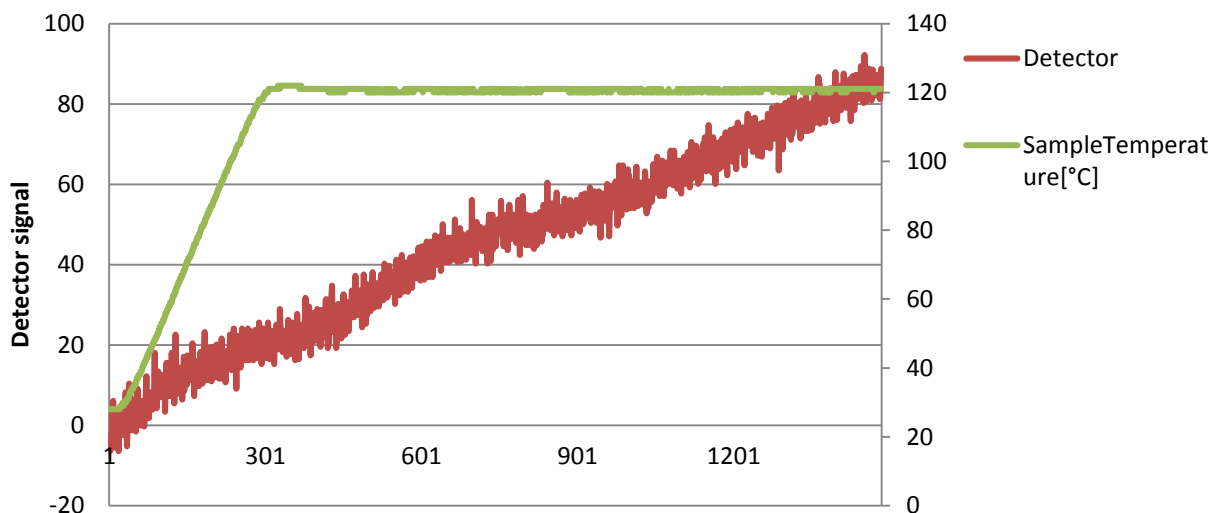


Figure 5.17: TPD plot of metofluthrin-impregnated nonwoven PET.

5.5.3 Results and discussion

The desorption begins within 3 min below 40 °C for nylon and cellulose and occurs faster on nylon than on cellulose. The desorption process is a two stage event for PET substrates, as indicated by the presence of two peaks. Polypropylene exhibits the slowest and the least desorption, as substantiated by previous studies.

The fastest desorption of nylon compared to other substrates points to the possible existence of weaker interactions with metofluthrin. It also suggests the presence of open pores accounting for a higher porosity within nylon.

Results highlighted in the thermal study including DTG, HSGC and TPD, qualitatively indicate that the extent of interaction between metofluthrin is the lowest in cellulose, in comparison to other substrates. Taking into conjunction, both sets of data, the relative release profiles of metofluthrin impregnated into various substrates follow the order:

Nylon~Cellulose>PP>PET

This study also interestingly indicates that weight loss trends observed in the thermo grams are directionally similar, and, in line with the ambient release rates which have been experimentally measured with cellulose and nylon. HSGC and DTG data indicate that, cellulose releases were higher than Nylon. One plausible reason could be the presence of a steady nitrogen stream within

DTG which might aid a better metofluthrin release during the study. It is likely that HSGC measurements from vials performed under non convective air draft conditions might influence release profiles accounting for the difference in data between these techniques.

It must be noted that HSGC release data for both PET and PP were silent, hence non informative thereby, allowing our inferences to be drawn based on DTG data solely. ..Earlier Sentence deleted since repeating. However, the order of release has been found different for PET and PP. The thermal data indicates impregnated PP releases a higher amount of metofluthrin when compared with PET, while, laboratory experiments conducted at ambient show the reverse.

We believe that intrinsic substrate porosities, as well as, possibly surface interactions of metofluthrin with individual substrates might be playing an important role in influencing metofluthrin release, and, hence will need to be considered for providing a scientific rationale of the release data obtained under ambient conditions. The pore distribution of these substrates may provide additional insights into this phenomenon.

5.6 Influence of substrate density on metofluthrin release

The influence of substrate density on metofluthrin release is investigated by GC for different substrates.

5.6.1 Experimental details

Materials and equipment

Metofluthrin

Isopropyl alcohol

Nonwoven nylon 10, 20, and 30 g/m² (10 × 60 cm²)

Cellulose 13 and 17 g/m²

Gas chromatograph Agilent 6820A, fitted with a flame ionization detector

Column: Capillary HP-5, 30 × 320 × 0.25 m³

Oven temperature Program: 220 °C for 150 min and heating at 1 °C/min to 300 °C

Injector temperature: 275 °C

Detector temperature: 300 °C

Method

Substrates impregnated with 66 mg of metofluthrin are prepared from active ingredient solutions in isopropyl alcohol. The prepared samples are kept open and unfolded to enable solvent evaporation and subsequently placed in three standard test rooms (30 m³). These rooms are equipped with a ceiling fan and maintained at 27 °C and 65 ± 5% RH.

The wind velocity is measured at different locations in the rooms using an anemometer and set to 0.5 m/s at these marked locations by adjusting the fan speed. The samples are placed at these test locations and allowed to release the active ingredient under ambient conditions for 60, 120, 180, 240, and 300 h.

At these scheduled exposure times, samples are collected and analyzed by GC to determine the residual metofluthrin content, and subsequently the released quantity. All measurements are conducted in triplicates.

5.6.2 Observations

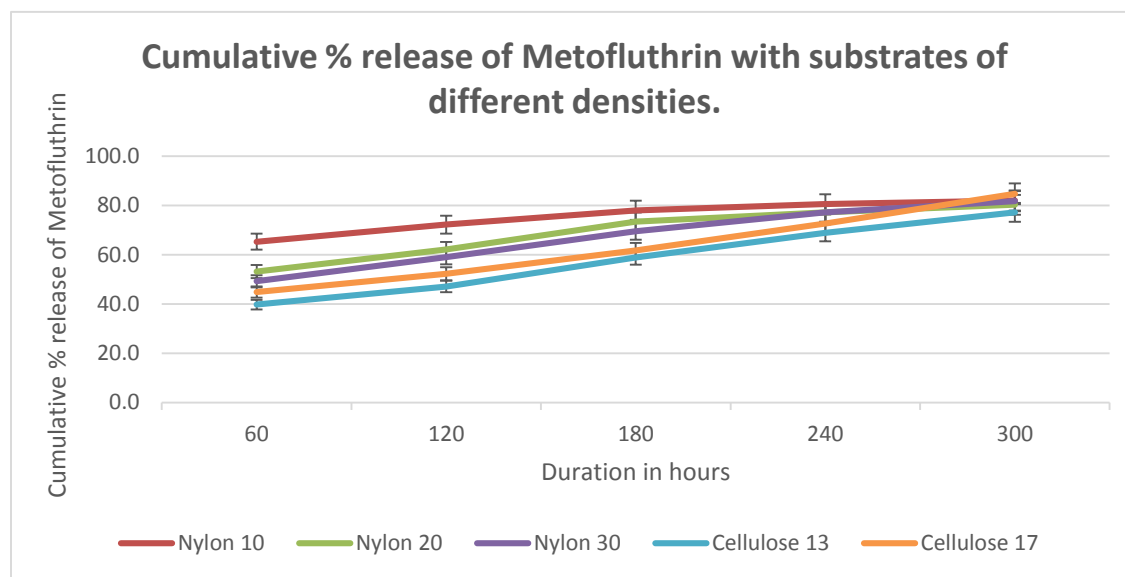


Figure 5.18: Cumulative metofluthrin release from different density substrates. Nylon 10, 20, and 30 refer to nonwoven nylon fabrics exhibiting densities of 10, 20, and 30 g/m², respectively. Cellulose 13 and 17 correspond to cellulose sheets with densities of 13 and 17 g/m², respectively.

5.6.3 Conclusion

The influence of the density parameter on metofluthrin release is evaluated for cellulose and nonwoven nylon substrates, which have previously demonstrated better release profiles than nonwoven PE and polypropylene. The difference in metofluthrin release kinetics is more pronounced during initial times between these substrates (Figure 5.18). However, the generated release data tend to converge after 300 h of exposure.

The data qualitatively indicates an inverse relationship between metofluthrin release and substrate density. It may be inferred that an increase in polymeric substrate density leads to a reduced void volume fraction within the substrate, hampering rapid diffusion than for substrates displaying a higher void volume fraction. This trend is slightly reversed for cellulosic substrates.

In addition, regardless of substrate density, metofluthrin release from nylon is initially higher than that from cellulosic substrates. Cellulosic substrates show gradual release over time and converge with nylon data toward the end-of-life.

5.7. Brunauer–Emmett–Teller surface area and pore characterization

The Brunauer–Emmett–Teller (BET) theory aims to explain the physical adsorption of gas molecules on a solid surface and serves as the basis for specific surface area measurements of a material. This precise specific surface area evaluation relies on the assessment of nitrogen multilayer adsorption as a function of relative pressure using a completely automated analyzer. This technique determines external and pore areas to estimate the total specific surface area expressed in m^2/g , providing important information regarding the effects of surface porosity and particle size in many applications. In addition to pore areas, BET analysis is employed to measure specific pore volume via adsorption and desorption techniques. This technique generates pore size distribution independent of external area because of the sample particle size. It has been utilized successfully in several applications [149,150,151] such as

- Rapid single point and multipoint specific BET surface area determinations.
- Complete BET surface area characterization of disperse, nonporous, or macro porous materials displaying pore diameters exceeding 50 nm (type II isotherms) and mesoporous materials with pore diameters between 2 and 50 nm (type IV isotherms).

- BET surface area characterization of micro porous materials (<2 nm, type I isotherms).
- Pore volume and pore area distributions in the mesopore and macro pore ranges using the Barrett–Joyner–Halenda (BJH) analysis with a complete complement of adsorbate thickness models.
- BJH adsorption and desorption average pore diameter (4 V/A) determinations. Here, the adsorption behavior of metofluthrin on different substrates is assessed. The adsorption process involves transferring a substance from a liquid (adsorbate) to a solid phase (adsorbent). Usually, the amount of adsorbed substance depends on the surface area and porosity of the adsorbent. Therefore, these characteristics are evaluated by measuring the adsorption isotherm of the substrates [148].

5.7.1 Methodology

Table 5.12: Operating conditions of the BET equipment

Sr. No	Details	
1	Name of the equipment	Micrometrics ASAP 2020
2	Manufacturer	Micrometrics
3	Model No.	ASAP 2020
4	Accessories used	Specific glass holder and glass condenser tube and two 3 liter liquid nitrogen container one is in condenser port and the another in the analysis port
5	Operating conditions such as carrier gas, flow rates, and temperatures	For adsorption measurement, we used very high purity nitrogen gas, and for back flush or dead space measurement, high purity helium gas was used. Outlet pressure (cylinder) of both the gas was maintained 1 kg/cm ² . During analysis, samples maintain the temperature of sample container ~77 K by liquid nitrogen.

5.7.2 Observations

BET results for cellulose and nonwoven nylon, PET, and polypropylene are summarized in Table 5.13, and representative plots are shown in Figures 5.19–5.22.

Table 5.13: BET results for cellulose and nonwoven nylon, PET, and polypropylene.

Surface area	Nylon	Cellulose	PET	Polypropylene
BET Surface Area	1.3583 m ² /g	1.9172 m ² /g	1.2987 m ² /g	0.7037 m ² /g
Langmuir Surface Area	2.2727 m ² /g	3.0790 m ² /g	2.1118 m ² /g	1.0066 m ² /g
t-Plot External Surface Area	1.8249 m ² /g	2.5011 m ² /g	1.5784 m ² /g	0.3858 m ² /g
Pore Volume				
Single point adsorption total pore volume of pores	0.00382 cm ³ /g	0.00822 cm ³ /g	0.00151 cm ³ /g	0.00125 cm ³ /g
t-Plot micro pore volume	0.000303 cm ³ /g	0.000368 cm ³ /g	0.000201 cm ³ /g	0.000192 cm ³ /g
Adsorption average pore width (4 V/A by BET)	112.3747 Å	171.4834 Å	46.6368 Å	70.9638 Å

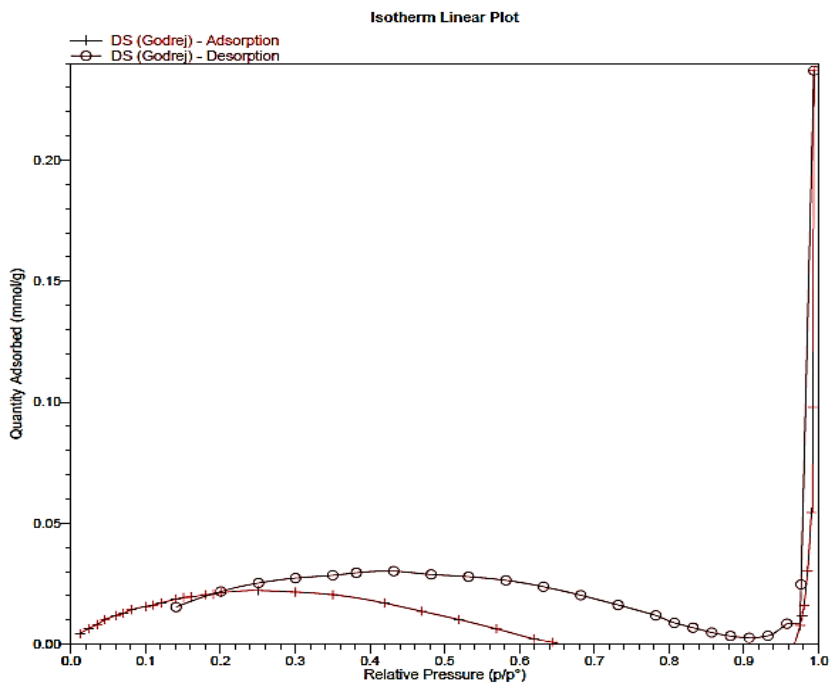


Figure 5.19: BET plot of cellulose.

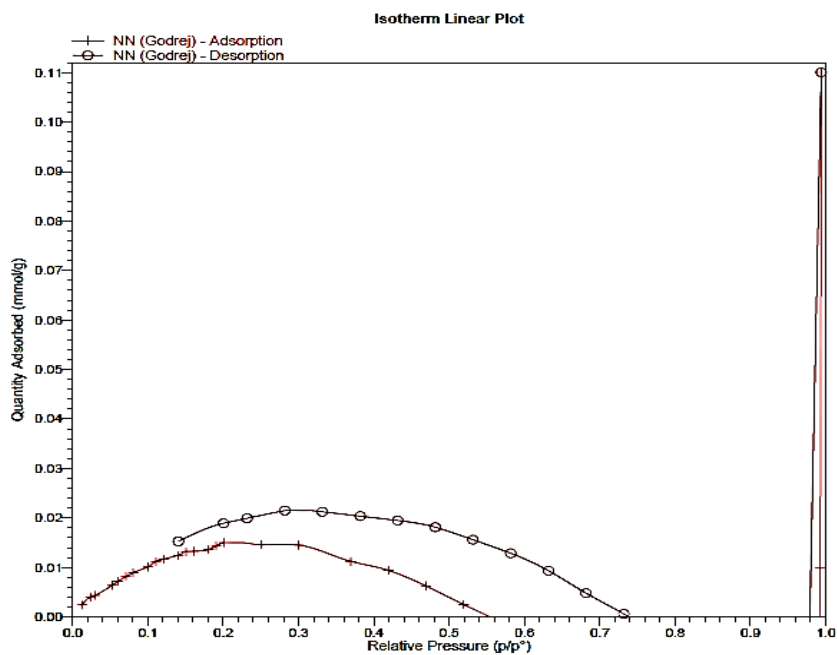


Figure 5.20: BET plot of nonwoven nylon.

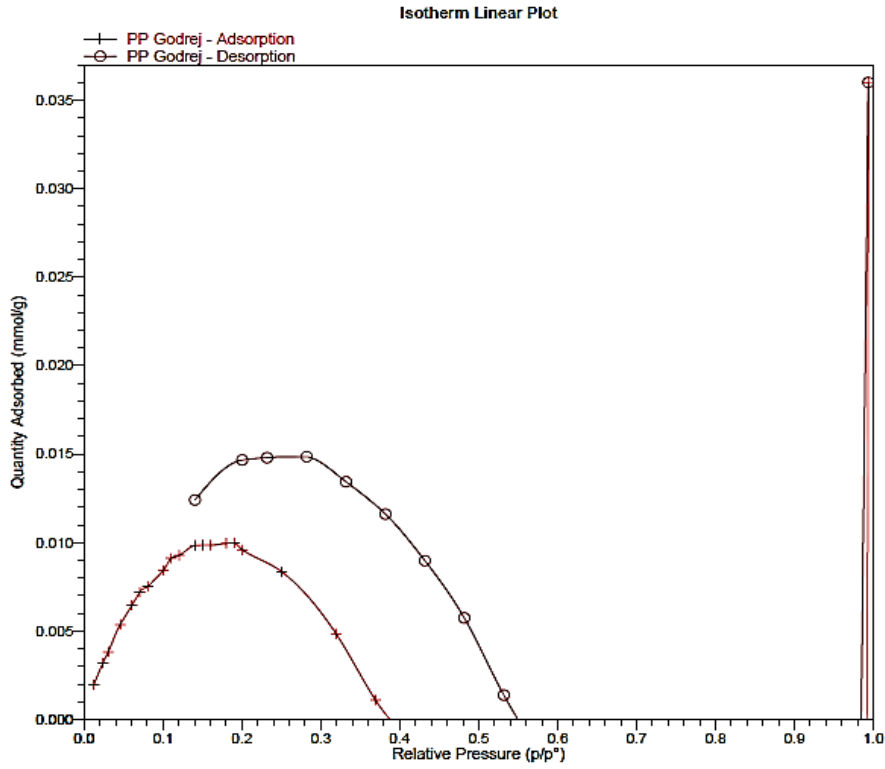


Figure 5.21: BET plot for nonwoven polypropylene.

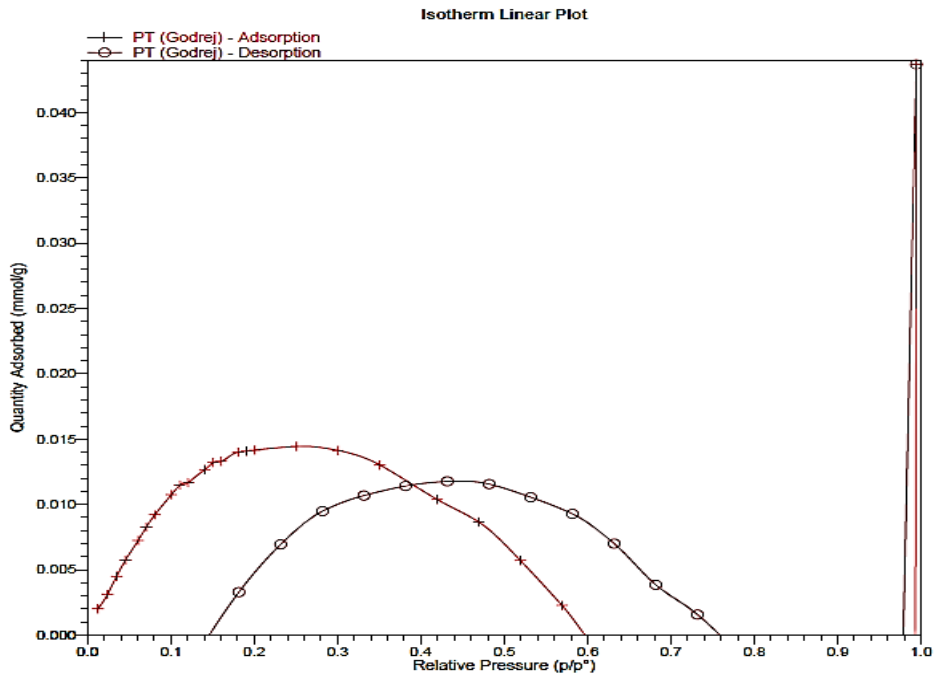


Figure 5.22: BET plot for nonwoven PET.

5.7.3 Conclusion

The independent pore size measurements by the BET method correlate well with the data obtained in the comparative study of metofluthrin release from different substrates (Section 5.2), which showed that release rates depend on the nature of the substrate.

Cellulose exhibits significantly higher BET surface area and pore volume than the other polymeric substrates. However, its pore size follows a similar trend to those polymeric substrates. The surface area behavior of the substrates is also consistent and in line with their metofluthrin release rates. Therefore, surface area, pore volume, and pore size influence the metofluthrin release from various substrates to a great extent.

5.8 Mercury intrusion porosimetry

Porosimetry is an analytical technique for determining various quantifiable aspects of material porosity, such as pore diameter, total pore volume, surface area, and bulk and absolute densities.

Surface areas are most widely evaluated by gas adsorption, in particular, BET N₂-desorption/adsorption. In addition, they are measured by mercury intrusion porosimetry (MIP), which also provides porosity, pore volume, and pore size distribution [154,155]. In this technique, a non-wetting liquid (often mercury) is introduced on a material at high pressure using a porosimeter. The pore size is determined from the external pressure needed to force the liquid into a pore against the opposing force of the liquid surface tension. MIP has widely been used to characterize pore size distributions in cement-based materials. This simple and quick indirect technique has shown limitations when applied to materials with irregular pore geometry [152,154]. MIP has been applied for the analysis of the liquid volume in the presence of poly (ϵ -caprolactone) mat deformation by buckling of the pores or elastic compression of the mat [153].

The previous section described the evaluation of the BET surface area of cellulose, nylon, polypropylene, and PET substrates for metofluthrin release. Average pore width and volume were also determined by the BET technique for these untreated substrates. These measured parameters are definitely key to the release of metofluthrin. However, pore volume and porosity may be more relevant to predict the impact of these substrates on metofluthrin release.

The differential reduction of porosity after metofluthrin loading and the subsequent porosity available for metofluthrin release may provide a clear indication of the relation with the release [155,156].

5.8.1 Methodology

Table 5.14: Experimental conditions for MIP measurements.

Sr. No.	Details	
1	Name of the equipment	Mercury Intrusion Porosimeter
2	Manufacturer	Quantachrome, USA
3	Model No.	Poremaster 33
4	Sampling procedure, if any	Rolls were prepared from the sample and tied with thin thread and inserted in the testing cell (called penetrometer). This cell was sealed with accessories provided by the manufacturer and inserted into the position in the equipment. Then, the cell was filled with mercury. Furthermore, analysis was performed in low pressure port (0–50 psi), and further analysis was performed in high pressure port (20–33000 psi) range. The instrument has volume and pressure sensors which record these values. The pore size is calculated by the software associated with the instrument (pore volume is determined from the pressure and volume).

5.8.2 Observations

Table 5.15: MIP data for various substrates.

Parameters	Untreated Cellulose	Treated Cellulose	Untreated Nylon	Metofluthrin treated Nylon	Untreated PET	Metofluthrin treated PET	Untreated polypropylene	Metofluthrin treated polypropylene
Total pore volume cc/g	3.935	1.8697	2.7685	2.34267	3.118395	2.0667574	4.92706	3.71565
Total porosity %	78.708	37.3953	55.3714	46.85349	62.3679	41.33514	116.377	74.3131
Reduction in porosity in % on loading with metofluthrin		52.49		15.38		33.78		36.15

5.8.3 Conclusion

MIP measurements reveal that for identical extents of metofluthrin incorporation within substrates exhibiting comparable surface areas, the porosity reduction is the highest for cellulose (52.34 %). Porosity reductions amount to 36.15%, 33.78%, and 15.38% for polypropylene, nylon, and PET, respectively. These data may explain correlations between diffusive metofluthrin losses from substrates of differing porosities. However, this data do not correlate with experimental diffusivity data on metofluthrin.

5. 9 Contact angle measurements

Conventionally measured through a liquid, the contact angle (θ) is formed by a liquid–vapor interface and a solid surface and quantifies the wettability of solid surface by this liquid via the Young’s equation.

$$\gamma_{SV} = \gamma_{SL} + \gamma_{LV} \cos\theta$$

A given system of solid, liquid, and vapor at a given temperature and pressure has a unique equilibrium contact angle. However, in practice, contact angle hysteresis is observed between the so-called advancing (maximal) contact angle and the receding (minimal) contact angle. The equilibrium contact angle, which reflects the relative strength of the liquid, solid, and vapor molecular interaction, belongs to this range and can be calculated from these values.

Contact angle and sliding angle measurements have provided insight in the energetics of solid surfaces and their effect on interaction with liquid surfaces. Their roles in adhesion strength have been studied [154,155].

Contact angle measurements have been used to determine and visualize the adsorption properties, and consequently the sorption capacity of a selected material. As a general rule, if $\theta > 90^\circ$, the liquid tends to form droplets on the surface. If $\theta < 90^\circ$, the liquid tends to spread out over the surface. For $\theta \approx 0^\circ$, the liquid forms a thin film. These surface properties are essential because the primary uptake of active adsorption involves surface adsorption (i.e., nonpolar interactions). Therefore, contact angle measurements are a simple way to assess the potential of a sorbent to take up liquid, i.e., the lower the liquid–solid contact angle, the greater the mutual attraction between the oil and sorbent. This is consistent with the higher sorption performance of the adsorbent [150]. In the previous sections , porosity of substrates have been studied. However the tendency of metofluthrin to spread in the pores on the substrates can be correlated with contact angles and surface tension of metofluthrin and substrates.

The contact angle of metofluthrin is measured for different substrates and correlated with porosity observations obtained in previous sections.

5.9.1 Equipment details

Table 5.16: Experimental conditions.

Sr. No	Details	
1	Name of the equipment	Contact angle meter
2	Manufacturer	DIGIDROP
3	Sampling procedure	Sessile drop method of contact angle measurement

5.9.2 Observations

Table 5.17: Contact angle of metofluthrin with various substrates.

	Contact angle of metofluthrin with various substrates in degrees			
Substrates	Cellulose	Nylon	PET	Polypropylene
Contact angle in Degrees	Not measurable	Not measurable	Not measurable	Not measurable

5.9.3 Conclusion

An extremely fast absorption process of metofluthrin on the substrates under consideration precludes the determination of contact angle using standard techniques. Surface irregularities of substrates also play a role in preventing precise contact angle measurements. Therefore, no comment can be made about either the substrate surface energetics or their interaction with metofluthrin.

5.10 Surface tensiometry

The Young's equation only applies to an ideal solid with a smooth, inert, homogeneous, and nonporous surface. An accurate determination of contact angles on porous substrates is challenging because surface irregularity leads to contact angle hysteresis. The static contact angle is normally defined as the average of various contact angle measurements. However, it can show large errors because of real surface irregularity. Dynamic contact angles are the extremes of the possible contact angle range and are detected when the three-phase boundary moves. They also provide information on surface topography and homogeneity [150,155].

Washburn sorption measurements, which are typically used to determine the surface energy of powders, are performed to determine the contact angles of the substrates of interest. A glass tube possessing a filter base is filled with the powder to be measured and suspended from the balance. Once the vessel has contacted the liquid, the speed at which the liquid rises through the bulk powder is measured by recording the increase in weight as a function of time.

The bulk powder through which a liquid flows can be regarded as a bundle of capillaries. Consequently, for calculating the advancing angle θ corresponding to the contact angle between the solid and liquid, the Washburn equation that applies to capillaries can be used.

$$\frac{l^2}{t} = \frac{\sigma_{L\gamma} \cos \theta}{2\eta}$$

Where l is the flow front, t is the flow time, σ is the surface tension of the liquid, r is the capillary radius, and η is the viscosity of the liquid. The capillary radius of the bulk powder must be replaced by the quantity $(c \cdot r)$, which describes the orientation of the microcapillaries c and their mean radius. Consequently, for a particular powder,

$$\frac{l^2}{t} = \frac{(c \cdot r) \sigma_{L\gamma} \cos \theta}{2\eta}$$

Because l cannot be measured directly, it is calculated from the measured increase in weight, the liquid density, and the tube diameter. Liquid viscosity and surface tension are known. Therefore, only two unknown quantities remain, i.e., the advancing angle θ and the material constant $(c \cdot r)$. A measurement with an optimally wetting liquid (e.g., hexane), which exhibits an advancing angle of virtually 0° , is conducted first, giving a value of approximately 1 for $\cos \theta$. Next, this constant can be inserted in the Washburn equation to determine the advancing angle for other liquids.

5.10.1 Equipment details

Table 5.18: Surface tensiometer operating conditions.

Sr. No	Details	
1	Name of the equipment	Surface Tensiometry and Contact Angle measurement
2	Manufacturer	Mettler Toledo
3	Model No.	A 201
4	Sampling procedure	The substrates were rolled into cylinder of about 10 mm diameter and 35 mm length.
5	Operating temperature	at 27 °C

5.10.2 Observations

Surface tensiometry using hexane

The mass gain is measured using hexane for all substrates and is used to calculate material constants for $\cos \theta \approx 1$.

Table 5.19: Calculated material constants using hexane.

Liquid	Solid	Constant
Hexane	Cellulose	267
	Nylon	8
	PET	1068
	Polypropylene	313

Surface tensiometry using metofluthrin

The contact angle θ is obtained from mass gain measurements using metofluthrin and material constants obtained from the experiments involving hexane.

Table 5.20: Contact angles of metofluthrin with various substrates using the Washburn equation.

Liquid	Solid	Contact Angle
Metofluthrin	Cellulose	0
	Nylon	0
	PET	90
	Polypropylene	70.6

5.10.3 Conclusion

The surface tensiometry data actually show low, near zero, contact angles between metofluthrin and cellulose and nylon powders, implying good wetting properties and the rapid deposition of metofluthrin on substrate fibers. Higher contact angles are observed between metofluthrin and PET and polypropylene powders, indicating the tendency of these substrates to resist metofluthrin wetting or deposition.

5.11 Surface morphologies of substrates

Scanning electron microscopy (SEM) produces images by scanning a sample with a focused electron beam. The electron beam interacts with atoms in the sample, producing various detectable signals that contain information about the sample surface topography and composition. SEM technique has been widely used to study paper properties and processing [158] and understand the nature of surface topographies in detail.

Equipment details

SEM images were acquired using a Hitachi TM1000 Tabletop Microscope equipped with a backscatter detector operating at an accelerating voltage of 15 kV.

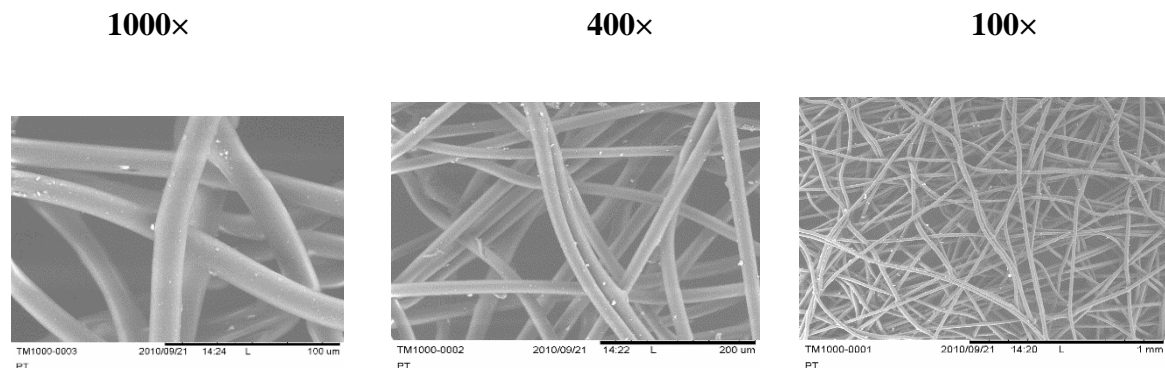


Figure 5.23: SEM micrograph of nonwoven PET.

Observations

SEM surface features show that cellulose comprises irregularly defined intertwined fibers that appear flattened. All other substrates consist of cylindrical long fibers.

Average fiber diameters calculated from the SEM images of the different substrates are shown in Table 5.19.

Table 5.21: Average fiber diameters in various substrates.

	Cellulose	Nylon	PET	Polypropylene
Substrate	Average fiber diameter in μm (approx)			
	35	20	17	16

Conclusion

SEM images of various substrates under evaluation for metofluthrin release are shown in Figures 5.23–5.26. These micrographs reveal that cellulose presents flat, non-uniform features, whereas the other substrates show arrays of cylindrical fibers. The shape and diameter/width of cellulosic fiber contribute to a sustained metofluthrin release. The fiber diameters of the nonwoven substrates correlate positively with their metofluthrin release rates. However, these diameters are very close to each other and do not explain for the large differences in their release rate.

5.12 Fourier transform infrared spectroscopy

Molecules are excited to a higher energy state when they absorb infrared radiation. Similar to any other absorption processes, the absorption of infrared radiation is a quantized process during which a molecule selectively absorbs certain infrared frequencies. These resonant frequencies are characteristic of its molecular structure and match the transition energies of the bonds or groups that vibrate. Energies are determined from the shape of the molecular potential energy surfaces, atom masses, and associated coupling. The absorption of infrared radiation corresponds to energy changes ranging from 8 to 40 kJ/mol [157].

Attenuated total reflectance (ATR) is used in conjunction with infrared spectroscopy to enable samples to be examined directly in the solid or liquid state without further specialized preparation.

In this approach, samples are pressed against the face of a single crystal. The infrared radiation passes through the crystal and only interacts with the sample at the interface between the two materials [159,160]. Surface interactions, especially surface adsorption, surface binding, and hydrogen bonding, have been assessed by FTIR [161–165]. Interactions between metofluthrin and cellulose and polymer substrates are evaluated using this technique.

5.12.1 Experimental details

Materials:

Metofluthrin (purity 98.5%)

Isopropyl alcohol A.R

Cellulose, Nonwoven PET, Nonwoven Polypropylene and Nonwoven nylon dosed with 32 mg metofluthrin/100 cm²

Method

Cellulose and polymer samples containing 66 mg of active ingredient are prepared using a metofluthrin solution in isopropyl alcohol. The resulting samples are kept open and unfolded to enable solvent evaporation.

Table 5.22: ATR–FTIR experimental conditions.

Sr. No.	Details	
1	Name of the equipment	FTIR
2	Manufacturer	Shimadzu
3	Model No.	IR Affinity-1
4	Sampling procedure	Cut into small discs
5	Accessories used	Single reflection ATR (Dura sampler)
6	Operating conditions such as carrier gas, flow rates, and temperatures	Samples were pressed using pressurizing tool of ATR for intimate contact of sample with the prism.

Observations

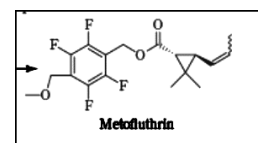
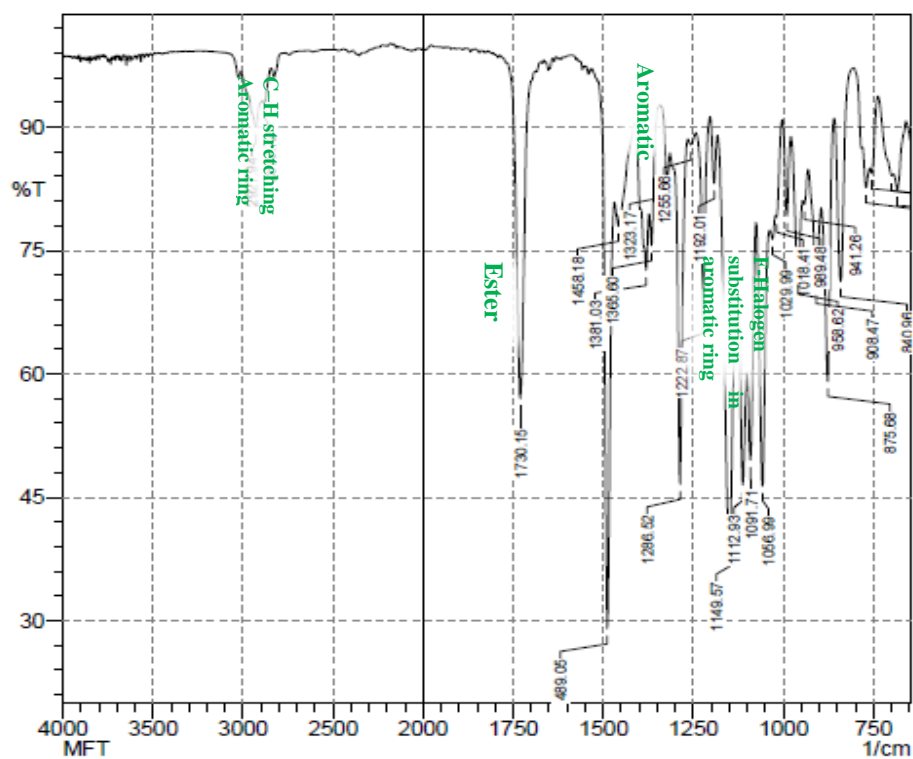


Figure 5.27: FTIR spectrum of liquid metofluthrin

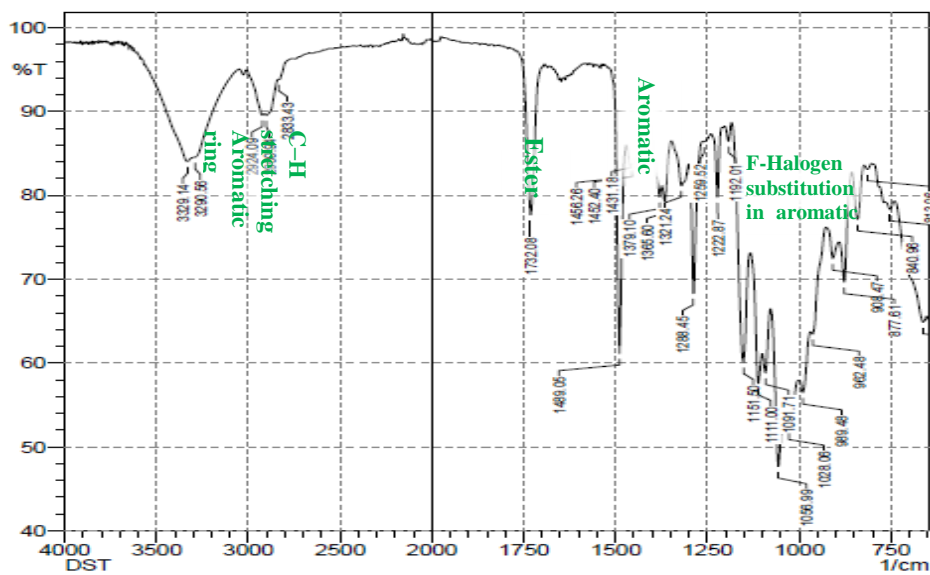


Figure 5.28: FTIR spectrum of metofluthrin-impregnated cellulose.

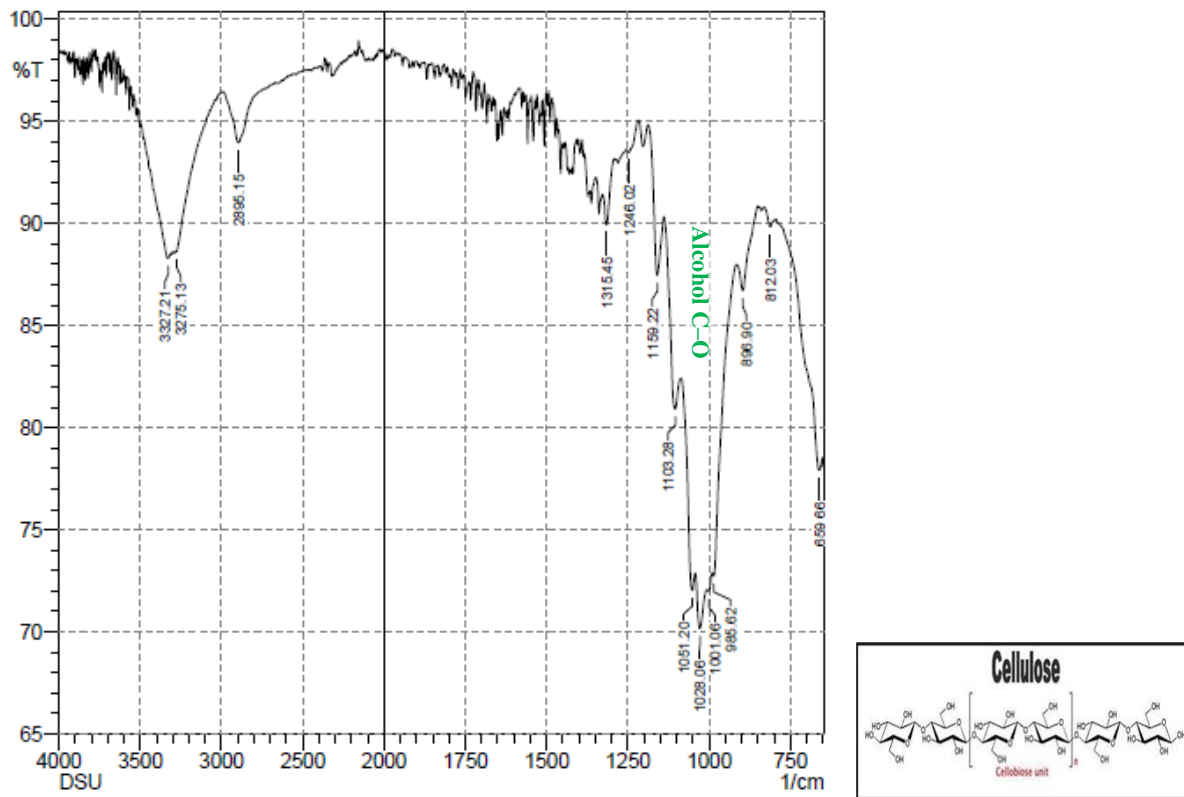


Figure 5.29: FTIR spectrum of cellulose.

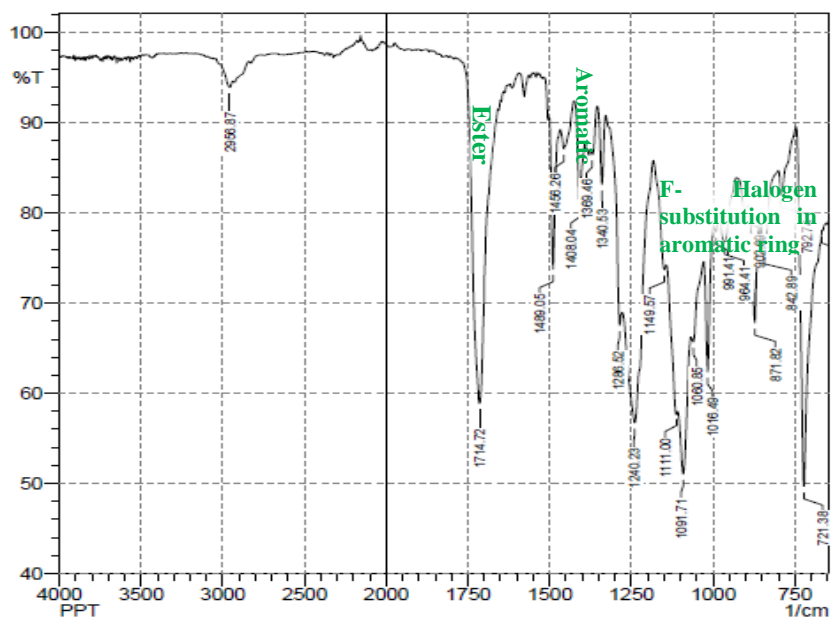


Figure 5.30: FTIR spectrum of metofluthrin-impregnated nonwoven PET.

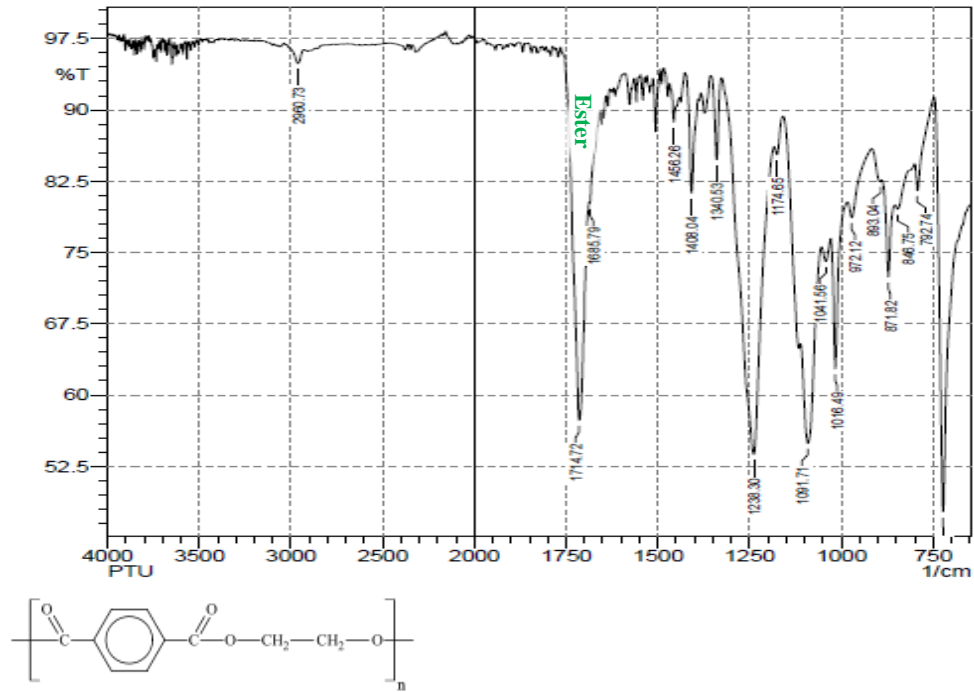


Figure 5.31: FTIR spectrum of nonwoven PET.

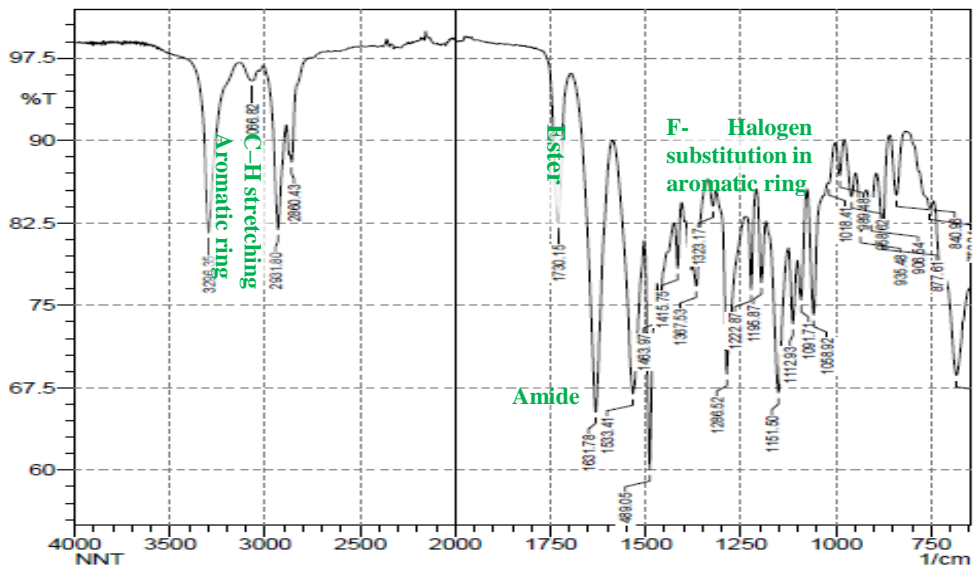


Figure 5.32: FTIR spectrum of metofluthrin-impregnated nonwoven nylon.

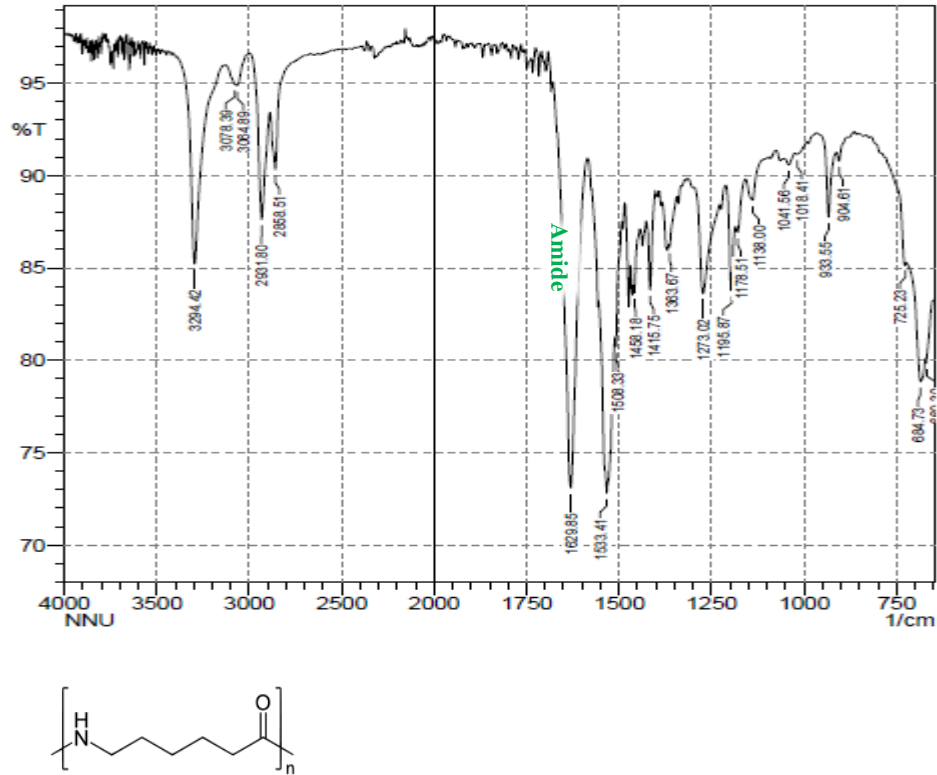


Figure 5.33: FTIR Spectrum for nonwoven nylon.

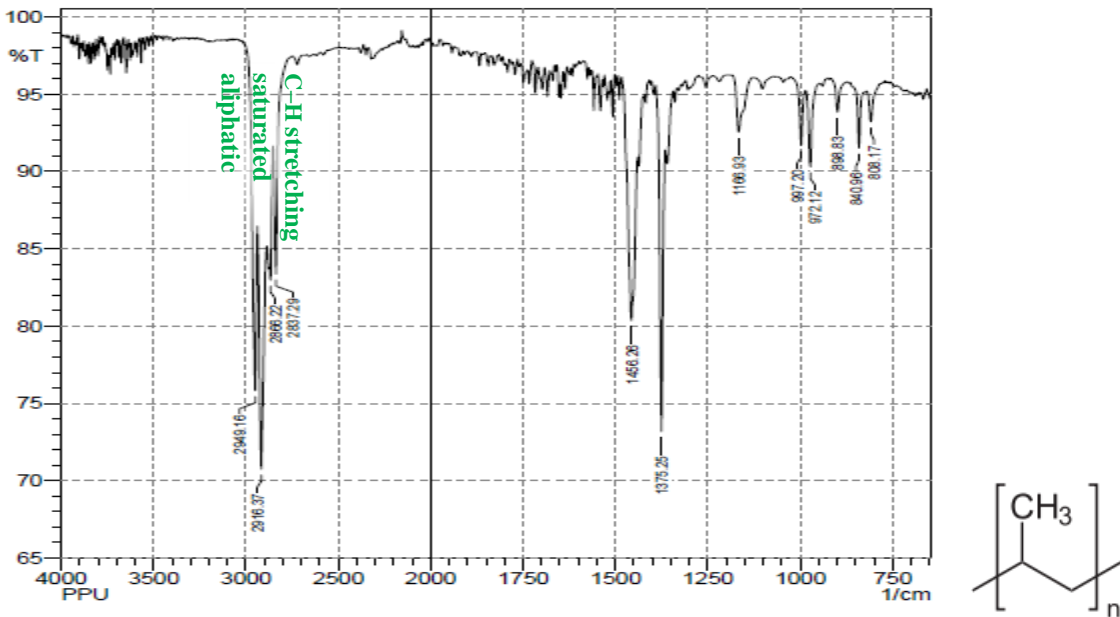


Figure 5.34: FTIR spectrum of nonwoven polypropylene.

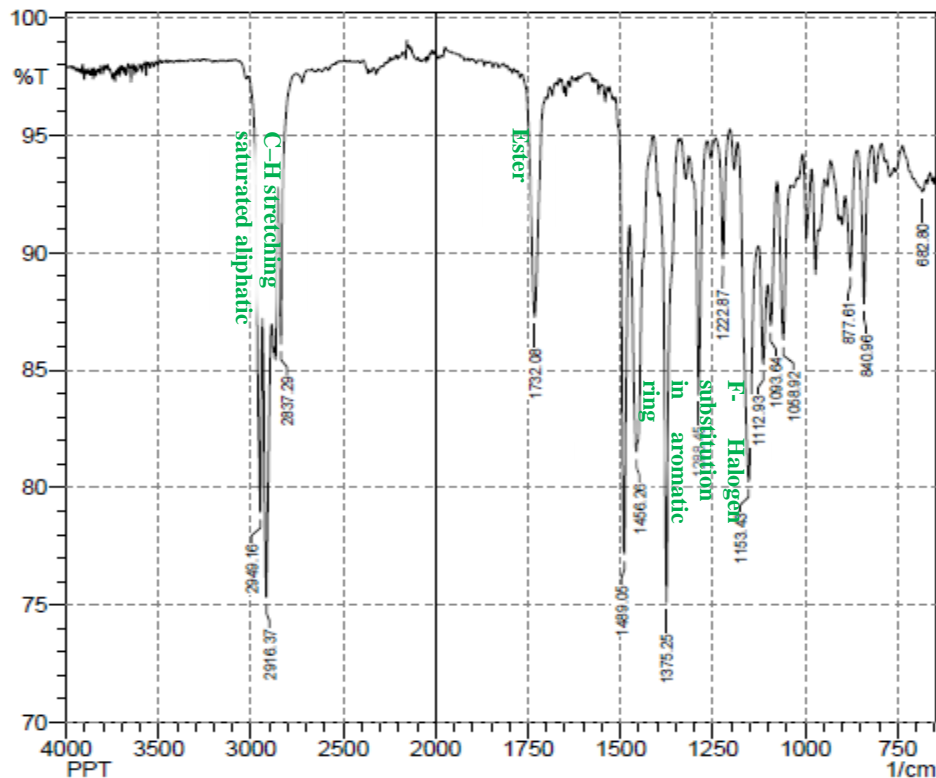


Figure 5.35: FTIR spectrum of metofluthrin-impregnated nonwoven polypropylene.

Table 5.23: Summary of Vibration frequencies of key functional groups from FTIR spectra.

	Ester group cm ⁻¹	Aromatic cm ⁻¹	Aromatic Halogen cm ⁻¹	Others
Metofluthrin	1730	1489	1149	
Cellulose	Nil	Nil	Nil	Alcohol C-OH 1001-1051 cm ⁻¹
Metofluthrin + Cellulose	1732	1489	1151	Alcohol C-OH 1001-1051 cm ⁻¹
Nylon	Nil	Nil	Nil	Amide NH ₂ -C=O 1533-1631 cm ⁻¹
Metofluthrin + Nylon	1730	1489	1151	Amide NH ₂ -C=O 1533-1631 cm ⁻¹
PET	Nil	Nil	Nil	Ester- 1714 cm ⁻¹
Metofluthrin + PET	1714	1489	1149	
Polypropylene	Nil	Nil	Nil	C-H stretching

				2837-2949 cm ⁻¹
Metofluthrin + polypropylene	1732	1489	1153	C-H stretching 2837-2949 cm ⁻¹

5.13 Surface FTIR of films

Various metofluthrin-impregnated substrates are further characterized by ATR spectroscopy to develop a much deeper understanding of surface interactions between metofluthrin and these substrates.

Materials

Metofluthrin

Isopropyl alcohol

Cellulose dosed 32 mg/100 cm²

Nonwoven PET

Nonwoven polypropylene

Nonwoven nylon

Method

Cellulose and polymer samples containing 66 mg of metofluthrin are prepared from a stock solution of metofluthrin in isopropyl alcohol. The obtained samples are kept open and unfolded to facilitate solvent evaporation.

Table 5.24: ATR–FTIR operating conditions

Sr. No.	Details	
1	Name of the equipment	FT-IR
2	Manufacturer	Perkin-Elmer
3	Model No.	FT1730

Observations

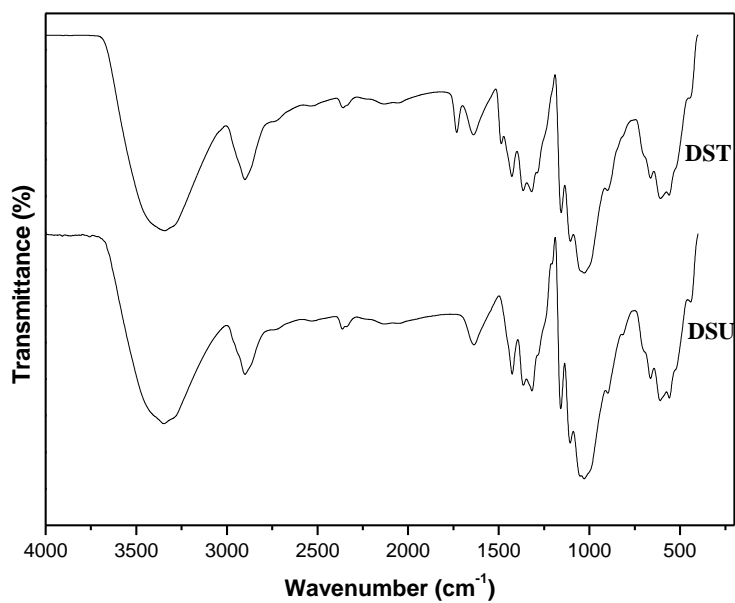


Figure 5.36: Overlay of surface FTIR untreated (DSU) and metofluthrin-impregnated cellulose (DST).

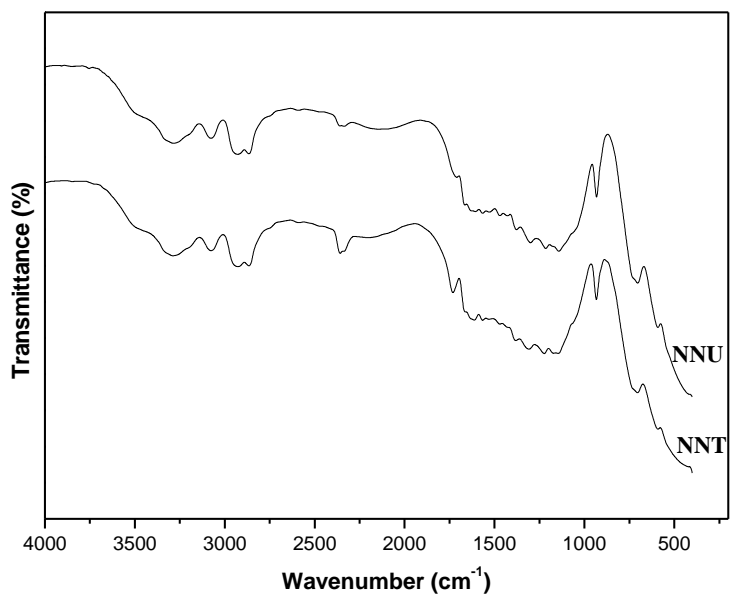


Figure 5.37: Overlay of surface FTIR of untreated (NNU) and metofluthrin-impregnated nonwoven nylon (NNT).

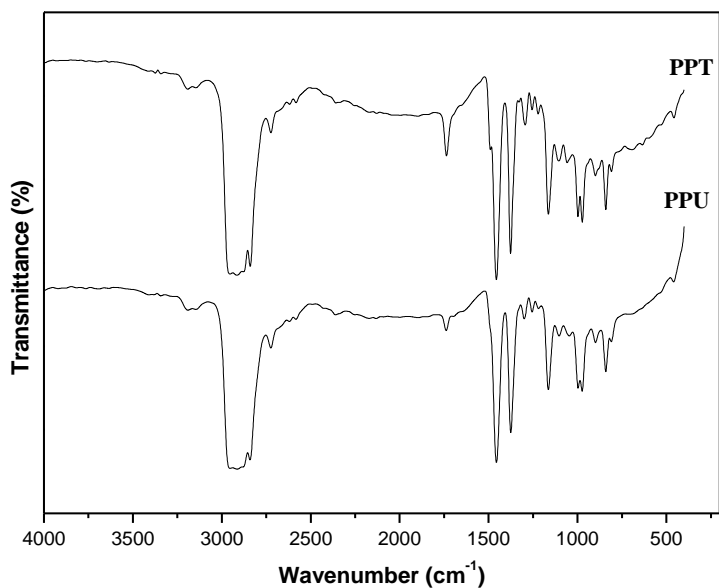


Figure 5.38: Overlay of surface FTIR of untreated (PPU) and metofluthrin-impregnated nonwoven polypropylene (PPT).

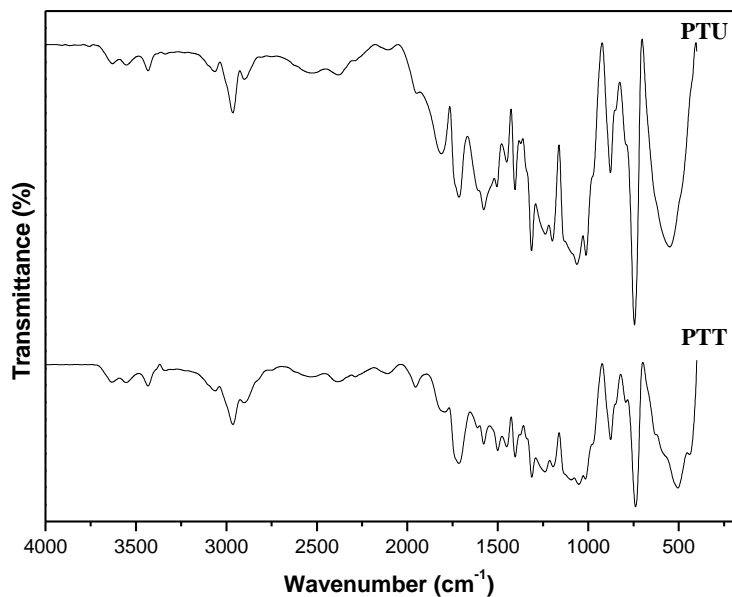


Figure 5.39: Overlay of Surface FTIR overlay of untreated (PTU) and metofluthrin-impregnated nonwoven PET (PTT).

Conclusion

Table 5.22 lists the vibration frequencies of key functional ester groups measured for metofluthrin alone and impregnated in various surfaces. Bulk and surface infrared measurements do not show any measurable shifts in substrate functional groups upon metofluthrin treatment. One would have expected weak hydrogen bonding associations between the aromatic fluoro group and ester functionality with surface –OH groups on substrate surfaces. However, surface FTIR measurements reveal no appreciable spectral shifts of the fluoro group, indicating the absence of strong chemical association between metofluthrin and substrates. This also points to the fact that metofluthrin diffusivity appears primarily influenced by the key physical properties of the considered substrates.

Table 5.25: Vibration frequencies of key functional groups.

Component	Ester group cm ⁻¹	Aromatic cm ⁻¹	Aromatic Halogen cm ⁻¹
Metofluthrin	1730	1489	1149
Metofluthrin + Cellulose	1732	1489	1151
Metofluthrin + Nylon	1730	1489	1151
Metofluthrin + PET	1714	1489	1149
Metofluthrin + polypropylene	1732	1489	1153

5.14 NMR spectroscopy

NMR spectroscopy is a spectral technique that exploits the magnetic properties of certain atomic nuclei to determine the physical and chemical properties of molecules or atoms within them. It relies on NMR and provides detailed information about the structure, dynamics, reaction state, and chemical environment of molecules [166].

NMR techniques have emerged as indispensable tools in fundamental and applied research in life science, physical science, and materials science. Their strength lies in the fact that they can provide intrinsic information at the molecular level in solid, liquid, and gaseous phases. Liquid-state NMR is very well established and routinely employed for structural elucidations and conformational studies of small and macromolecules. NMR spectra of solids (powder) are very broad and

featureless because of additional line-broadening processes resulting from various spin interactions under the influence of magnetic field. In solutions, most of these interactions are averaged to the Brownian motions of the molecules, resulting in narrow lines. In such cases, these interactions are negligible on the NMR experiment timescale [167,168]. The advent of techniques, such as magic angle spinning (MAS), cross-polarization (CP), and high power decoupling, have revolutionized solid-state NMR and opened up a new dimension in materials chemistry. A combination of these techniques is the method of choice for most popular spin- $1/2$ nuclei such as ^{13}C , ^{31}P , and ^{15}N . Spinning speeds usually range between 5 and 15 kHz for routine analysis but may exceed these values. In MAS experiments, the sample is kept at 54.7° (“magic angle”) with respect to the magnetic field and spun at high speed. For these experiments, the best results are obtained when the spinning rate exceeds the width of the static spectrum. Magic angle spinning leads to the formation of spinning side bands if the spinning speed is lower than the total width of the static signal. The high-power decoupling technique is analogous to decoupling of J-coupled spectra in solution except that it employs much higher power (a few kilowatts in solids vs. about 5 W in solution). The CP technique involves the transfer of magnetization from abundant ^1H spins to dilute spins, such as ^{13}C or ^{15}N , using a pulse sequence under certain conditions (Hartmann–Hahn match). Its combination with MAS is one of the most powerful solid-state NMR techniques because of the considerable sensitivity improvement. However, these techniques are not ideal for solid-state NMR measurements of quadrupolar nuclei ($I > 1/2$). In fact, variable angle spinning, dynamic angle spinning, and multiple quantum magic angle spinning techniques are essential for these measurements [169,170].

Solid state NMR was employed to further investigate on presence of interactions between adsorbent surface acidic protons and adsorbed organic molecules and hydrogen bonding between surface hydroxyl groups and adsorbate [171].

5.14.1 Experimental details

Materials

Metofluthrin

Isopropyl alcohol

Cellulose, Nonwoven PET, Nonwoven polypropylene and Nonwoven nylon dosed with metofluthrin to achieve an effective concentration $32 \text{ mg}/100 \text{ cm}^2$

Method

Cellulose and polymer samples containing 66 mg of active ingredient are prepared from a metofluthrin solution in isopropyl alcohol. The generated samples are kept open and unfolded to promote solvent evaporation.

Table 5.26: NMR experimental conditions.

Sr. No.	Details
1	Name of the equipment 300 MHz wide bore NMR spectrometer
2	Manufacturer Bruker
3	Model No. AV 300
4	Sampling procedure Samples cut into small pieces and packed in a 4 mm Zirconia rotor and spun at 8–10 KHz
5	Accessories used 4 mm CP–MAS probe
6	Any other specific information Measurements were performed with a relaxation delay of 5 s and contact time of 1 ms

Proton NMR at 8 kHz

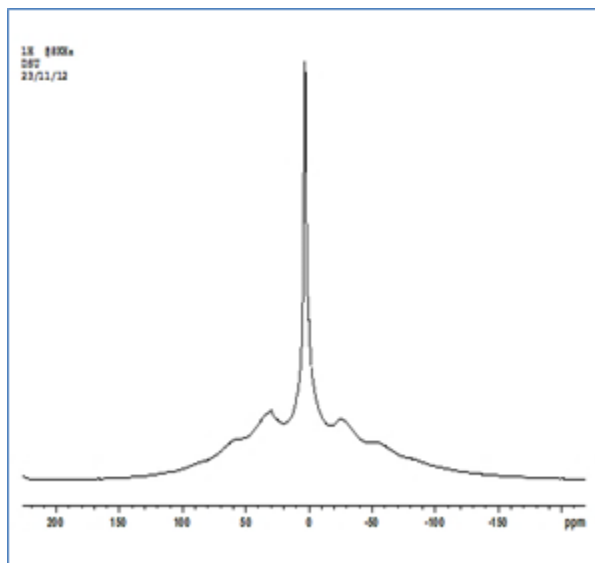


Figure 5.40: Solid-state ¹H NMR untreated cellulose.

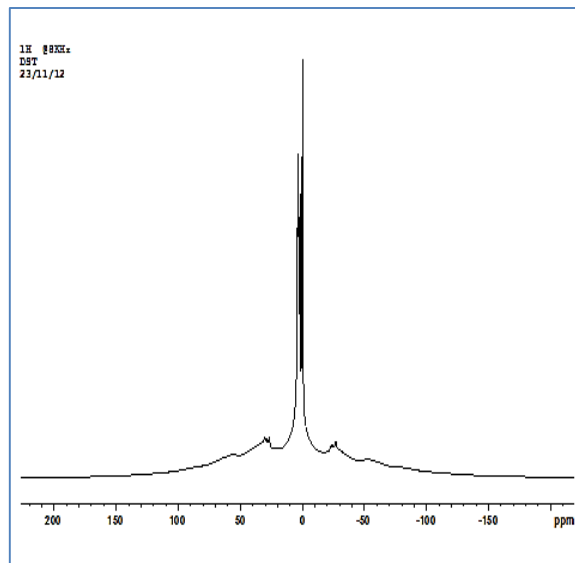


Figure 5.41: Solid-state ¹H NMR spectrum of metofluthrin impregnated cellulose

Proton NMR at 8 kHz

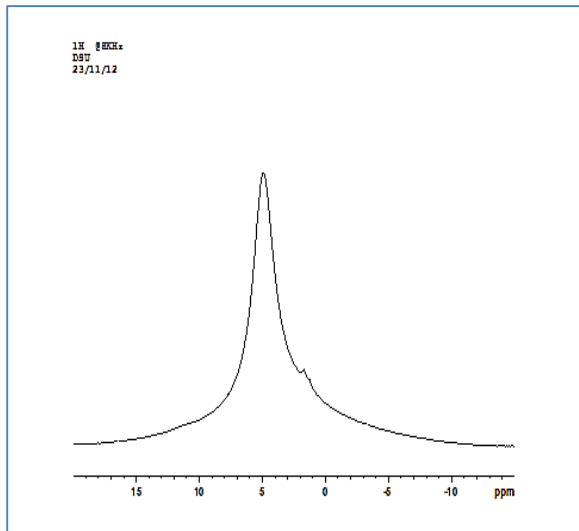


Figure 5.42: Solid-state ^1H NMR Untreated cellulose.

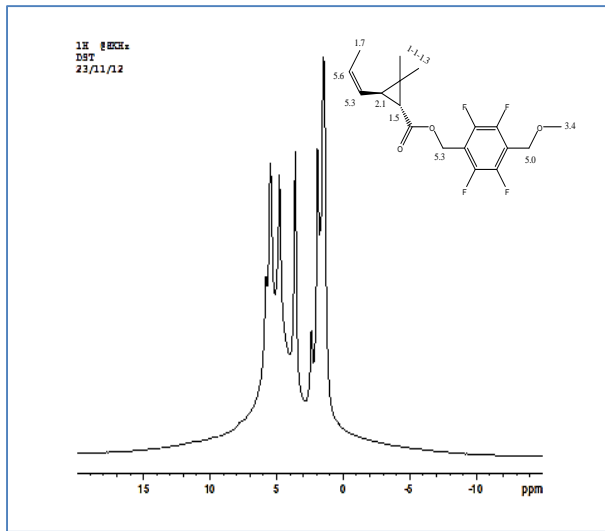


Figure 5.43: Solid-state ^1H NMR spectrum of metofluthrin-impregnated cellulose.

Proton NMR at 8 KHz

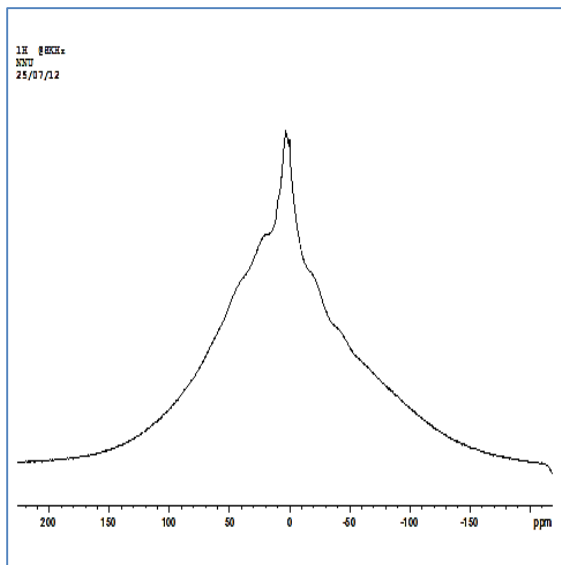


Figure 5.44: Solid-state ^1H NMR spectrum of untreated nonwoven nylon.

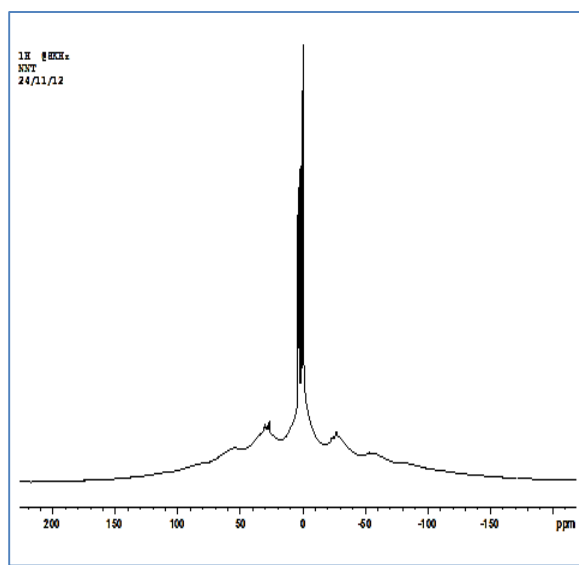


Figure 5.45: Solid-state ^1H NMR spectrum metofluthrin-impregnated nonwoven nylon

Proton NMR at 8 KHz

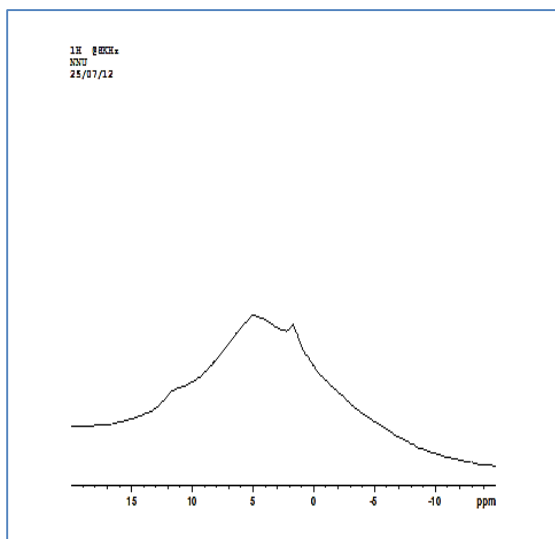


Figure 5.46: Solid-state ^1H NMR spectrum Of untreated nonwoven nylon.

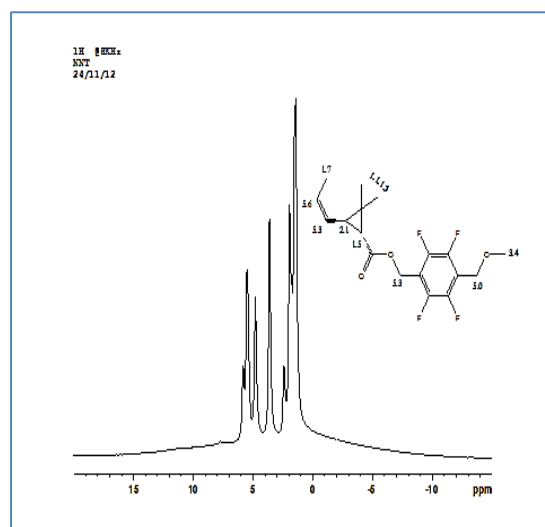


Figure 5.47: Solid-state ^1H NMR spectrum of metofluthrin-impregnated nonwoven nylon.

Proton NMR at 8 KHz

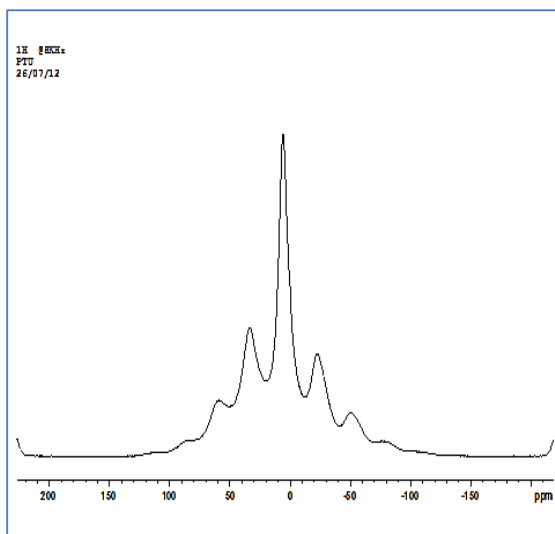


Figure 5.48: Solid-state ^1H NMR spectrum of untreated nonwoven PET.

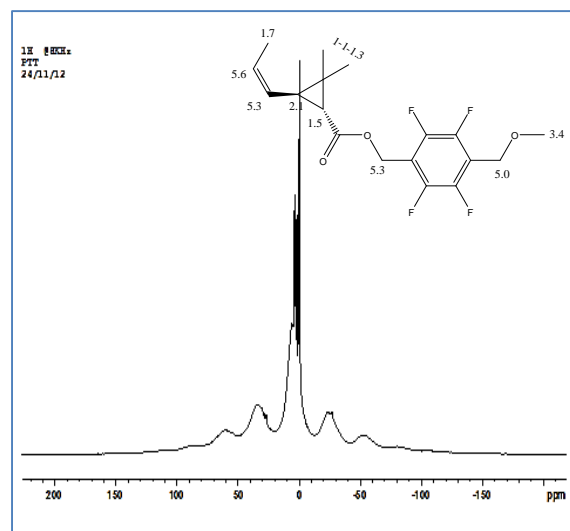


Figure 5.49: Solid-state ^1H NMR spectrum of metofluthrin-impregnated nonwoven PET

Proton NMR at 8 KHz

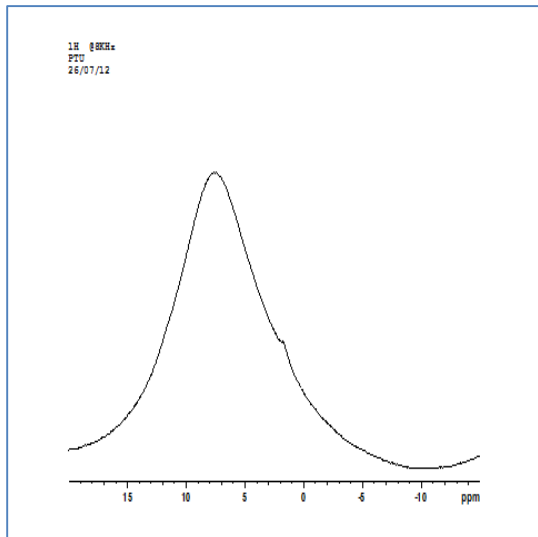


Figure 5.50: Solid-state ^1H NMR spectrum of untreated nonwoven PET.

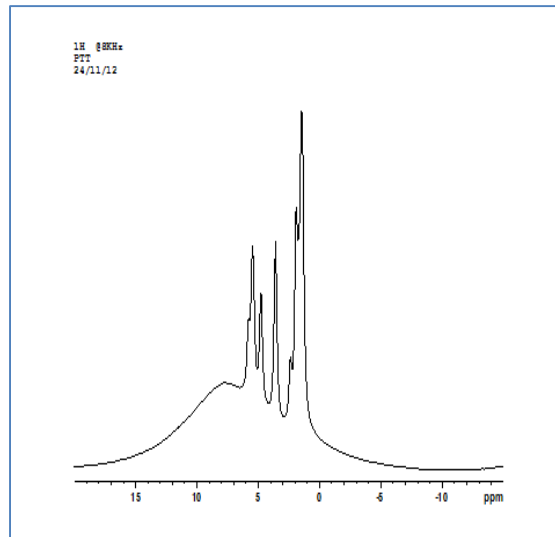


Figure 5.51: Solid-state ^1H NMR spectrum of metofluthrin-impregnated nonwoven PET.

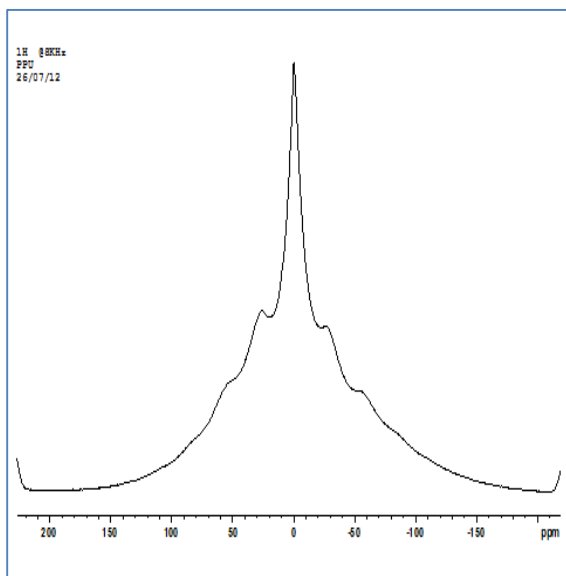


Figure 5.52: Solid-state ^1H NMR spectrum of untreated nonwoven polypropylene.

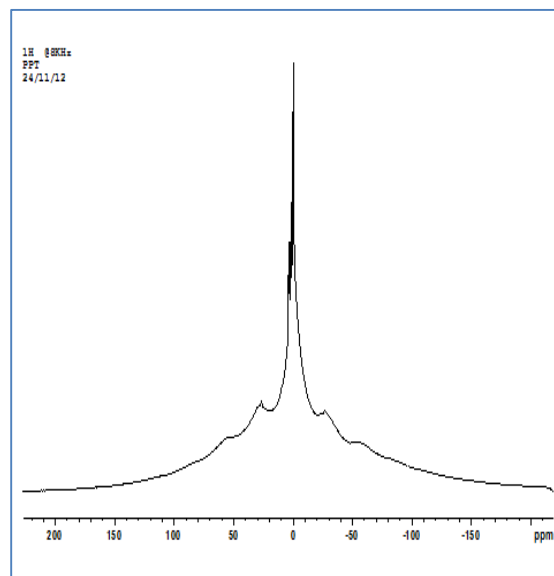


Figure 5.53: Solid-state ^1H NMR spectrum of metofluthrin-impregnated nonwoven PP.

Proton NMR at 8 KHz

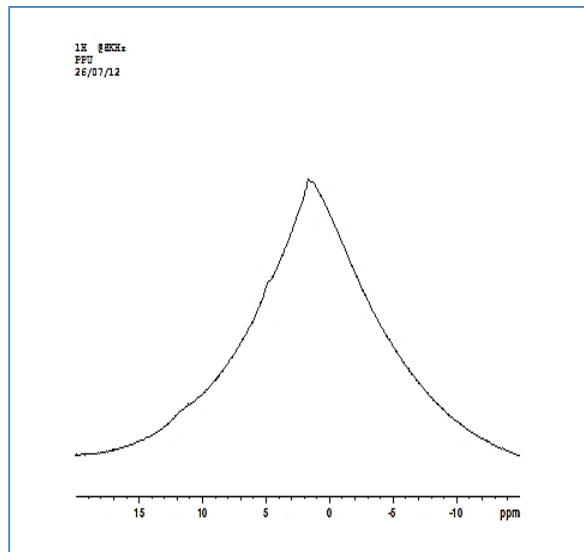


Figure 5.54: Solid-state ^1H NMR spectrum of untreated nonwoven polypropylene.

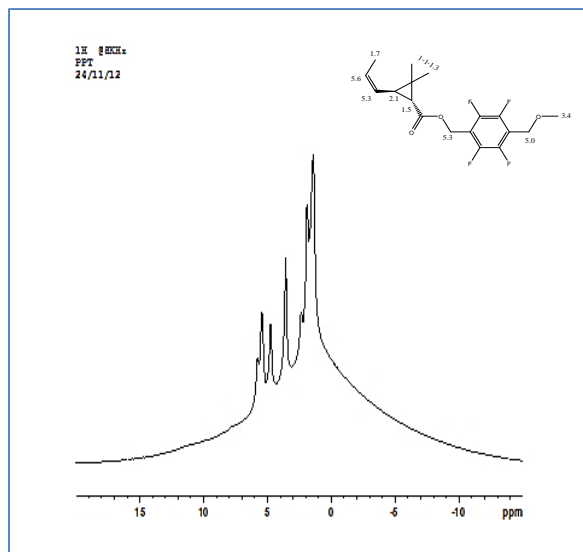


Figure 5.55: Solid-state ^1H NMR spectrum of metofluthrin-impregnated nonwoven PP

Table: 5.27 ^1H NMR chemical shifts in untreated and metofluthrin impregnated substrates

Proton environment	chemical shift (ppm)	Proton environment	chemical shift (ppm)
Cellulose		Metofluthrin impregnated Cellulose	
C=C-H	5.3	C=C-H	5.3
		H-C-OH	3.4
Polypropylene		Metofluthrin impregnated Polypropylene	
R-CH ₃	0.9	R-CH ₃	0.9
R ₂ -CH ₂	1.3	R ₂ -CH ₂	1.3
R ₃ -CH	1.5	R ₃ -CH	1.5
		C=C-H	5.3
		H-C-OH	3.4
PET		Metofluthrin impregnated PET	
RCOO-CH	4.1	RCOO-CH	4.1
		C=C-H	5.3
		H-C-OH	3.4
Nylon		Metofluthrin impregnated Nylon	
R-NH ₂	5	R-NH ₂	5
		C=C-H	5.3
		H-C-OH	3.4

^{13}C NMR spectra at 8 KHz

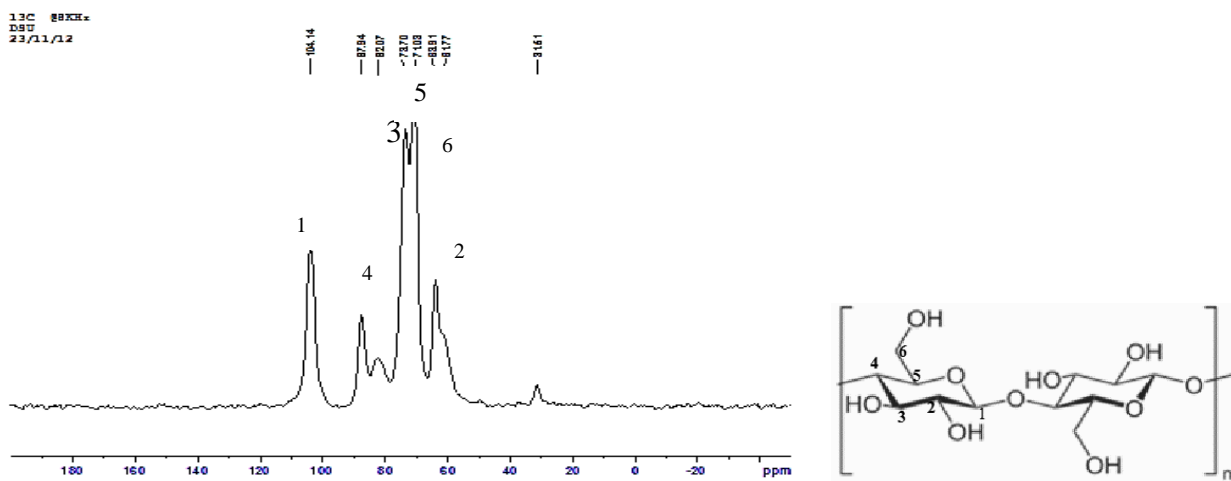


Figure 5.56: Solid-state ^{13}C NMR spectrum of untreated cellulose.

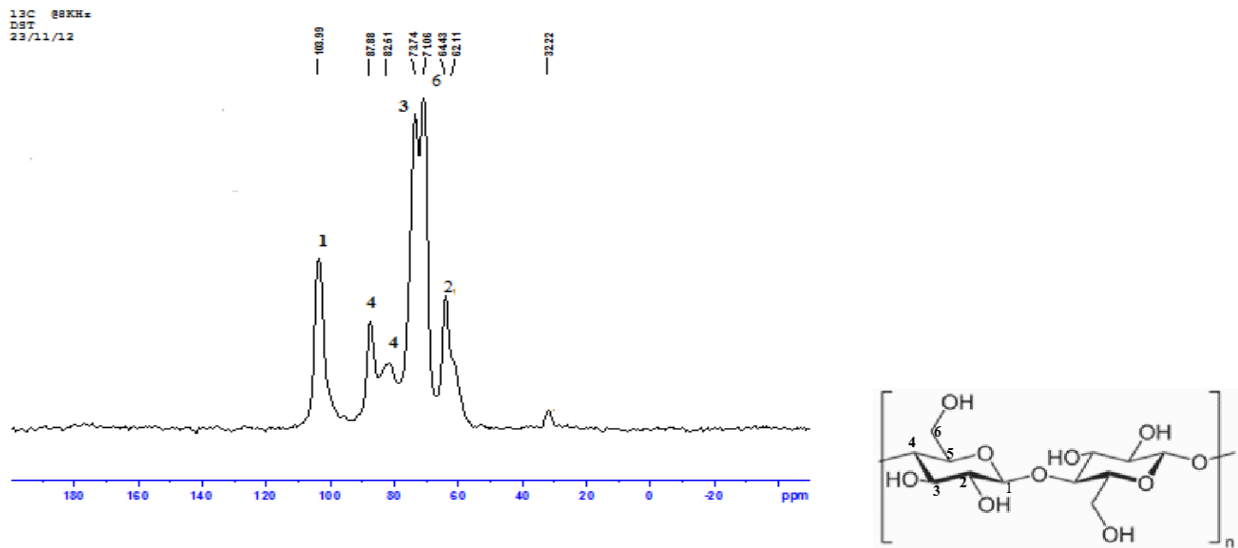


Figure 5.57: Solid-state ^{13}C NMR spectrum of metofluthrin-impregnated cellulose.

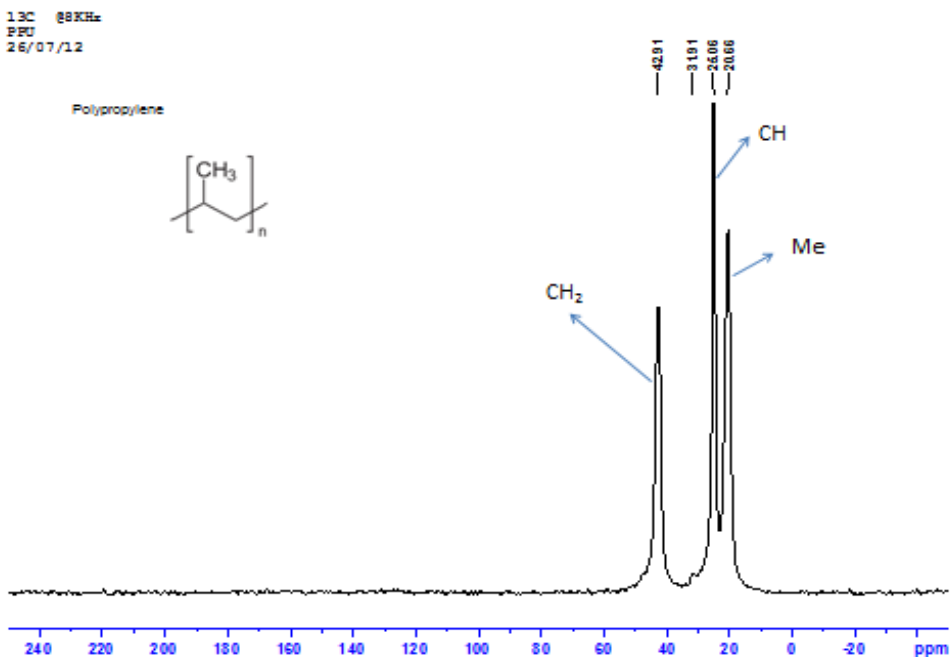


Figure 5.58: Solid-state ¹³C NMR spectrum of untreated nonwoven polypropylene.

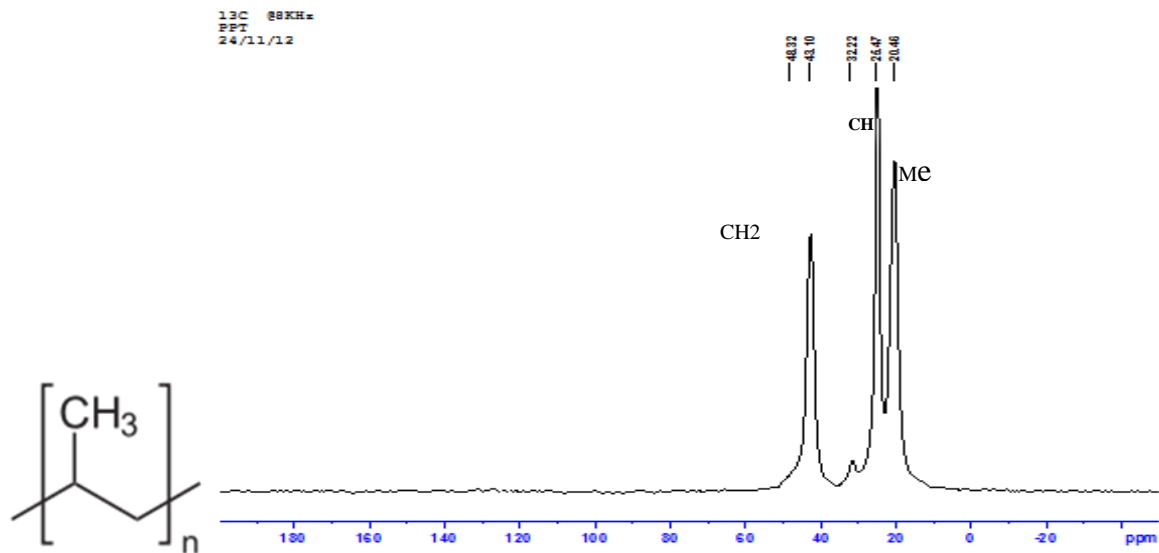


Figure 5.59: Solid-state ¹³C NMR spectrum of metofluthrin-impregnated nonwoven polypropylene.

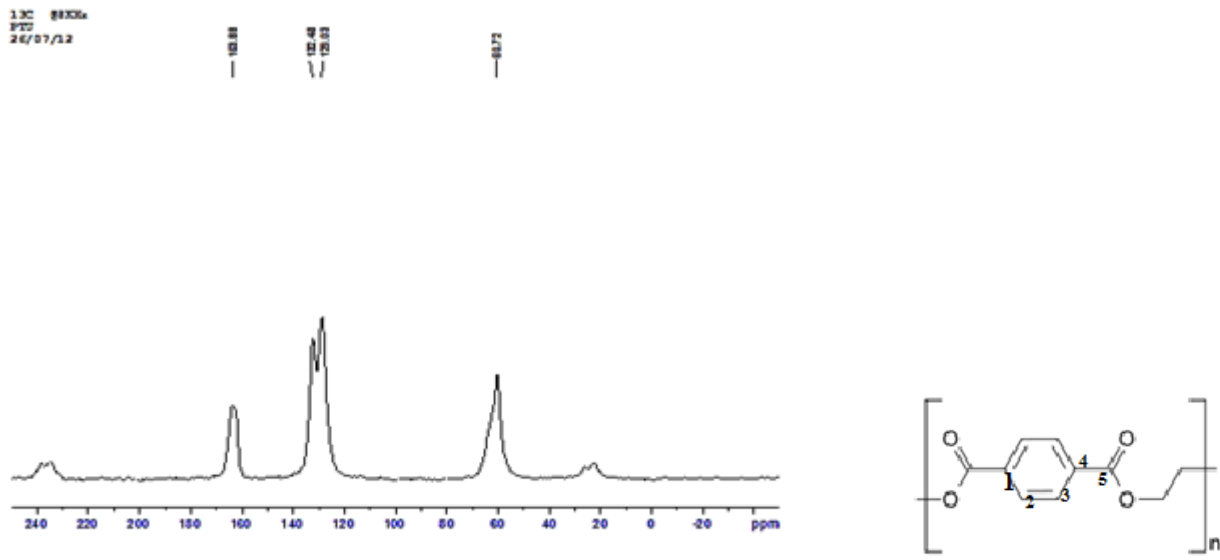


Figure 5.60: Solid-state ¹³C NMR spectrum of untreated nonwoven PET.

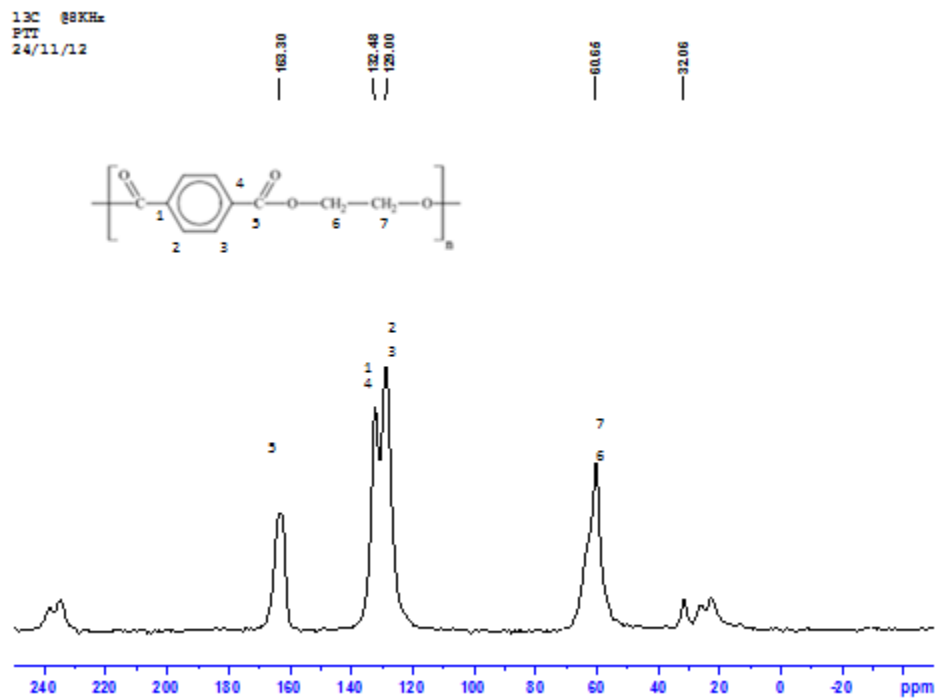


Figure 5.61: Solid-state ¹³C NMR spectrum of metofluthrin-impregnated nonwoven PET.

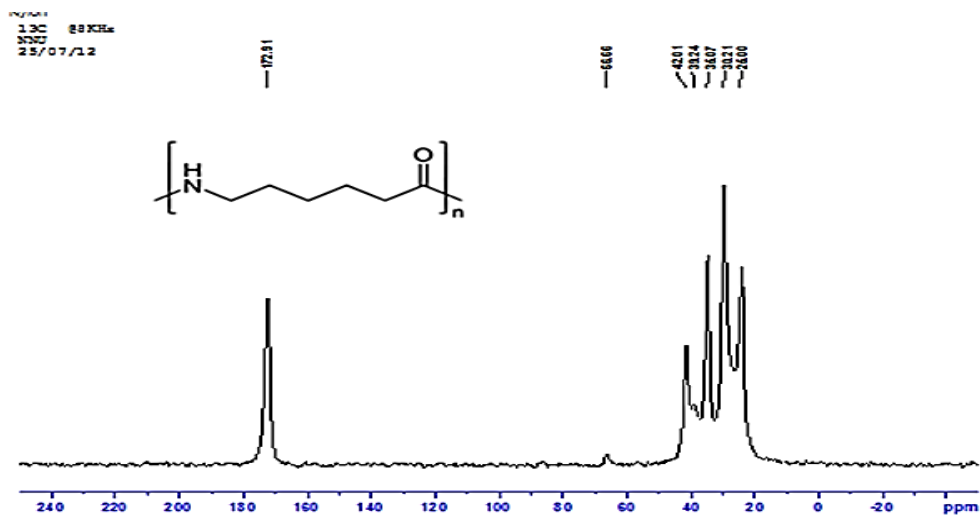


Figure 5.62: Solid-state ^{13}C NMR spectrum of untreated nonwoven nylon.

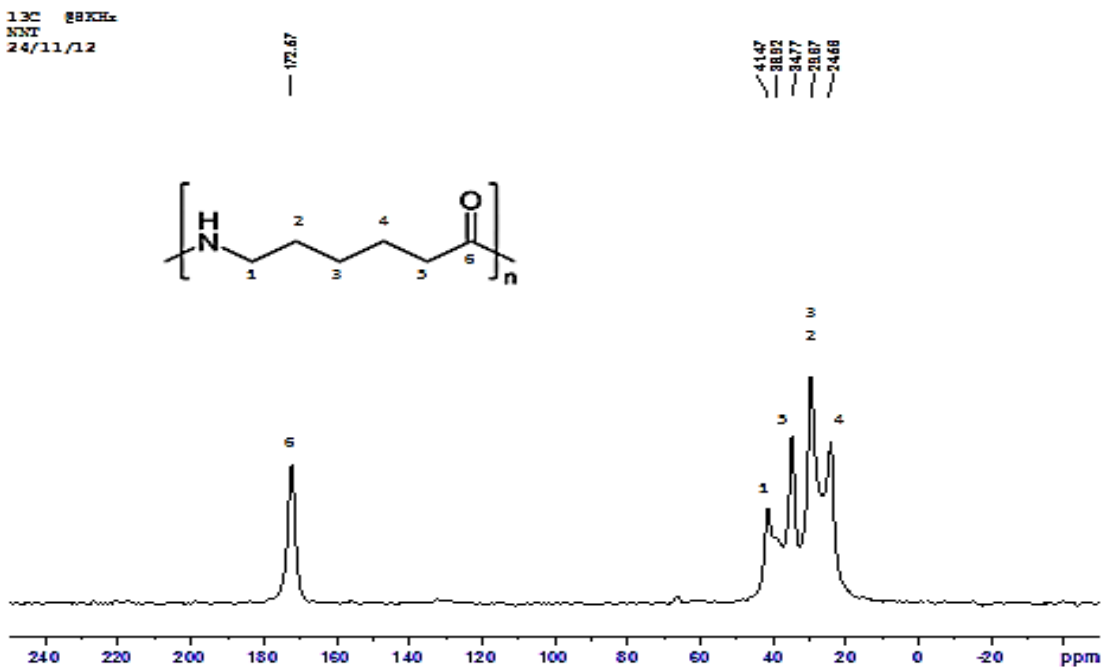


Figure 5.63: Solid-state ^{13}C NMR spectrum of metofluthrin-impregnated nonwoven nylon.

Table: 5.28 ¹³C NMR chemical shifts in untreated and metofluthrin impregnated substrates

Carbon environment	chemical shift (ppm)	Carbon environment	chemical shift (ppm)
Cellulose		Metofluthrin impregnated Cellulose	
C-O	104.14	C-O	103.99
C-C=O	87.94	C-C=O	87.68
C-OH	73.70	C-OH	73.79
C-C-OH	63.61	C-C-OH	64.43
Polypropylene		Metofluthrin impregnated Polypropylene	
C-H₂	42.91	C-H₂	43.10
C-H	25.06	C-H	25.47
C-H₃	20.85	C-H₃	20.47
PET		Metofluthrin impregnated PET	
C=O	163.8	C=O	163.3
C-Aromatic ring	129.03	C-Aromatic ring	129.0
C-H₂	60.72	C-H₂	60.65
Nylon		Metofluthrin impregnated Nylon	
C-H₂	42.91	C-H₂	43.10
C-H	25.06	C-H	25.47
C-H₃	20.85	C-H₃	20.47

5.14.3 Conclusion

A comprehensive study of solid state NMR (¹H and ¹³C) of various impregnated substrates were undertaken as represented in the figures. The assignments for signals obtained in both ¹H and ¹³C spectra for metofluthrin, as well as, the dosed substrates have been shown alongside. No evidence of any interaction between metofluthrin and the various substrates in question have been noted, as evident from the ¹H and ¹³C spectra of the treated and the untreated substrates. Therefore, clearly, spectral data seems to indicate the absence of any bulk interactions between metofluthrin and various substrates.

It can be reasonably conjectured therefore, that the differences in metofluthrin release profiles from the various substrates which has been experimentally determined are largely dependent on the substrate physical properties. Hence, it seems likely that in the absence of any chemical interactions, substrate properties like surface morphologies, surface areas, pore volumes and intrinsic porosities might be key determinants influencing release.

5.15 X-ray Diffraction

X-ray crystallography identifies the atomic and molecular structure of crystals, in which the atoms cause an incident X-ray beam to diffract into many specific directions. The measured angles and intensities of these diffracted beams produce a three-dimensional picture of the electron density within the crystal. In turn, this electron density provides the mean atom positions in the crystal along with chemical bonds, disorder, and other structural information.

In addition to characterizing the atomic structure of new materials, X-ray diffraction (XRD) distinguishes materials that appear similar in other experiments. It also determines unusual electronic or elastic properties of materials and shed light on chemical interactions and processes [158]. Here, the differences between substrate solid-state structures are evaluated by powder XRD to determine the crystalline or amorphous nature of these substrates. Fundamentally powder XRD was resorted to gain insights into the crystalline / amorphous nature of substrates.

5.15.1 Experimental details

Materials

Metofluthrin (purity 98.5%)

Isopropyl alcohol A.R

Cellulose, Nonwoven PET, Nonwoven polypropylene and Nonwoven nylon dosed with metofluthrin 32 mg/100 cm²

Table 5.29: Powder XRD experimental conditions.

Sr. No	Details	
1	Name of the equipment	Powder XRD
2	Manufacturer	Rigaku Corporation
3	Model No.	Miniflex II, Desktop X-ray diffractometer (Sr. No: FD-41521)
4	Operating conditions	2 θ , range 5–70°, step size 0.04°, scan speed 1.5°/min

5.14.2 Results

Table 5.30: XRD peak list of untreated cellulose.

2 θ (deg)	d (ang.)	Height (cps)	Int. I(cps·deg)	FWHM (deg)	Size
5.78 (6)	15.28 (16)	40 (6)	38 (3)	0.52 (9)	160 (29)
14.99 (10)	5.91 (4)	92 (9)	465 (30)	3.1 (2)	27.2 (19)
22.73 (2)	3.908 (4)	595 (22)	1264 (28)	1.68 (3)	50.4 (8)
28.4 (4)	3.14 (4)	14 (3)	10 (6)	0.7 (3)	121 (55)

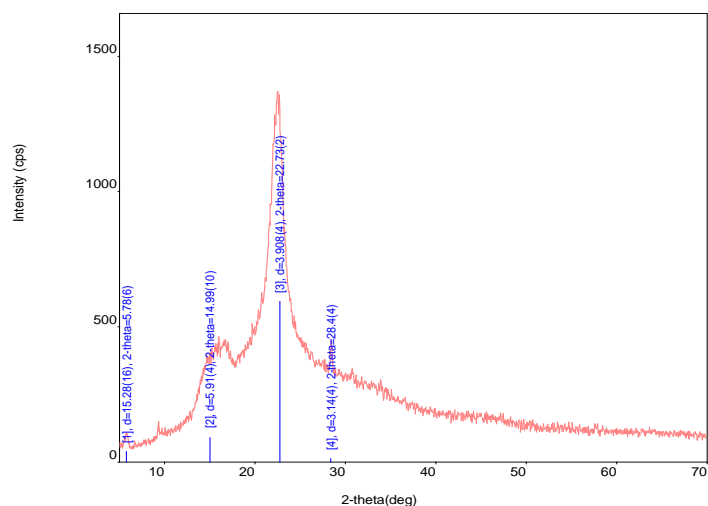


Figure 5.64: XRD plot of untreated cellulose.

Table 5.31: XRD peak list of untreated nonwoven nylon.

2 θ (deg)	d (ang.)	Height (cps)	Int. I(cps·deg)	FWHM (deg)	Size
20.096 (17)	4.415 (4)	552 (21)	1254 (36)	1.36 (4)	62.0 (18)
23.53 (2)	3.778 (3)	700 (24)	2893 (79)	2.44 (4)	34.8 (6)

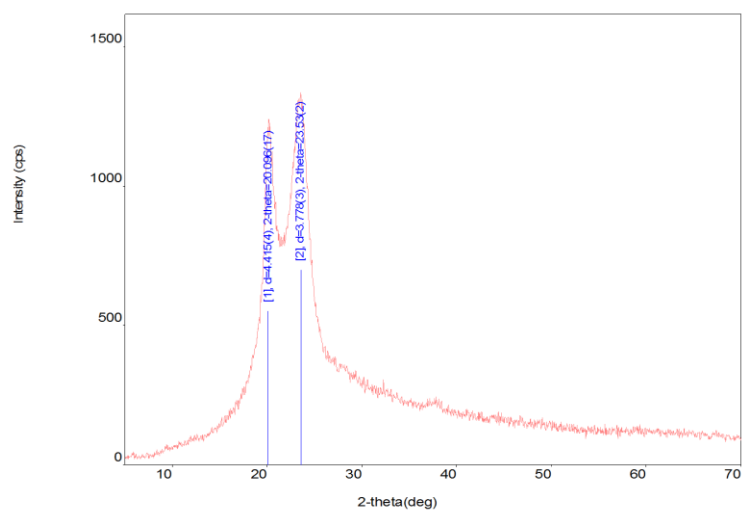


Figure 5.65: XRD plot of untreated nonwoven nylon.

Table 5.32: XRD peak list of untreated nonwoven polypropylene.

2 θ (deg)	d (ang.)	Height (cps)	Int. I(cps·deg)	FWHM (deg)	Size
13.956 (10)	6.340 (5)	1283 (33)	835 (10)	0.493 (11)	169 (4)
16.778 (8)	5.280 (3)	972 (28)	649 (7)	0.503 (9)	167 (3)
18.366 (10)	4.827 (3)	795 (26)	639 (8)	0.596 (11)	141 (3)
25.33 (4)	3.514 (6)	128 (10)	79 (7)	0.58 (4)	147 (10)
28.23 (3)	3.158 (3)	89 (9)	63 (3)	0.46 (4)	185 (16)

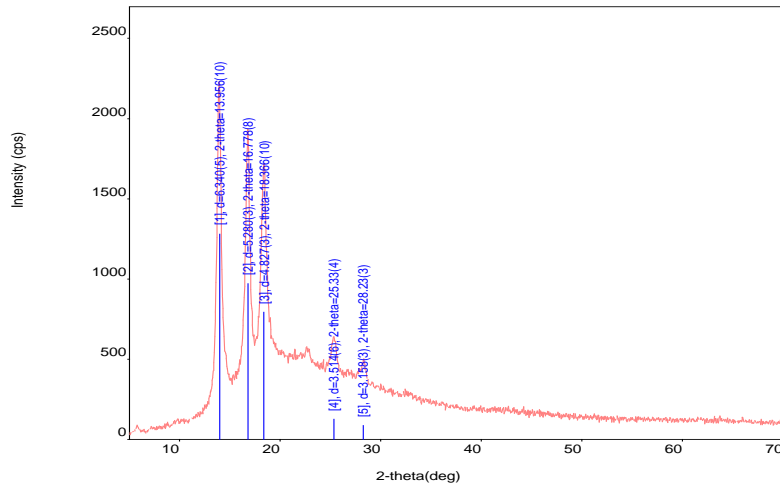


Figure 5.66: XRD plot of untreated nonwoven polypropylene.

Table 5.33: XRD peak list of untreated nonwoven PET.

2 θ (deg)	d (ang.)	Height (cps)	Int. I(cps·deg)	FWHM (deg)	Size
No measurable data					

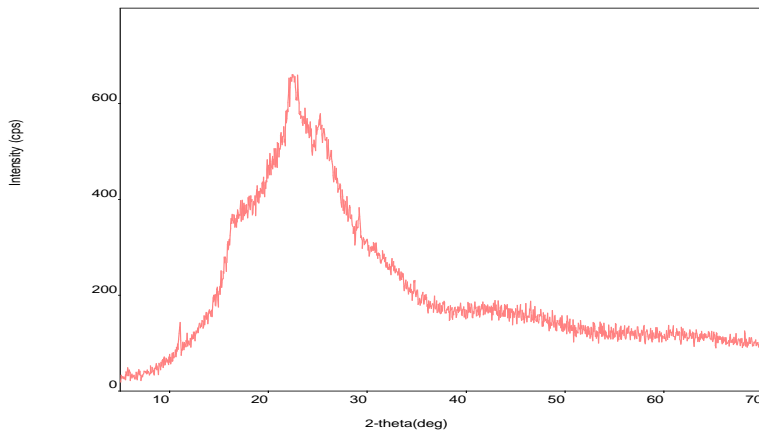


Figure 5.67: XRD plot of untreated nonwoven PET.

5.14.3 Conclusion

The relative crystallinities of cellulose and polymer substrates are characterized by powder XRD. The powder XRD patterns exhibit weak reflections with typically low intensities, indicating the weakly crystalline nature of the substrates. It can be commented, therefore, all substrates under investigation display a high degree of amorphosity, and thus weak interplanar ordering within their molecular structures.

CHAPTER 6

Model Formulation

This thesis seeks to develop a critical understanding of factors that influence metofluthrin release from metofluthrin impregnated polymer matrices. Effort have been directed to understand the role of external factors, such as temperature, wind velocity, porosities and exposed surface area amongst others in release process. Normal household conditions are expected to differ from controlled laboratory conditions of study. Hence, designing a model for these real-life factors is necessary. This chapter attempts to address metofluthrin diffusion following a model constructed using various controlled experimental data. A solution that integrates the effects of several variable factors in metofluthrin release is investigated. This design study is also expected to offer a much deeper understanding of the effect of substrate types on metofluthrin release.

The present study continues the assessment of metofluthrin release rates from a polymer matrix. The study is performed using a metofluthrin-impregnated matrix placed at the center of a room with a known bulk air velocity to determine the effect of several parameters on the metofluthrin release. These parameters include temperature, initial loading, wind velocity, substrate surface areas, and, the polymer substrate type in terms of their crystallinities and intrinsic properties.

Modelling studies were conducted using unsteady state mass balances and assuming that metofluthrin diffusivity inside the matrix follows an Arrhenius dependence on the temperature and the mass transfer coefficient linearly depends on the bulk fluid velocity. A model that measures metofluthrin diffusivity in cellulose is proposed using the data generated from our experimental studies. Experimental and simulation results were subsequently compared. Finally, the accuracy of the mathematical model is tested by applying this on a previously reported system and compared with current results.

In a polymer matrix, the active ingredient is transported from the matrix core to its surface being released to external atmosphere. For simplicity, a cellulose strip for loading of Metofluthrin of the same area is used (1200 cm^2) is considered to study the diffusion. In cellulose and polymer

systems, the air flow is parallel to the substrate surfaces, resulting in similar convection-related mass transfer. The effect of gravity is not considered. Therefore, substrate orientation (horizontal or vertical) is neglected.

6.1 Geometry

The model used for the simulation consists of a rectangular strip instead of a folded semicircular substrate to save time and efforts. To check whether this simplification introduces any appreciable change in the results, semicircular and circular strips exhibiting the same surface area are also studied. Circular and semicircular strips provide the same results as the rectangular strip, indicating that shape changes do not affect simulations when the surface area remains the same. Therefore, the rectangular strip is used for all simulations.

Figure 6.1 shows the system configuration. The cuboidal polymer matrix ($0.6 \text{ m} \times 0.1 \text{ m} \times 50 \text{ }\mu\text{m}$) is positioned at the center of a room ($3.1 \times 3.1 \times 3.1 \text{ m}^3$).

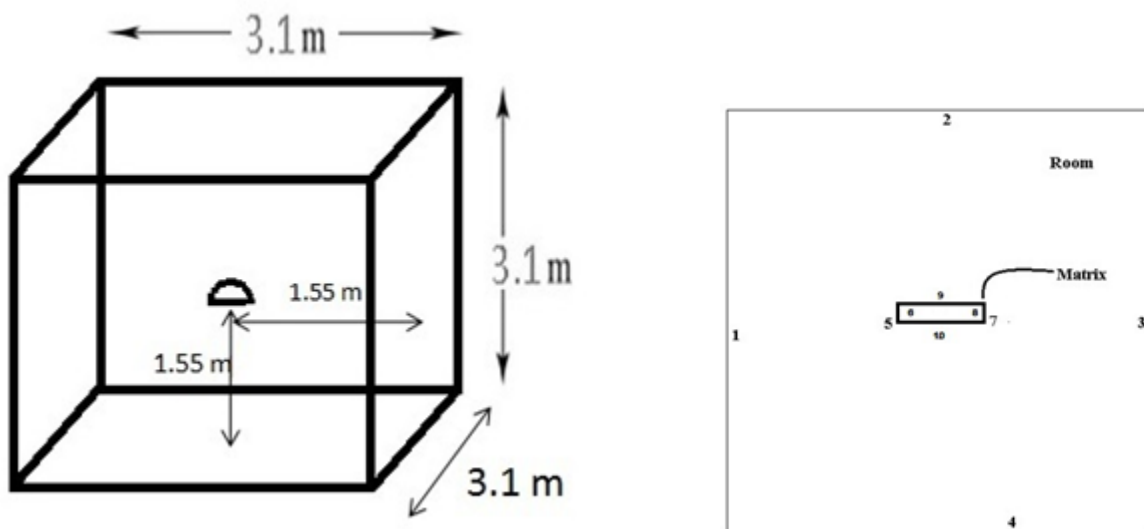


Figure 6.1: a) The polymer matrix inside the room.

b) System geometry.

6.2 Assumptions

It is assumed that the polymer matrix is kept at the geometric center of the room and metofluthrin diffuses from the matrix to the room. Several factors, such as temperature, initial loading, and air velocity, affect the release rate. Various assumptions are made during this study.

1. The density of the polymer matrix does not vary with space and time.
2. Mass transfer occurs only by diffusion inside the matrix and by diffusion and convection external to the matrix.
3. No reaction occurs anywhere, and thus the entire system is in thermodynamic equilibrium.
4. The matrix and metofluthrin are assumed to maintain their physical and chemical properties in this space and time.
5. The temperature inside and outside the polymer matrix is assumed to be uniform with space and time.

6.3 Mathematical model

Unsteady state mass balance is used to capture the movement of metofluthrin inside and outside the matrix. As discussed in the previous section, the mass transfer is assumed to follow a diffusion process inside the matrix, and, combine diffusion and convection outside the matrix. Therefore,

$$\frac{\partial C_1}{\partial t} = D_{eff} \left(\frac{\partial^2 C_1}{\partial x^2} + \frac{\partial^2 C_1}{\partial y^2} + \frac{\partial^2 C_1}{\partial z^2} \right) \quad \text{Equation 6.1}$$

Where C_1 is the concentration of metofluthrin in the matrix (in mol/m³) and D_{eff} is the effective diffusion coefficient of metofluthrin in the matrix (in m²/s).

The mass balance equation in the surrounding air is given by [48].

$$\frac{\partial C_2}{\partial t} + \left(u_x \frac{\partial C_2}{\partial x} + u_y \frac{\partial C_2}{\partial y} + u_z \frac{\partial C_2}{\partial z} \right) = D_a \left(\frac{\partial^2 C_2}{\partial x^2} + \frac{\partial^2 C_2}{\partial y^2} + \frac{\partial^2 C_2}{\partial z^2} \right) \quad \text{Equation 6.2}$$

Where C_2 is the concentration of metofluthrin in the air (in mol/m³), D_a is the diffusion coefficient of metofluthrin in the air (1×10^{-5} m²/s, and μ_x and μ_y are the air velocities along x and y axis (in m/s), respectively).

Boundary conditions are established according to the number assignment shown in Figure 6.1. The flux at the boundary is directly proportional to the concentration difference at the surface. The constant concentration boundary condition and the concentration build-up are also studied.

Boundary conditions for the polymer matrix could be represented as follows:

$$n \cdot (-D_{eff} \nabla C_1) = 0 \quad \text{At the centre (symmetry)}$$

$$-n \cdot N = -k_c (C_{1b} - C_{2b}) \quad \text{At boundaries 5,6,7,8,9,10}$$

The boundary conditions for the room are defined as follows:

$$-n \cdot N = 0 \quad (\text{Insulation}) \text{ at boundaries 1,2,3,4}$$

$$-n \cdot N = k_c (C_{1b} - C_{2b}) \quad \text{At boundaries 5,6,7,8,9,10}$$

Where, C_{1b} and C_{2b} are the concentrations of metofluthrin at the boundary inside and outside the polymer matrix, respectively, N is the vector quantity for the velocity of metofluthrin along the x axis at any point, and k_c is the mass transfer coefficient at the matrix–air interface. Here, the μ_x boundary condition applies, in which μ_x is proportional to the concentration difference at the boundary.

Initially,

$$C_1 = C_{10} \quad \forall_x \quad \text{At } t=0 \text{ (Polymer Matrix)}$$

$$C_2 = 0 \quad \forall_x \quad \text{At } t=0 \text{ (Room)}$$

Where C_{10} amounts to 61.05, 120.26, and 180.38 mol/m³ when the initial loading of metofluthrin equals 65, 130, and 195 mg, respectively. The velocity inside the room varies from 0.1 to 1 m/s.

A molecule impregnated into a solid needs to diffuse through this solid before getting released externally. The average thermal energy of a molecule (0.026 eV/molecule) is much lower than that needed for a jump (1 eV/molecule). A jump only occurs when a fluctuation in the system may result in a concentration of energy at one point. The frequency of this fluctuation is exponentially temperature dependent according to an Arrhenius relation. In addition, the probability of the jump is exponentially temperature dependent. Therefore, the expression of diffusion must capture these effects using an Arrhenius expression for the diffusivity.

The Arrhenius equation has been applied to diffusion coefficients. Kolhapure and Venkatesh [119] used the Arrhenius relationship between diffusion coefficients and temperature to explain the movement of water inside a hygroscopic medium, a solid matrix that strongly interact with water. In their system, water was assumed to diffuse through the solid matrix, driven by the concentration gradient, similar to our system.

The same relationship has been exploited by Dhoot *et al.* to study eugenol diffusion from linear low-density polyethylene films [160]. It has also been utilized by Gegner [172] to explain the diffusion of carbon in a Fe–C austenite lattice. In this system, carbon was assumed to diffuse through the Fe–C austenite lattice according to the concentration gradient. Here, a polymer matrix is assumed to partly behave like a crystal lattice.

Therefore, the diffusion coefficient of metofluthrin in the polymer matrix is expressed as follows:

$$D_{eff} = A. \exp\left(-\frac{E_a}{RT}\right) \quad \text{Equation 6.3}$$

Where A is the pre-exponential factor (m^2/s), E_a is the activation energy of the molecule diffusion (J/mol), and R is the universal gas constant (8.314 J/Kmol).

At the boundary, mass transfer follows a convection process. According to Osbourne Reynolds [118], the mass transfer between two phases consists of natural diffusion, which occurs even if the bulk fluid in one phase is at rest, and eddies due to bulk fluid movement. These eddies give rise to mixing and continually brings fresh molecules from the bulk in contact with the surface. Consequently, the mass transfer coefficient should be a linear function of velocity.

This linear dependence of the mass transfer coefficient on the velocity has been mentioned previously. Zhang *et al.* [123] investigated the emission of volatile organic compounds from field laboratory emission cells comprising an inner chamber formed by a wire and mesh matrix. They used this linear model to explain the mass transfer rate of these compounds from this matrix system. The present system also involves mass transfer from a polymer matrix in the air.

Ghosh *et al.* also used a similar relationship to describe the dissolution of oxygen from bulk to living cells. Their system involved an inter-phase mass transfer, similar to the present system [173]. The linear dependence of the mass transfer coefficient has been described by Cussler [118].

If v is the velocity of the bulk fluid, then

$$k_c = a + bv \quad \text{Equation 6.4}$$

Where a and b are constants.

The model relies on four parameters, including the pre-exponential factor, the energy of activation E_a , and constants a and b . The system consists of two partial differential equations coupled together. Because it cannot be solved analytically, a simplified system comprising only one partial differential equation is considered. In this simplified system, a material diffuses out from a semi-infinite solid substrate. Furthermore, the outside medium is considered infinite, giving an outside concentration of zero.

Values for the pre-exponential factor A and the energy of activation E_a are determined using the simplified system. For each system, the solution comprises a D_{eff} term, which is substituted with Eq. 6.3 and then fitted with experimental data for zero bulk air velocity ($v = 0$).

This fit gives A and E_a values of $4.54 \times 10^{-12} \text{ m}^2/\text{s}$ and 23824 J/mol , respectively (Figure 6.2), which are quite close to the values obtained by the Carslaw–Jaeger solution ($A = 4.3 \times 10^{-12} \text{ m}^2/\text{s}$, $E_a = 23754 \text{ J/mol}$).

The mass transfer coefficient is estimated from experimental data for different bulk air velocities to find a and b (Figure 6.6). The k_c values are chosen so that simulation results satisfactorily match the experimental data. Because several k_c values are available for different velocities, the constants a and b are found by linear fitting.

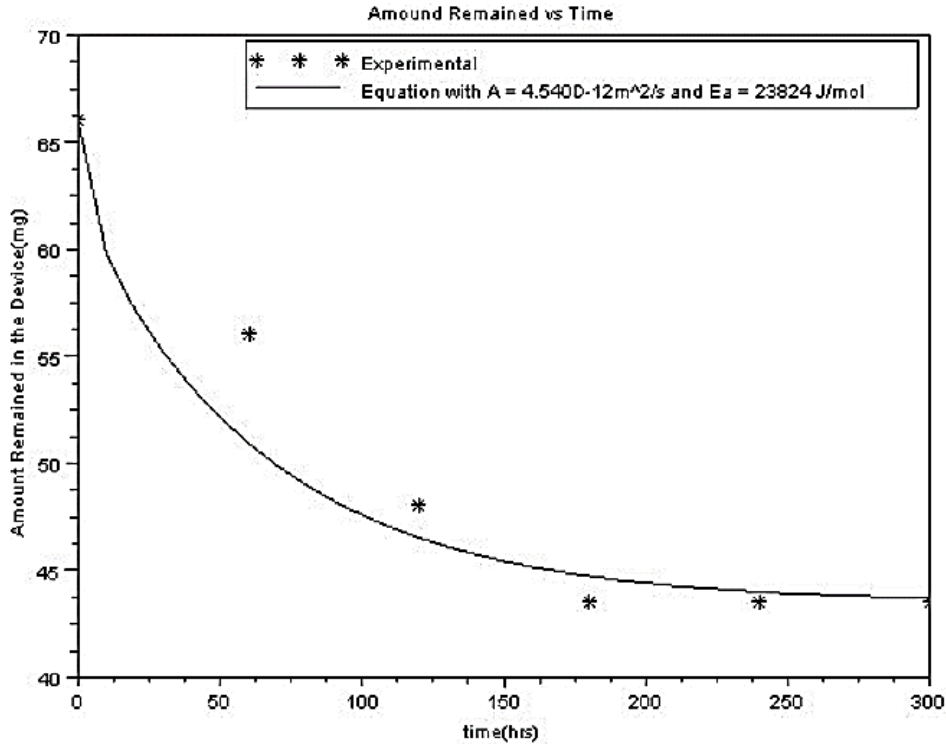


Figure 6.2: Analytical solution fitted with experimental data for $v = 0$. Experimental data were reported at temperature of 27°C for an initial loading of 61.05 M . The obtained A and E_a values amount to $4.54 \times 10^{-12}\text{ m}^2/\text{s}$ and 23824 J/mol , respectively.

6.4 Computational approach

The system is solved by the finite element technique using the commercial COMSOL Multi-physics 3.5a software. In this technique, both matrix and air domain are discretized into a total number of 6524 finite elements. In particular, the mesh consists of 116 tetrahedral elements inside the matrix and 6408 tetrahedral elements within the air domain. Figure 6.3 shows the computer model used for the simulation.

As discussed earlier, a rectangular matrix is used for simplicity. The effect of changing the polymer matrix geometry has been discussed above. The system is solved for 300 h for a typical computational time of about 30 min.

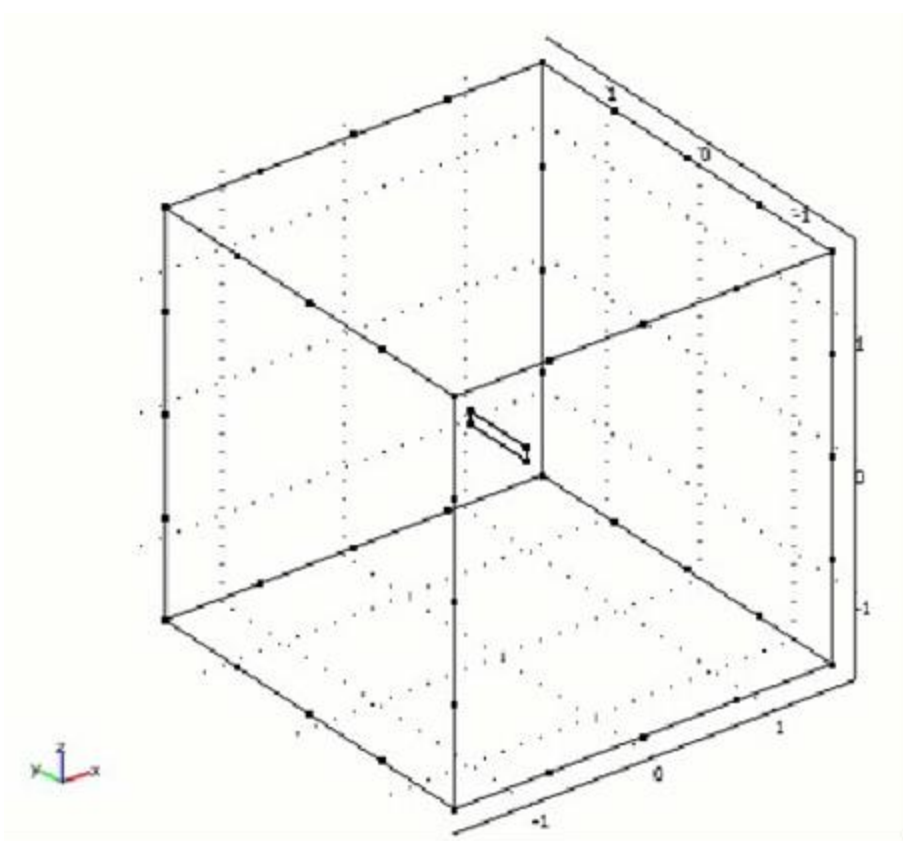


Figure 6.3: Model used for the three-dimensional simulation.

Although A and E_a values have been found, a and b need to be determined. This chapter describes how these values are evaluated and presents a validation of the model. However, it is important to validate the software used first.

6.4.1 Software validation

Software is validated by choosing a dummy system and performing a simulation with it. The analytical result is then compared with the simulation result. To check the accuracy of the software, a simple system of diffusion into a falling liquid is considered, in which a gas A is absorbed by a laminar falling film of liquid B . Gas A is assumed to be only slightly soluble in B [174] Therefore, the viscosity of B is not affected.

If D_{AB} is the diffusivity of A into B , then

$$v_z \frac{\partial C_A}{\partial z} = D_{AB} \frac{\partial^2 C_A}{\partial x^2} \quad \text{Equation 6.5}$$

The boundary conditions are as follows:

$$\text{At } z = 0, C_A = 0$$

$$\text{At } x = 0, C_A = C_{A0}$$

$$\text{At } x = \delta, \frac{dC_A}{dx} = 0$$

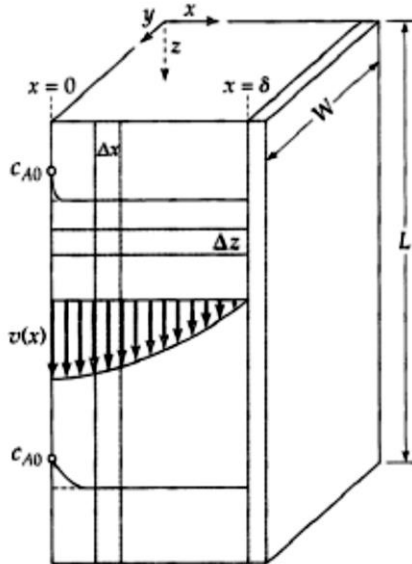


Figure 6.4: Gas absorption by a falling film [178].

The solution is written as follows:

$$\frac{C_A}{C_{A0}} = 1 - \operatorname{erf} \frac{x}{\sqrt{4D_{AB}z/v_{max}}} \quad \text{Equation 6.6}$$

Where, erf is the error function of x , C_A is the concentration of gas molecule A , and C_{A0} is the concentration of gas molecule A at the interface of falling film B .

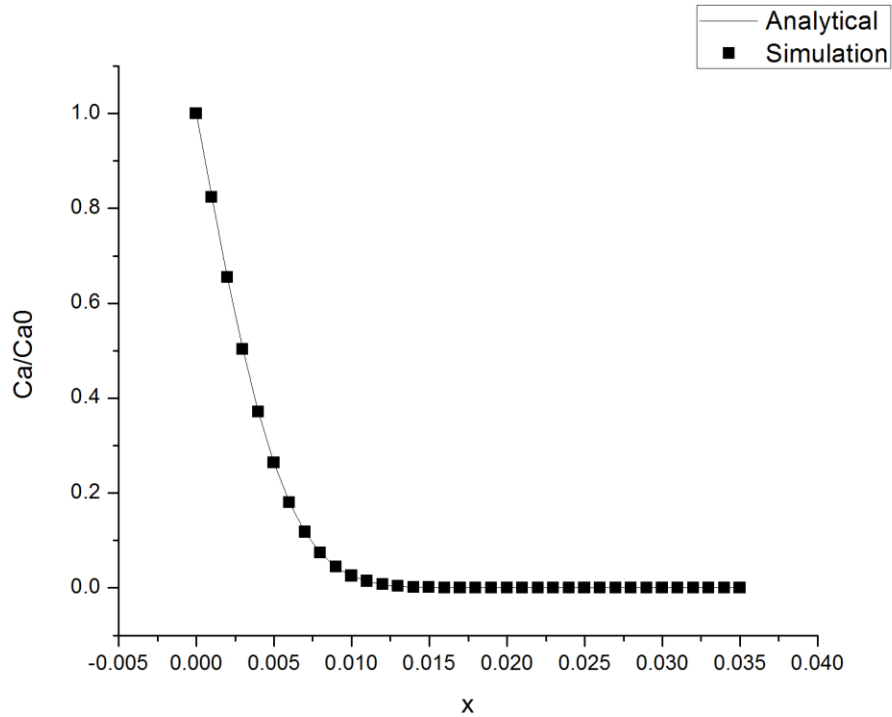


Figure 6.5: Validation of the modelling software.

Figure 6.5 shows the analytical and simulated plots of C_A/C_{A0} as a function of the distance x . Simulation and analytical results match, validating the modelling software.

6.4.2 Evaluation of a and b

The constants a and b are evaluated using the experimental data reported at different bulk air velocities ($v = 0, 0.2, 0.25, 0.5, \text{ and } 0.8 \text{ m/s}$). Simulations are performed with known values of A and E_a and a k_c value is found for each velocity. Then, a and b values are obtained using a linear fit of k_c with v .

As discussed in Section 6.4.1, $A = 4.54 \times 10^{-12} \text{ m}^2/\text{s}$ and $E_a = 23824 \text{ J/mol}$.

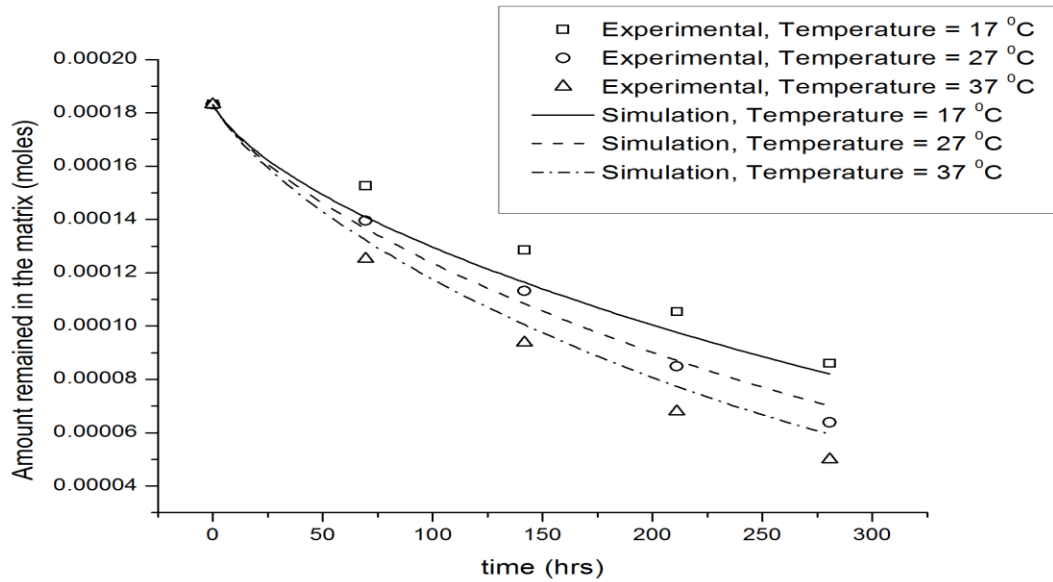


Figure 6.6: Effect of temperature on metofluthrin release. Experimental data are reported for an initial concentration of 61.05 M and air velocity of 0.2 m/s. Simulations are run with $A = 4.54 \times 10^{-12} \text{ m}^2/\text{s}$, $E_a = 23824 \text{ J/mol}$, and $kc = 6.25 \times 10^{-11} \text{ m/s}$.

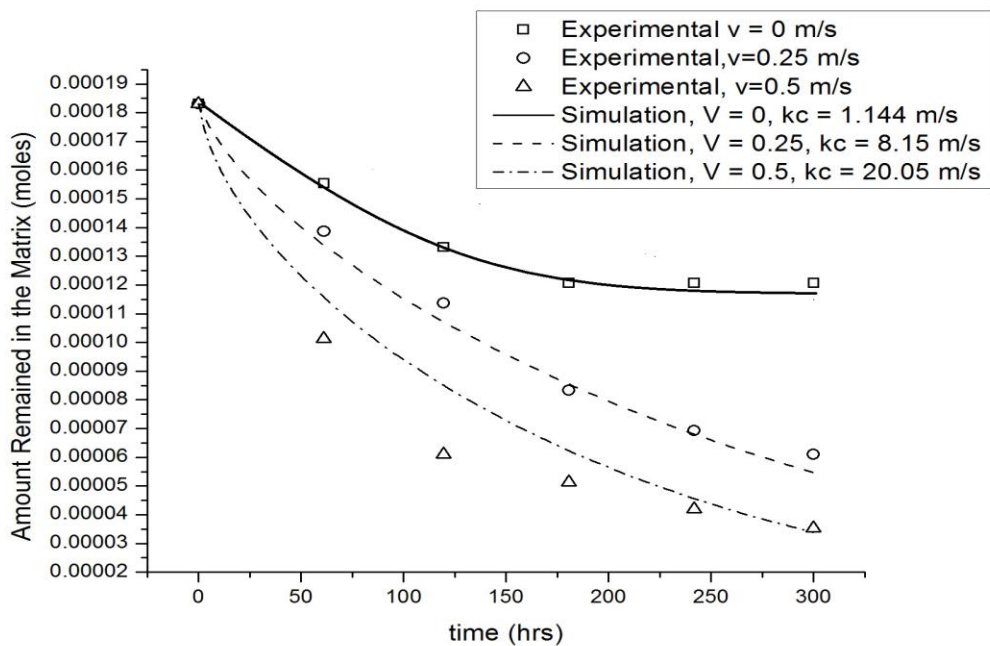


Figure 6.7: Effect of air velocity on metofluthrin release. Experiments are conducted at a temperature of 27 °C and an initial loading of 61.05 M. Simulations are run with $A = 4.54 \times 10^{-12} \text{ m}^2/\text{s}$ and $E_a = 23824 \text{ J/mol}$.

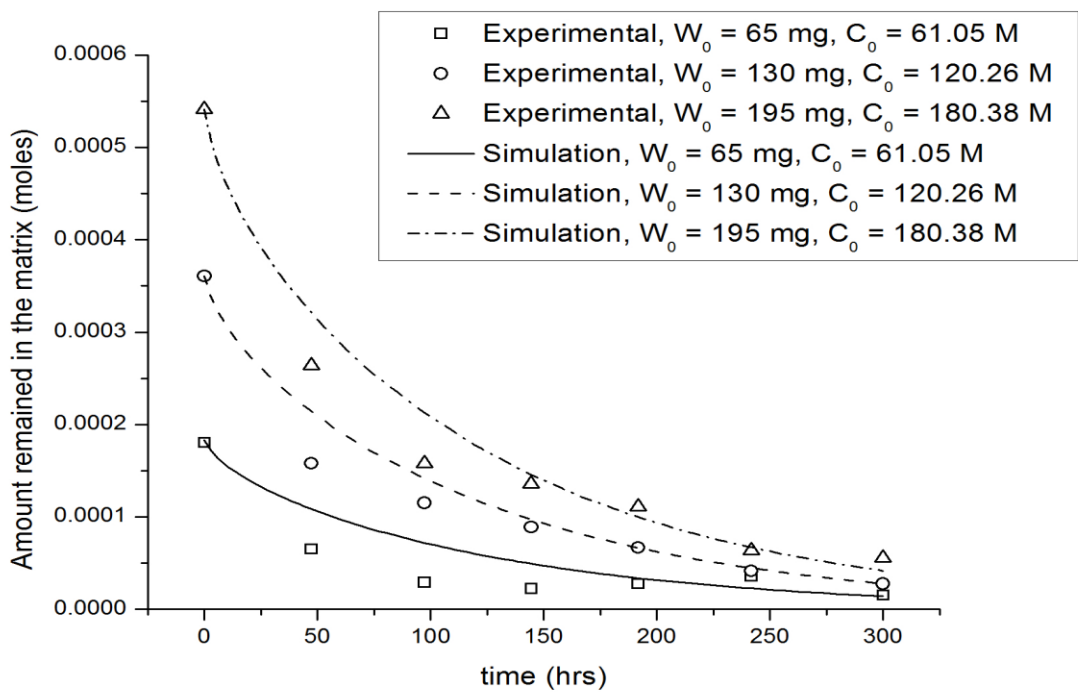


Figure 6.8: Effect of concentration on metofluthrin release. Experimental data are performed at a temperature of 27 °C and an air velocity of 0.8 m/s. Simulations are run with $A = 4.54 \times 10^{-12} \text{ m}^2/\text{s}$, $E_a = 23824 \text{ J/mol}$, and $kc = 25.67 \times 10^{-11} \text{ m/s}$.

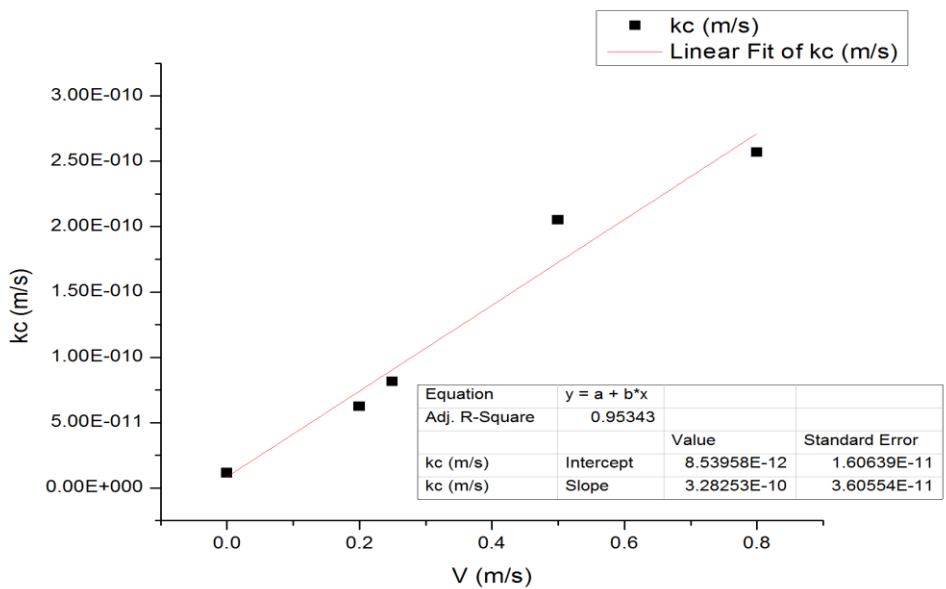


Figure 6.9: Linear fit of k_c with v .

In statistics, the coefficient of determination (R^2) indicates how well data fit a statistical model, and its main purpose is either the prediction of future outcomes or the testing of hypotheses based on other related information.

The use of an adjusted R^2 is an attempt to take account of the phenomenon of the R^2 automatically and spuriously increasing when extra explanatory variables are added to the model.

Table 6.1: Values of the parameters A , E_a , a , and b

Parameters	Values
E_a	23824 J/mol
A	$4.54 \times 10^{-12} \text{ m}^2/\text{s}$
a	$0.854 \times 10^{-11} \text{ m/s}$
b	$32.82 \times 10^{-11} \text{ m/s}$

As shown in Table 6.1, the activation energy of the process is quite close to common activation energies of diffusion (approximately 25 kJ/mol). The order of magnitude of the effective diffusion coefficient comes out at $10^{-16} \text{ m}^2/\text{s}$. A plausible reason for this low order of magnitude is discussed below.

6.5 Model accuracy testing

To test the accuracy of the model, the system is solved using the parameter values obtained for an air velocity of 1 m/s. The results are compared with the experimental data.

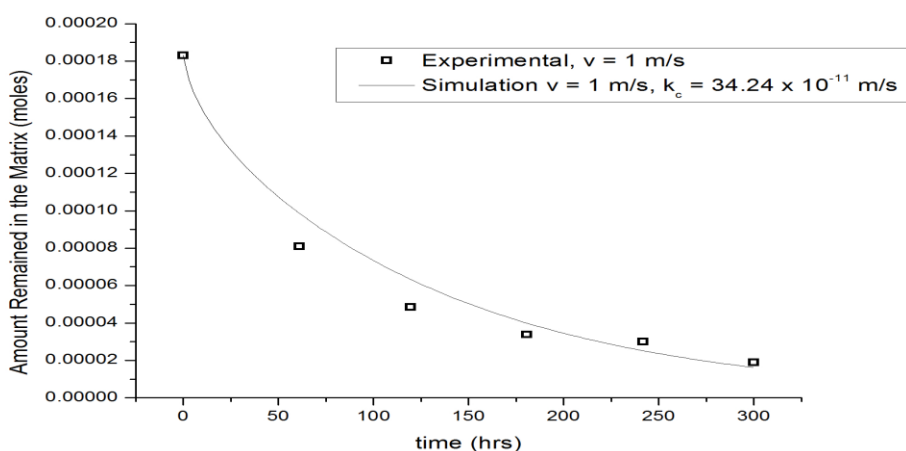


Figure 6.10: Metofluthrin release for an air velocity of 1 m/s. Experimental data are acquired at a temperature of 30 °C and an initial loading of 61.05 M. Simulations are performed with $A = 4.54 \times 10^{-12} \text{ m}^2/\text{s}$, $E_a = 23824 \text{ J/mol}$, $a = 0.85 \times 10^{-11} \text{ m/s}$, and $b = 32.82 \times 10^{-11} \text{ m/s}$.

The accuracy of the model is further assessed by replicating a system reported by Lucas *et al* [97]. In this system, a Denguri strip impregnated with 200 mg of metofluthrin (Figure 6.12) is suspended in a fumehood at an air velocity of 0.6 m/s [175–177]. The model is solved with the parameter values found using the Carslaw–Jaeger solution, and simulation results are compared with experimental data.

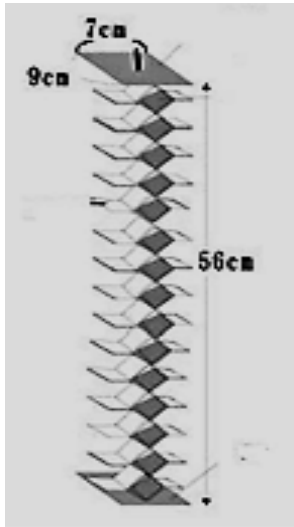


Figure 6.11: Denguri strip used by Lucas et al. This arrangement combines eight ($9 \times 7 \text{ cm}^2$) squares (Figure 6.10).

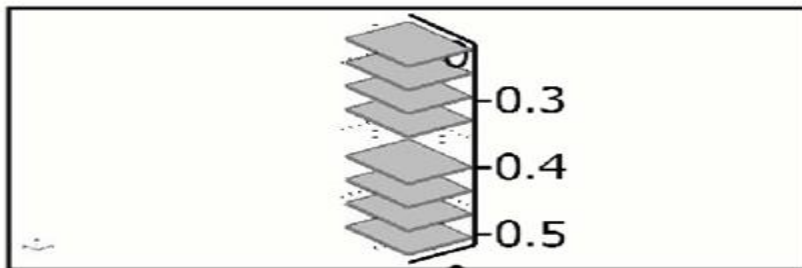


Figure 6.12: Computer model generated in COMSOL.

Simulation and experimental results are shown in Figure 6.13.

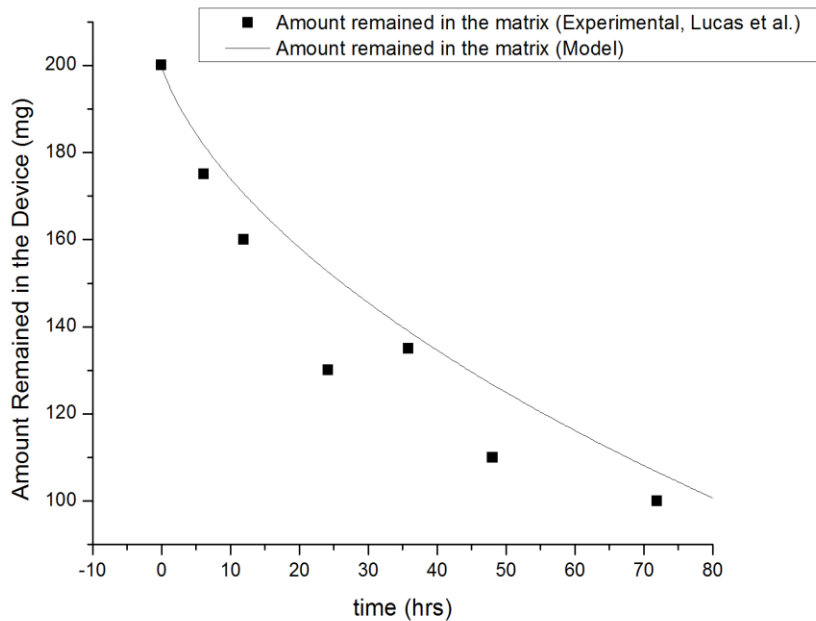


Figure 6.13: Amount remained in the device. Experimental data are acquired at 25 °C and an air velocity of 0.6 m/s. Simulations are performed with $A = 4.54 \times 10^{-12} \text{ m}^2/\text{s}$, $E_a = 23824 \text{ kJ/mol}$, $a = 0.85 \times 10^{-11} \text{ m/s}$, and $b = 32.82 \times 10^{-11} \text{ m/s}$.

6.6 Effect of the polymer matrix geometry

As discussed previously, it is important to check if a change in matrix geometry introduces any change in the results. To this end, three geometries including rectangular, circular, and semicircular are taken.

Since, the actual matrix is a semicircular cellulose substrate with many folds, a full, circular matrix is chosen for the simulation instead of the rectangular strip.

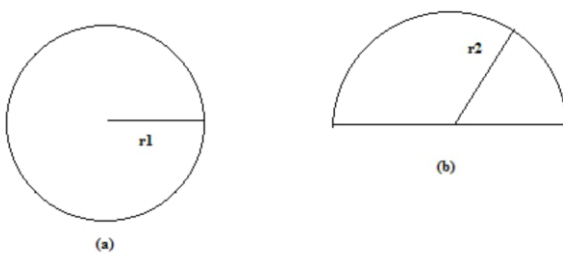
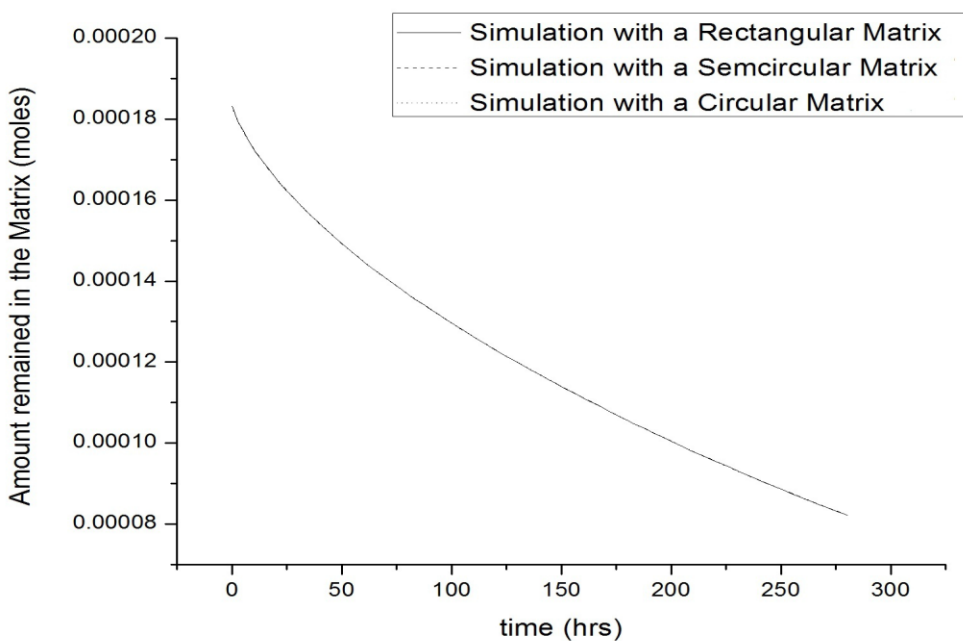


Figure 6.14: Circular and semicircular strips are chosen for the simulation.

The external exposed area of the matrix amounts to 1200 cm² (with both sides included). Therefore, the radii of the circular (r1) and semicircular (r2) matrices equal 13.82 and 19.54 cm, respectively.

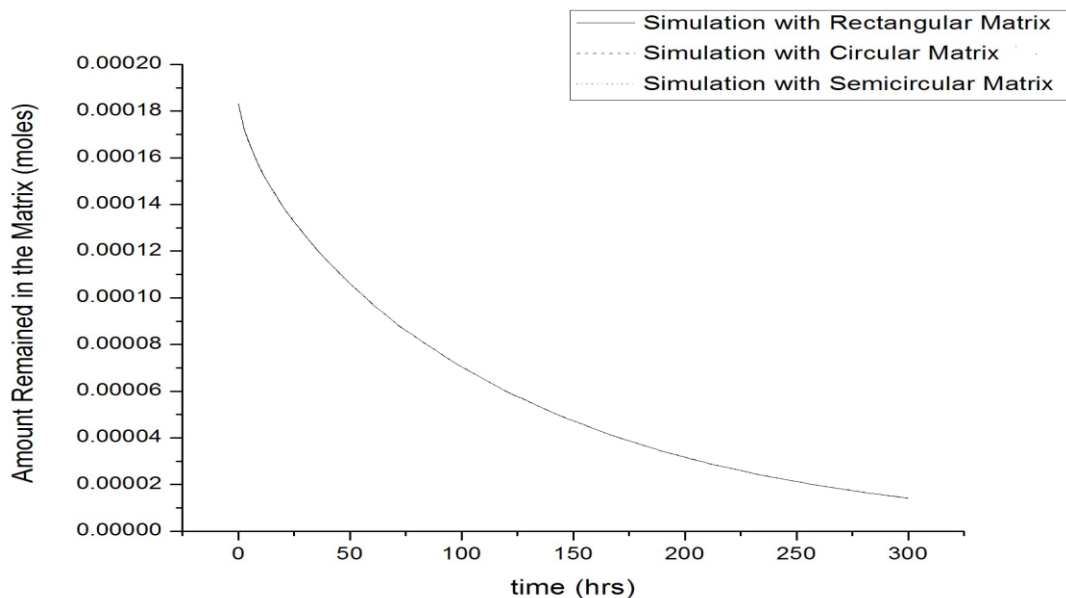
To determine whether changing the polymer matrix geometry affect metofluthrin release, simulations were conducted for three polymer matrix geometries (all with thickness 5×10^{-5} m) including a rectangular strip (0.1×0.6 m²), a semicircular strip with a radius of 19.54 cm, and a circular strip with a radius of 13.82 cm

All these simulations use a uniform velocity profile. To check if the geometry introduces any changes using the exact velocity profile, the mass transfer coefficient is allowed to vary with space (Section 6.7).



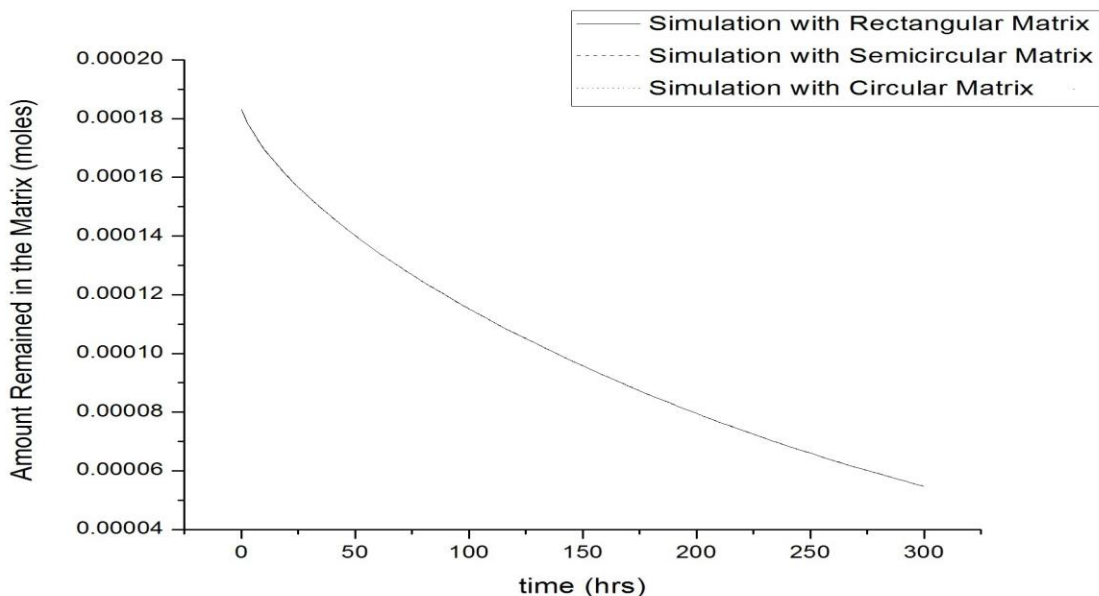
Note: All three lines have converged

Figure 6.15: Amounts of metofluthrin retained in the matrix as a function of time for rectangular, semicircular, and circular geometries at 27 °C with an initial loading of 61.05 M and an air velocity of 0.2 m/s. Simulations are performed with $A = 4.54 \times 10^{-12}$ m²/s, $E_a = 23824$ J/mol, $a = 0.85 \times 10^{-11}$ m/s, and $b = 32.82 \times 10^{-11}$ m/s.



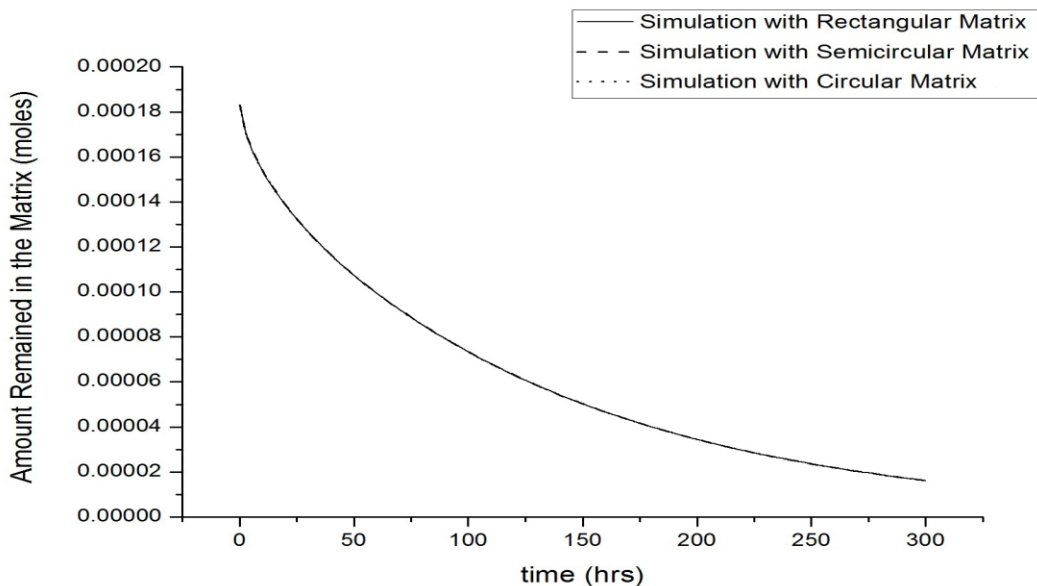
Note: All three lines have converged.

Figure 6.16: Comparison between rectangular, semicircular, and circular geometries at 27 °C with an initial loading of 61.05 M and an air velocity of 0.8 m/s. Simulations are performed with $A = 4.54 \times 10^{-12} \text{ m}^2/\text{s}$, $E_a = 23824 \text{ J/mol}$, $a = 0.85 \times 10^{-11} \text{ m/s}$, and $b = 32.82 \times 10^{-11} \text{ m/s}$.



Note: All three lines have converged.

Figure 6.17: Comparison between rectangular, semicircular, and circular geometries at 30 °C for an initial loading of 61.05 M and an air velocity of 0.25 m/s. Simulations are conducted with $A = 4.54 \times 10^{-12} \text{ m}^2/\text{s}$, $E_a = 23824 \text{ J/mol}$, $a = 0.85 \times 10^{-11} \text{ m/s}$, and $b = 32.82 \times 10^{-11} \text{ m/s}$.



Note: All three lines have converged.

Figure 6.18: Amounts of metofluthrin retained in rectangular, semicircular, and circular matrices as a function of time at 27 °C for an initial loading of 61.05 M and an air velocity of 1 m/s. Simulations are performed with $A = 4.54 \times 10^{-12} \text{ m}^2/\text{s}$, $E_a = 23824 \text{ J/mol}$, $a = 0.85 \times 10^{-11} \text{ m/s}$, and $b = 32.82 \times 10^{-11} \text{ m/s}$.

The simulation plots were found to be exactly the same for all three geometries, clearly indicating that changes in geometry do not affect the results. Therefore, simulations performed using a rectangular strip as the polymer matrix introduces no change, hence, could be used as a convenient geometry.

6.7 Effect of bulk air velocity profile

As discussed in earlier section, simulations are conducted using a uniform velocity profile primarily to save computational time and effort. To check if this impacts on the results, some fan geometries are chosen and matrix-free models are designed for each of them. Their angular velocities (rpm) are adjusted so that the air velocity at the center matches the required velocity. The steady-state solution is imported in the main model, which is run using velocity-dependent kc values.

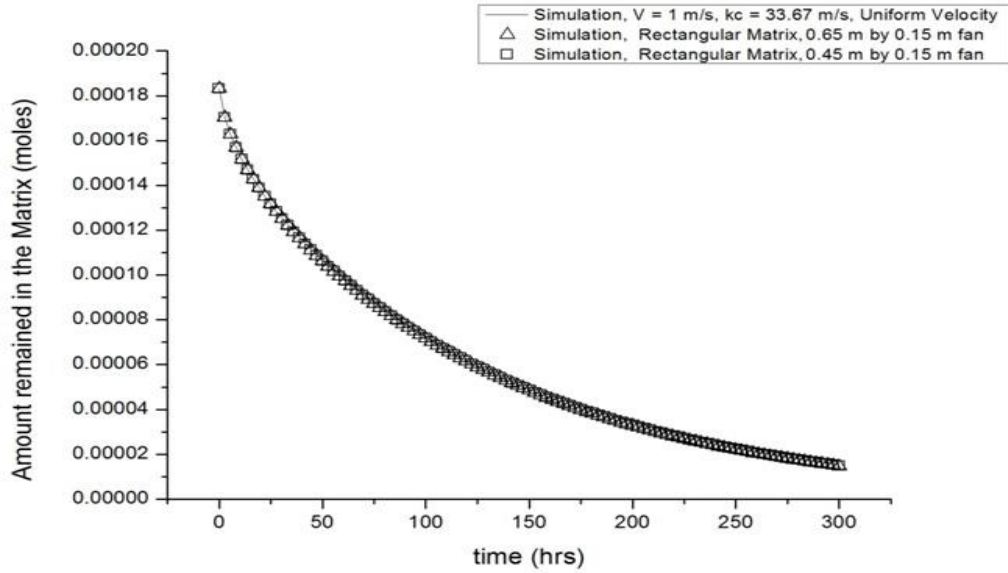
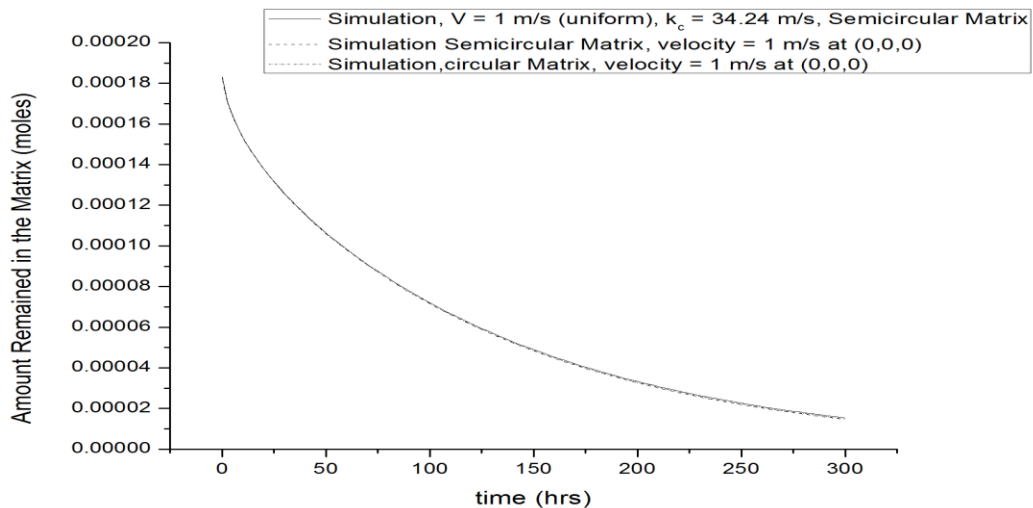


Figure 6.19: Simulation results run using a rectangular strip as the polymer matrix. Simulations were conducted at 27 °C for an initial loading of 61.05 M and an air velocity of 1 m/s at (0, 0, 0).

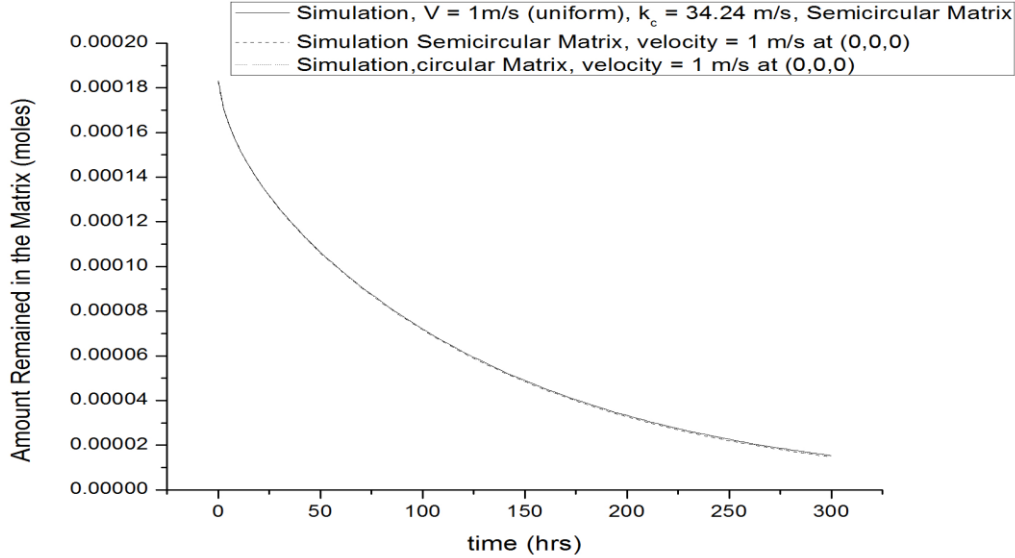
The mass transfer coefficient varies according to the spatial wind velocity.

With the rectangular matrix, the results are not very different for each fan configuration. To check if the same is true for other polymer matrix geometries, the same algorithm is adopted for semicircular and circular matrices.



Note: All three lines have converged.

Figure 6.20: Simulation results obtained using a $0.65 \times 0.45 \text{ m}^2$ fan. Simulations are conducted at 27 °C for an initial loading of 61.05 M and an air velocity of 1 m/s at (0, 0, 0).



Note: All three lines have converged.

Figure 6.21: Simulation results obtained using a $0.45 \times 0.15 \text{ m}^2$ fan. Simulations are conducted at $300 \text{ }^\circ\text{C}$ for an initial loading of 61.05 M and an air velocity of 1 m/s at $(0, 0, 0)$.

The mass transfer coefficient varies according to spatial wind velocity.

Figures 6.19–6.21 show that when the exact velocity profile is used, velocity-dependent variations of k_c do not introduce appreciable changes in the results. The computational time is considerably higher when the exact velocity is used. Therefore, the uniform velocity profile is preferable to its exact counterpart.

6.8 Effect of changing surface area

Experimental data are available for different matrix surface areas. To capture the effect of surface area, simulations are performed using semicircular matrices exhibiting different areas at $27 \text{ }^\circ\text{C}$ for an initial loading of 66 mg and a bulk air velocity of 0.5 m/s at $(0, 0, 0)$. In addition, $A = 4.54 \times 10^{-12} \text{ m}^2/\text{s}$, $E_a = 23824 \text{ J/mol}$, and $k_c = 17.26 \text{ m/s}$.

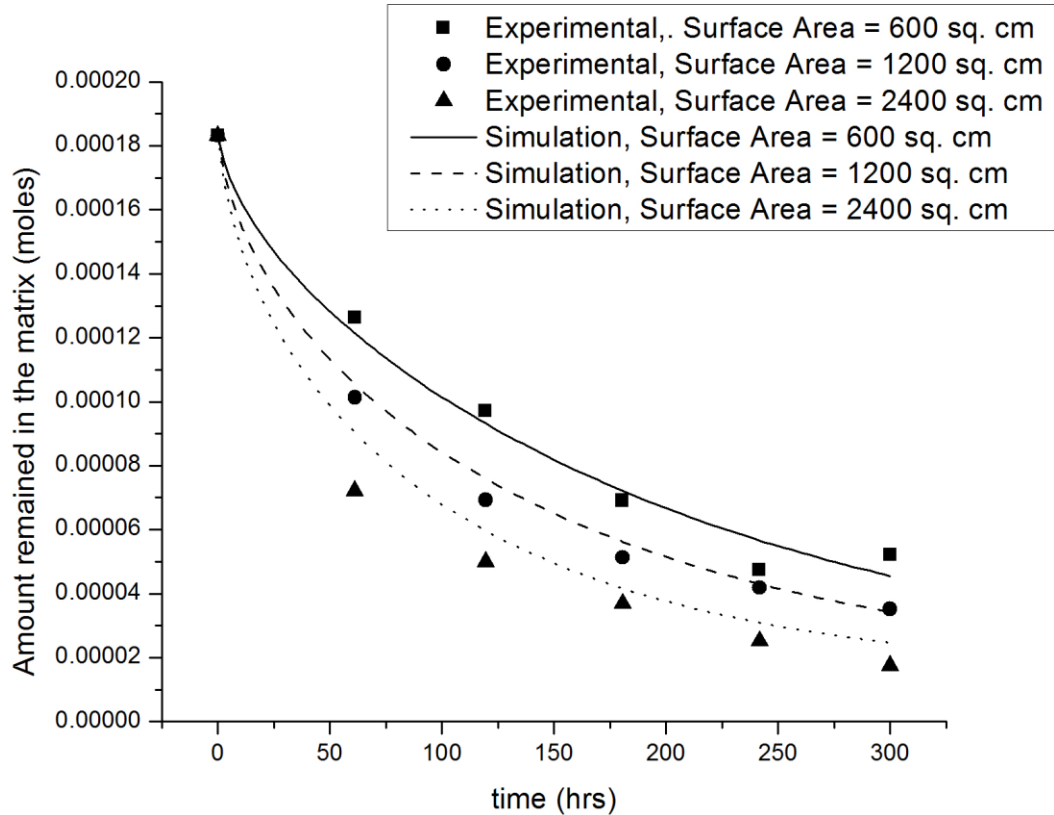


Figure 6.22: Effect of surface area on metofluthrin release. Experiments are conducted at 27 °C for an initial loading of 66 mg and a bulk air velocity of 0.5 m/s. Simulations are performed $A = 4.54 \times 10^{-12} \text{ m}^2/\text{s}$, $E_a = 23824 \text{ J/mol}$, and $kc = 17.26 \text{ m/s}$.

6.9 Parameter evaluation using other substrates on metofluthrin release

For all reported results, experiments are conducted using a cellulose matrix. All unknown parameters are applicable for other polymers as well. Experimental data are available for a few other polymer substrates at 30 °C for an initial loading of 61.05 M and a bulk air velocity of 0.5 m/s. Although an exact evaluation of all parameters is not possible (because it would require more experimental data), their determination is attempted as follows. Although the mass transfer coefficient significantly depends on the material, the constants a and b are assumed to mostly depend on the bulk fluid. Consequently, in a very crude attempt, the mass transfer coefficient is kept constant while the effective diffusion coefficient is varied to obtain a satisfactory match between simulation and experimental data for PET and nylon surfaces.

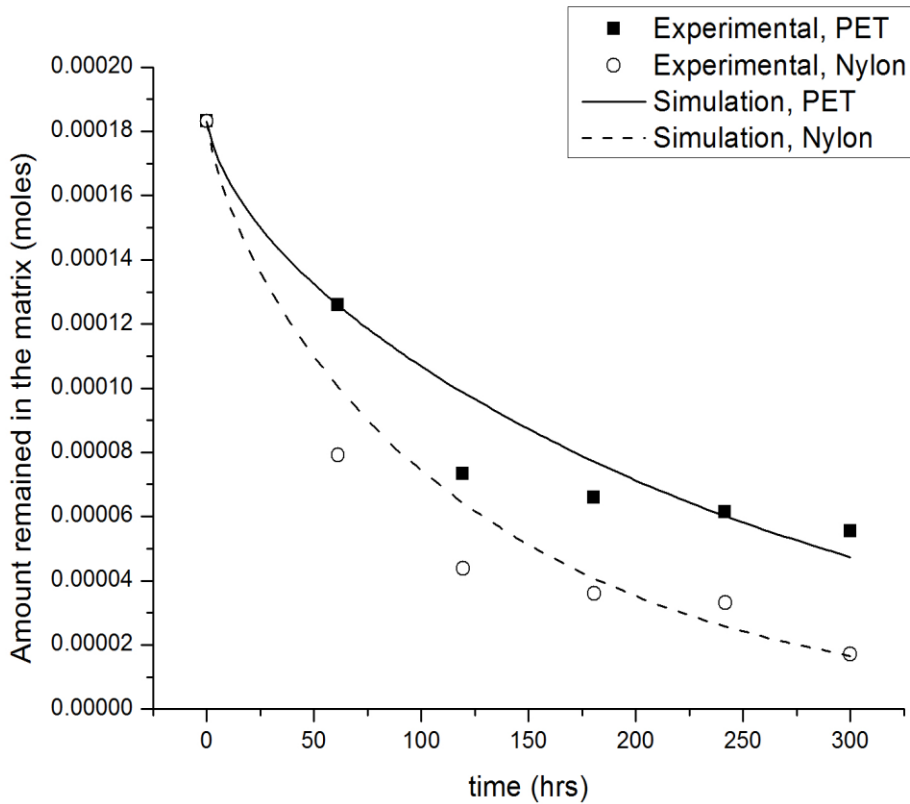


Figure 6.23: Effect of substrate on metofluthrin release. Experiments are conducted at 27 °C for an initial loading of 61.05 M and a bulk air velocity of 0.5 m/s. Simulations are performed with (a) $k_c = 17.26$ m/s and $D_{eff} = 2.7 \times 10^{-16}$ m²/s for PET; (b) $k_c = 17.26$ m/s and $D_{eff} = 7.3 \times 10^{-16}$ m²/s for nylon.

More experiments are needed for other substrates to determine the four parameters using the same algorithm as for cellulose. Results presented in Figure 6.23 are obtained by trial and error by varying the effective diffusion coefficient while keeping the same mass transfer coefficient.

6.10 Plausible reasons for low metofluthrin diffusivity

Using the values mentioned in Table 6.1 in Eq. 6.1 and at a temperature of 30 °C, a D_{eff} value of 3.47×10^{-16} is obtained, which is a few orders of magnitude lower than the diffusivity reported for common volatile materials. For example, the reported diffusivity of acetone is reported to be of the order of 10^{-12} m²/s. Several explanations have been advanced to explain

the abnormally low diffusivity observed. We believe, that substrate material properties for instance surface areas, intrinsic properties and Metofluthrin vapor pressure plays a key role in influencing diffusion process.

This chapter discusses and attempts to explain the difference between diffusion and mass transfer coefficient values obtained for metofluthrin and those reported in literature for common volatile compounds.

6.10.1 Hindered diffusion in a pore

Hindered diffusion in a pore is observed when solute particles need to diffuse through a solvent inside a pore. In this case, Van der Waals forces related to the pore walls may act on the solvent, making it more viscous. Ratikon *et al.* [178] studied the diffusivity of glucose in water-filled silica of various pore sizes and determined that an increase in pore size from 7.4 to 116 Å alters the diffusivity from 10^{-13} to 10^{-10} m²/s. They suggested that these changes in diffusion coefficient are due to Van der Waals forces. In our present study, it is likely that metofluthrin transport within the pores could be through the intermediacy of voids existing with in pores, and, that Van der Waals forces would influence the void properties.

For the diffusion of glucose, an effective diffusion coefficient D_e corresponding to the diffusivity inside a pore was proposed in addition to the molecular diffusivity D_0 , which is the diffusivity under normal conditions (not inside any pore) [179].

$$D_e = D_0 \cdot F_1(\lambda_s) \cdot F_2(\lambda_s) \quad \text{Equation 6.7}$$

Where F_1 and F_2 are the correction factors. The expression for the steric position coefficient F_1 has been derived by Anderson and Quinn [180] as well as by Deen [181]

A simple force balance is established first.

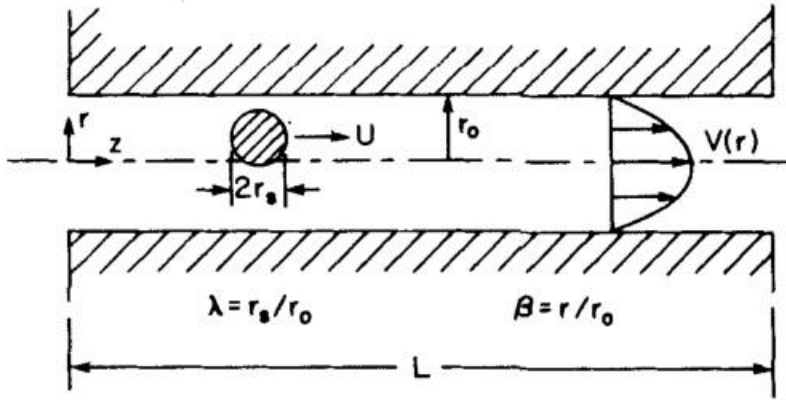


Figure 6.24: Particle located off the centerline inside a pore (Deen, 1987).

$$kT \frac{d(\ln C)}{dz} = -6\pi\eta aK[U_s - GV] \quad \text{Equation 6.8}$$

Where U_s is the velocity of the particle with respect to the walls. A particle experiences one force resulting from a concentration gradient (L.H.S) and another originating from viscosity (R.H.S). These forces are assumed to be equal because the solute particle moves at a constant velocity.

$$F = -\nabla\mu_k(r) \frac{1}{N_A}$$

$$F_{dx} = -\frac{\partial\mu_k(r)}{\partial x} \times \frac{1}{N_a}$$

Now,

$$\mu_k = \mu_k^0 + RT \ln(C)$$

Hence,

$$F = \frac{-1}{N_a} RT \frac{d \ln(C)}{dz} = L.H.S \quad \text{Equation 6.9}$$

From Eq. 6.9,

$$N = \frac{-D_0}{k} \frac{dC}{dz} + GCV \quad \text{Equation 6.10}$$

$\langle N \rangle$ is defined as N averaged over the cross-section area and

$$\langle N \rangle = \frac{\int_0^1 N\beta d\beta}{\int_0^1 \beta d\beta} = 2 \int_0^{1-\lambda} N\beta d\beta \quad \text{Equation 6.11}$$

The denominator in Eq. 6.11 is half and the upper limit of the integral becomes $(1 - \lambda)$ because no movement occurs in the outermost region.

Averaging this equation gives

$$\langle N \rangle = -2D_\infty \int_0^{1-\lambda} k^{-1} \frac{\partial C}{\partial z} \beta d\beta + 4 \langle v \rangle \int_0^{1-\lambda} GC(1 - \beta^2)\beta d\beta$$

An appropriate form for C is

$$C = g(z). \exp[-E(\beta)/(kT)] \quad \text{Equation 6.12}$$

Where E is a potential describing long range interactions between solute and pore wall.

For $\langle v \rangle = 0$, Biener and Gaydos have shown that this equation is consistent for a particle with Brownian motions. For $\langle v \rangle = 0$, this is not exact, and its use is equivalent to neglecting Taylor dispersion.

Using Eqs. 6.11 and 6.12,

$$\langle N \rangle = -k_d D_\infty \frac{d \langle C \rangle}{dz} + k_c \langle v \rangle \langle c \rangle$$

$$k_d = \frac{\int_0^{1-\lambda} k^{-1} e^{-E/kT} \beta d\beta}{\int_0^{1-\lambda} e^{-E/kT} \beta d\beta}$$

$$k_c = \frac{2 \int_0^{1-\lambda} G(1-\beta^2)e^{-E/kT} \beta d\beta}{\int_0^{1-\lambda} e^{-E/kT} \beta d\beta} \quad \text{Equation 6.13}$$

The concentrations at pore extremities ($z = 0$ and $z = L$) are in equilibrium with outside concentration. In addition, the probability of finding a particle at a given radial position should be a function of $\exp[-E(\beta)/kT]$. This is consistent with Eq. 6.11 if $g(0) = C_0$ and $g(L) = C_L$ (Deen, 1987). At $z = 0$ or $z = L$,

$$C_{0,inside} = C_0 \exp\left[\frac{-E(\beta)}{kT}\right] \quad \text{Equation 6.14}$$

Consequently, the ratio between the average concentration (averaged over the area) and the concentration outside in the bulk is written as follows:

$$\phi = \frac{\langle c_0 \rangle}{c_0} = 2 \int_0^{1-\lambda} \exp\left(\frac{-E}{kT}\right) \beta d\beta \quad \text{Equation 6.15}$$

If $E = 0$ and the interaction is purely steric, then

$$\phi = (1 - \lambda)^2 \quad \text{Equation 6.16}$$

Anderson and Quinn [180] and later Netrabukkana *et al.* suggested that the same quantity F_1 may be used to calculate the effective diffusivity inside a pore because this is the fractional area available inside a pore. Therefore, to account for the effect of pore wall-induced Van der Waals forces on the solvent,

$$F_1(\lambda) = \phi = (1 - \lambda)^2$$

Ternan [181] further introduced another quantity F_2 defined as follows:

$$F_2(\lambda) = \frac{1}{1+\lambda} \quad \text{Equation 6.17}$$

The expression for this correction factor is derived as follows:

The viscosity of the solvent is assumed to increase near the wall because of Van der Waals forces. If the radius of a solute particle is r_m and the distance from the wall where the viscosity is higher is r_w , the region in which the higher viscosity is effective is $r_m + r_w$.

Therefore, the area at which the viscosity is higher is

$$xA = \pi r_p^2 - \pi (r_p - r_m - r_w)^2 \quad \text{Equation 6.18}$$

The overall viscosity inside the pore is obtained using

$$\pi r_p^2 L \mu_p = \pi r_p^2 L \mu_\beta + (xA_l \Delta \mu_w)$$

$$\text{With } \beta = \frac{r_w}{r_p}$$

$$\mu_p = \mu_\beta + \lambda[2 - \lambda + \beta/\lambda(2 - 2\lambda - \beta)]\Delta\mu_w$$

$$\text{Or } \frac{\mu_\beta}{\mu_p} = \frac{1}{1+P\lambda}$$

Where,

$$P = [2 - \lambda + B/\lambda(2 - 2\lambda - \beta)] \frac{\Delta\mu_w}{\mu_\beta} \quad \text{Equation 6.19}$$

Netrabukkana *et al.* suggested that P could be used as a diffusivity correction factor.

$$\frac{D_c}{D_0} = \frac{(1 - \lambda)^2}{(1 + P\lambda)}$$

$$P = [2 - \lambda \frac{b}{\lambda}(2 - 2\lambda - \beta)] \frac{\Delta\mu_w}{\mu_\beta} \quad \text{Equation 6.20}$$

A metofluthrin molecule displays a molecular volume of 306.55 \AA^3 (Chemspider Database), and, thus a molecular radius of 4.18 \AA . For cellulose, the pore diameter is determined by considering the space between cellulose fibers as a pore.

$$\text{Therefore, } \lambda = \frac{4.18 \text{ \AA}}{40 \text{ nm}}$$

The diffusivity of water and metofluthrin are compared using the ratio of their individual effective diffusivities.

$$\frac{D_{e,\text{water}}}{D_{e,\text{metofluthrin}}} = \frac{\left[\frac{(1-\lambda)^2}{1+P\lambda}\right]_w}{\left[\frac{(1+\lambda)^2}{1+P\lambda}\right]_m} \times \frac{D_{0,w}}{D_{0,m}} \quad \text{Equation 6.21}$$

Substituting the values for water and metofluthrin provides a ratio of 1202.4. Therefore, the size of the metofluthrin molecule introduces a change of two orders of magnitude.

The mass transfer coefficient of metofluthrin from cellulose to air may also be affected by the molecule size. Further investigations are needed to determine the differences in diffusion and mass transfer coefficient magnitudes [182,183].

6.11 Solid State Theory

The diffusivity and mass transfer coefficient obtained for metofluthrin may also be explained if the system is considered as a diffusion in a solid lattice.

Water and acetone molecules are smaller than metofluthrin. Smaller molecules need less energy to jump from one site to another vacant site and show less distortion in the lattice during the jump. In contrast, metofluthrin is expected to demand a lot of energy for a jump and cause greater distortions upon jumping. When it is released in the air, it has to overcome significant steric hindrance. Moreover, the momentum needed to be taken along with the air molecules may also be high. Water and acetone would leave the surface and go in the air more readily. Consequently, the mass transfer coefficient is lower for metofluthrin than that for smaller molecules. These effects must be quantified but no study has addressed the diffusion of water or acetone in a solid lattice so far.

CHAPTER 7

Conclusion and Future scope

7.1 Conclusion

In recent times, the household insecticide industry has witnessed a rapid developmental surge in line with the growing incidence of mosquito menace on human population. Typically, household insecticidal compounds belong to the class of synthetic pyrethroids, for which the chemical architecture and efficacy have witnessed an evolution in terms of safety, efficacy, and toxicity potential.

The present study attempts to address key factors influencing the release of metofluthrin, a recently developed synthetic pyrethroid exhibiting a relatively high vapor pressure under ambient conditions. This insecticide has been impregnated on various substrates.

HS-GC and TGA measurements corroborate the experimentally observed higher diffusivity of metofluthrin in cellulose and provide a rational explanation for the different diffusivities noted on various substrates. Spectral studies, including surface FTIR, solid-state ^{13}C and ^1H NMR, and XRD, reveal negligible chemical interactions between substrate and active ingredient. Therefore, physical properties are proposed to play a determinant role in the diffusivity of metofluthrin-impregnated substrates. Experiments demonstrate that for all conditions maintained constant, the metofluthrin diffusivity follows the order cellulose > nylon > PET > polypropylene. The obtained diffusivities correlate with the overall substrate surface areas and surface spreadability, as evidenced by contact angle observations.

This thesis investigated the influence of external variable factors, such as temperature, wind velocity, and surface area on metofluthrin release from various substrates impregnated with similar amounts of active ingredient.

A diffusion model based on the classical Fickian diffusion theory has been employed to simulate the self-diffusion process and estimate metofluthrin diffusion coefficients from experimental release data. The proposed model relies on four parameters including the pre-exponential factor A ,

the energy of activation E_a , and constants a and b . When all parameters are evaluated for cellulose, the model has been found to predict experimental data well. The diffusion coefficient of metofluthrin has an order of magnitude 10^{-16} m²/s and its mass transfer coefficient equals 10^{-10} m/s.

Validation of the model and its extension

The insecticidal efficacy of metofluthrin is attained only when a specific aerial threshold concentration is reached (1.51×10^{-5} mol/m³ in this case). The model is refined to predict the time taken to achieve threshold concentrations depending on the initial loading amounts. Figure 7.1 shows the results obtained.

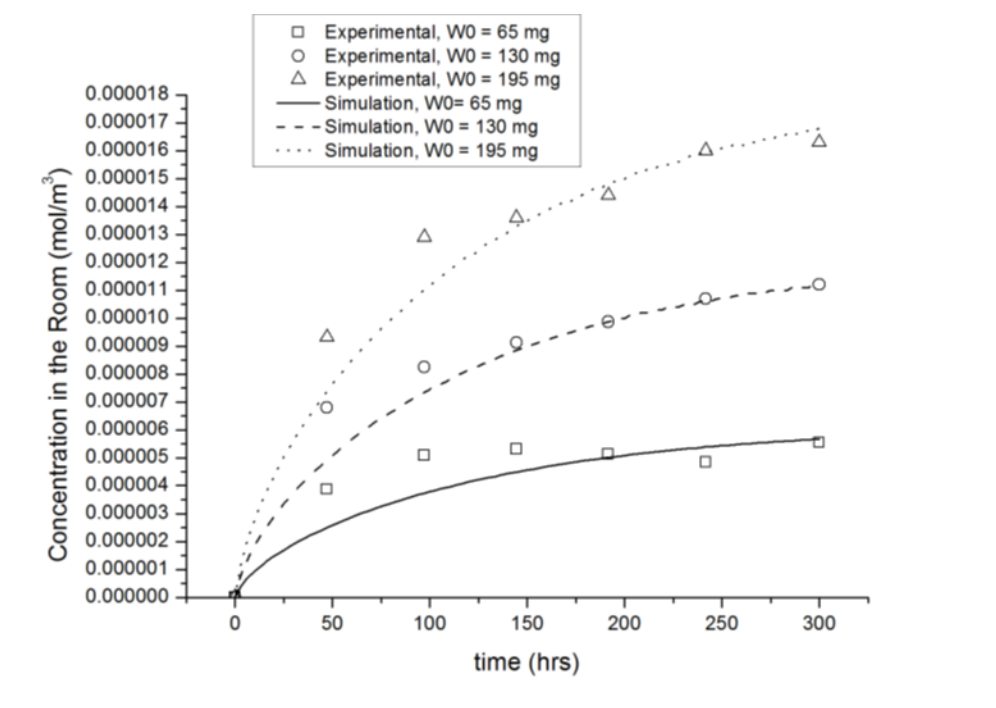


Figure 7.1: Metofluthrin concentration in the room at 27 °C with an air velocity of 0.8 m/s for different initial loading values.

Different initial loading configurations take different times to reach the threshold concentration. Specifically, initial loadings of 65, 130, and 195 mg take about 20, 8, and 5 min, respectively, to express bio-efficacy according to the simulation results. Consequently, the onset of efficacy depends significantly upon the initial loading on substrates. A higher initial loading enables a quick onset of efficacy of the product to be expressed. For more accurate conclusions, experiments need

to be conducted in open spaces that facilitate the verification of the modelling results. A higher matrix surface area is expected to dissipate metofluthrin at a higher rate, whereas a low surface area requires more time for metofluthrin to attain threshold concentrations. An optimal surface area, therefore, ensures a balance between the onset of efficacy and its longevity.

The mass transfer coefficient of metofluthrin from cellulose to air has been determined to have an order of magnitude of 10^{-11} m/s. This value which has been obtained is one order lower than the mass transfer evaporation coefficient between water to external environment (to air). The hindered pore diffusion model provides an explanation for such low mass transfer values. We believe that it should be possible to involve this model to rationalize and explain the low mass transfer coefficient noted. This model essentially addresses differential gradients in viscosity across the pore dimension from the periphery to within the bulk.

7.2 Future scope

It is desirable to verify the inferences made in the last section of this thesis. Experiments need to be conducted in open rooms to find the optimum surface area and initial loading of the product. The development of a more generalized algorithm that includes other external factors is required for a better prediction of diffusivity.

In addition, an extension of this study to various substrates may be undertaken to gather significantly more information on the types of interactions involving metofluthrin, and thus their influence on the diffusion process.

The modelling section suggests that, along with the diffusion, other transport mechanisms are also involved inside the matrix, such as strong interactions between liquid and pore walls. It would be interesting to investigate and understand all possible mechanisms of release kinetics from the polymer matrix and incorporate these mechanisms in the present model.

The newly developed model has considered humidity as an invariant with respect to metofluthrin diffusion. RH effects should be studied systematically.

A highly predictable model for metofluthrin release from the substrate is expected to provide understanding on the optimal metofluthrin amounts required to exhibit insecticidal action.

Finally, a comparison between metofluthrin release and that of its close congeners, such as transfluthrin, will also be interesting.

REFERENCES

1. WHO, Communicable diseases prevention and control, WHO pesticide evaluation scheme (WHOPES), *Guidelines for safe and effective use of household insecticides products*, 2000:1–3.
2. <http://www.who.int/mediacentre/factsheets/fs327/en/> accessed on August 17, 2014.
3. http://www.who.int/malaria/media/world_malaria_report_2013/en/ accessed on August 17, 2014.
4. <http://www.searo.who.int/india/topics/malaria/en/Malar> accessed on August 14, 2014.
5. Singh, N., Dash, A. P., and Thimasarn, K. (2009). Fighting malaria in Madhya Pradesh (Central India): Are we loosing the battle. *Malaria Journal*, 8, 93.
6. <http://www.who.int/mediacentre/factsheets/fs117/en/> accessed on August 14, 2014.
7. <http://cdc.gov/malaria/hidtory/ross.htm> accessed on July 11, 2009.
8. <http://nobelprize.org/nobelprizes/medicne/laurates/1902/ross-bio.html> accessed on July 11, 2009.
9. http://whqlibdoc.who.int/trs/WHO_TRS_857.pdf (Vector control for malaria and other mosquito borne diseases accessed on March 23, 2013).
10. Bellini, R., Veronesi, R., and Rizzoli, M. (1994). Efficacy of various fish species (*Carassius auratus* [L.], *Cyprinus carpio* [L.], *Gambusia affinis* [Baird and Girard]) in the control of rice field mosquitoes in Northern Italy. *Bull. Soc. Vector Ecol.*, 19(2), 87–99.
11. Prasad, H., Prasad, R. N., and Haq, S. (1993). Control of mosquito breeding through *Gambusia affinis* in rice fields. *Indian Journal of Malariology*, 30(2), 57–65.
12. Chatterjee, S. N., and Chandra, G. (1997). Feeding pattern on *Gambusia affinis* and *Lebistes reticulatus* on *Anopheles subpictus* larvae in the laboratory and field condition. *Journal of Applied Zoological Researches*, 8(2), 152–153.
13. Victor, T. J., Chandrasekaran, B., and Reuben, R. (1994). Composite fish culture for mosquito control in rice fields in southern India. *The Southeast Asian journal of tropical medicine and public health*, 25(3), 522–527.

14. Mulla, M. S. (1994). Mosquito control then, now, and in the future. *Journal of the American Mosquito Control Association*, 10(4), 574–584.
15. http://www.nobelprize.org/nobel_prizes/medicine/laureates/1948/press.html
16. www.epa.gov/history/topics/ddt/01.htm accessed on August 09, 2009.
17. Roberts, D., and Tren, R. (2010). *The excellent powder: DDT's political and scientific history*. Dog Ear Publishing.
18. Sadasivaiah, S., Tozan, Y., and Breman, J. G. (2007). Dichlorodiphenyltrichloroethane (DDT) for indoor residual spraying in Africa: how can it be used for malaria control? *The American journal of tropical medicine and hygiene*, 77(6), 249–263.
19. Smith, A., and Webley, D. J. (1969). A veranda-trap hut for studying the house-frequenting habits of mosquitoes and for assessing insecticides. III. The effect of DDT on behaviour and mortality. *Bulletin of Entomological Research*, 59(1), 33–46.
20. Kennedy, J. S. (1947). The excitant and repellent effects on mosquitos of sub-lethal contacts with DDT. *Bulletin of entomological research*, 37(4), 593–607.
21. Adams, M. E., and Miller, T. A. (1980). Neural and behavioral correlates of pyrethroid and DDT-type poisoning in the house fly, *Musca domestica* L. *Pesticide Biochemistry and Physiology*, 13(2), 137–147.
22. http://www.mrcindia.org/MRC_profile/profile2/profile.htm. Integrated vector management/Studies on reliance of BHC, DDT and Malathion in vector control programme, 198–200, accessed on August 29, 2009.
23. Lacey, L. A. (2007). *Bacillus thuringiensis* serovariety *israelensis* and *Bacillus sphaericus* for mosquito control. *Journal of the American Mosquito Control Association*, 23(2), 133–163.
24. Zahiri, N.S., Federici, B. A., Mulla, M.S. (2004). Biolarvicides in vector control: challenges and prospects. *Journal of Medical Entomology*, 41(3), 423–429.
25. Chandra, G., Bhattacharjee, I., Chatterjee, S. N., and Ghosh, A. (2008). Mosquito control by larvivorous fish. *Indian Journal of Medical Research*, 127(1), 13.
26. Rogers Jr, L. E. J., and USJVR, M. (1989). Fabric against human body lice. *Military medicine*, 154, 90.

27. Wu, N., Liao, G. H., Li, D. F., Luo, Y. L., and Zhong, G. M. (1991). The advantages of mosquito biocontrol by stocking edible fish in rice paddies. *The Southeast Asian journal of tropical medicine and public health*, 22(3), 436–442.
28. Wu, N., Liao, G. H., Li, D. F., Luo, Y. L., and Zhong, G. M. (1991). The advantages of mosquito biocontrol by stocking edible fish in rice paddies. *The Southeast Asian journal of tropical medicine and public health*, 22(3), 436–442.
29. Zahiri, N. S., Federici, B. A., and Mulla, M. S. (2004). Laboratory and simulated field evaluation of a new recombinant of *Bacillus thuringiensis ssp. israelensis* and *Bacillus sphaericus* against *Culex* mosquito larvae (Diptera: Culicidae). *Journal of Medical Entomology*, 41(3), 423–429.
30. Atieli, F. K., Munga, S. O., Ofulla, A. V., and Vulule, J. M. (2010). The effect of repeated washing of long-lasting insecticide-treated nets (LLINs) on the feeding success and survival rates of *Anopheles gambiae*. *Malaria Journal*, 9(304), 29.
31. WHO: Insecticide-Treated Mosquito Nets: a position statement. [<http://www.who.int/entity/malaria/publications/atoz/itnspospaperfinal.pdf>] website 2007.
32. Chandre, F., Dabire, R. K., Hougard, J. M., Djogbenou, L. S., Irish, S. R., Rowland, M., and N' Guessan, R. (2010). Field efficacy of pyrethroid treated plastic sheeting (durable lining) in combination with long lasting insecticidal nets against malaria vectors. *Parasit Vectors*, 3(1), 65.
33. Antonio-Nkondjio, C., Demanou, M., Etang, J., and Bouchite, B. (2013). Impact of cyfluthrin (Solfac EW050) impregnated bed nets on malaria transmission in the city of Mbandjock: lessons for the nationwide distribution of long-lasting insecticidal nets (LLINs) in Cameroon. *Parasites & vectors*, 6(10).
34. Faulde, M. K., and Nehring, O. (2012). Synergistic insecticidal and repellent effects of combined pyrethroid and repellent-impregnated bed nets using a novel long-lasting polymer-coating multi-layer technique. *Parasitology Research*, 111(2), 755–765.
35. Miller, J. E., Lindsay, S. W., and Armstrong, J. R. M. (1991). Experimental hut trials of bednets impregnated with synthetic pyrethroid or organophosphate

- insecticide for mosquito control in The Gambia. *Medical and Veterinary Entomology*, 5(4), 465–476.
36. Bill and Melinda Gates Foundation and Boston Consulting Group. Market Assessment for Public Health Pesticide Products. Boston: Boston Consulting Group; 2007.
 37. Hoffmann, E. J., and Miller, J. R. (2002). Reduction of mosquito (Diptera: Culicidae) attacks on a human subject by combination of wind and vapor-phase DEET repellent. *Journal of Medical Entomology*, 39(6), 935–938.
 38. Curtis, C. F., Lines, J. D., Ijumba, J., Callaghan, A., Hill, N., and Karimzad, M. A. (1987). The relative efficacy of repellents against mosquito vectors of disease. *Medical and Veterinary Entomology*, 1(2), 109–119.
 39. Rao, S. S., and Rao, K. M. (1991). Insect repellent N, N-diethylphenylacetamide: an update. *Journal of Medical Entomology*, 28(3), 303–306.
 40. Rao, K. M., Prakash, S., Kumar, S., Suryanarayana, M. V. S., Bhagwat, M. M., Gharia, M. M., and Bhavsar, R. B. (1991). N, N-diethylphenylacetamide in treated fabrics as a repellent against *Aedes aegypti* and *Culex quinquefasciatus* (Diptera: Culicidae). *Journal of Medical Entomology*, 28(1), 142–146.
 41. Debboun, M., Frances, S. P., and Strickman, D. A. (Eds.). (2006). *Insect repellents: principles, methods, and uses*. CRC Press.
 42. Schreck, C. E., Haile, D. G., and Kline, D. L. (1984). The effectiveness of permethrin and deet, alone or in combination, for protection against *Aedes taeniorhynchus*. *The American Journal of Tropical Medicine and Hygiene*, 33(4), 725–730.
 43. Gupta, R. K., Sweeney, A. W., Rutledge, L. C., Cooper, R. D., Frances, S. P., and Westrom, D. R. (1987). Effectiveness of controlled-release personal-use arthropod repellents and permethrin-impregnated clothing in the field. *Journal of the American Mosquito Control Association*, 3(4), 556–560.
 44. Lindsay, S. W., and Janneh, L. M. (1989). Preliminary field trials of personal protection against mosquitoes in The Gambia using deet or permethrin in soap, compared with other methods. *Medical and Veterinary Entomology*, 3(1), 97–100.

45. Yap, H. H. (1986). Effectiveness of soap formulations containing deet and permethrin as personal protection against outdoor mosquitoes in Malaysia. *Journal of American Mosquito Control Association*, 2(1), 63–67.
46. Miot, H. A., Ferreira, D. P., Mendes, F. G., Carrenho, F. R., de Oliveira Amui I., Carneiro, C. A., Madeira, N. G. (2008). Efficacy of topical permethrin as repellent against *Aedes aegypti*'s bites. *Dermatol Online*, 14(7), 1.
47. Frances, S. P. (1987). Effectiveness of deet and permethrin, alone, and in a soap formulation as skin and clothing protectants against mosquitoes in Australia. *Journal of American Mosquito Control Association*, 3, 648–650.
48. Schreck, C. E., Mount, G. A., and Carlson, D. A. (1982). Wear and wash persistence of permethrin used as a clothing treatment for personal protection against the lone star tick (Acari: Ixodidae). *Journal of Medical Entomology*, 19(2), 143–146.
49. Rutledge, L. C., Hooper, R. L., Wirtz, R. A., and Gupta, R. K. (1989). Efficacy of diethyl methylbenzamide (deet) against *Aedes dorsalis* and a comparison of two end points for protection time. *Journal of the American Mosquito Control Association*, 5(3), 363–368.
50. Costantini, C., Badolo, A., and Ilboudo-Sanogo, E. (2004). Field evaluation of the efficacy and persistence of insect repellents DEET, IR3535, and KBR 3023 against *Anopheles gambiae* complex and other Afrotropical vector mosquitoes. *Transactions of the Royal Society of Tropical Medicine and Hygiene*, 98(11), 644–652.
51. Feaster, J. E., Scialdone, M. A., Todd, R. G., Gonzalez, Y. I., Foster, J. P., and Hallahan, D. L. (2009). Dihydronepetalactones deter feeding activity by mosquitoes, stable flies, and deer ticks. *Journal of Medical Entomology*, 46(4), 832–840.
52. B Polsomboon, S., Grieco, J. P., Achee, N. L., Chauhan, K. R., Tanasinchayakul, S., Pothikasikorn, J., and Chareonviriyaphap, T. (2008). Behavioral responses of catnip (*Nepeta cataria*) by two species of mosquitoes, *Aedes aegypti* and *Anopheles harrisoni*, in Thailand. *Journal of the American Mosquito Control Association*, 24(4), 513–519.

53. Chauhan, K. R., Klun, J. A., Debboun, M., and Kramer, M. (2005). Feeding deterrent effects of catnip oil components compared with two synthetic amides against *Aedes aegypti*. *Journal of Medical Entomology*, 42(4), 643–646.
54. Hao, H., Wei, J., Dai, J., and Du, J. (2008). Host-seeking and blood-feeding behavior of *Aedes albopictus* (Diptera: Culicidae) exposed to vapors of geraniol, citral, citronellal, eugenol, or anisaldehyde. *Journal of Medical Entomology*, 45(3), 533–539.
55. Lindsay, L. R., Surgeoner, G. A., Heal, J. D., and Gallivan, G. J. (1996). Evaluation of the efficacy of 3% citronella candles and 5% citronella incense for protection against field populations of *Aedes* mosquitoes. *Journal of the American Mosquito Control Association*, 12(2 Pt 1), 293–294.
56. Müller, G. C., Junnila, A., Kravchenko, V. D., Revay, E. E., Butler, J., Orlova, O. B., Weiss, R. W., and Schlein, Y. (2008). Ability of essential oil candles to repel biting insects in high and low biting pressure environments. *Journal of the American Mosquito Control Association*, 24(1), 154–160.
57. Ritchie, S. A., Williams, C. R., and Montgomery, B. L. (2006). Field evaluation of New Mountain Sandalwood Mosquito Sticks® and New Mountain Sandalwood Botanical Repellent against mosquitoes in North Queensland, Australia. *Journal of the American Mosquito Control Association*, 22(1), 158–160.
58. Revay, E. E., Junnila, A., Kline, D. L., Xue, R. D., Bernier, U. R., Kravchenko, V. D., Yefremova, Z. A., and Müller, G. C. (2012). Reduction of mosquito biting pressure by timed-release 0.3% aerosolized geraniol. *Acta Tropica*, 124(1), 102–105.
59. Brady, J., Costantini, C., Sagnon, N., Gibson, G., and Coluzzi, M. (1997). The role of body odours in the relative attractiveness of different men to malarial vectors in Burkina Faso. *Annals of Tropical Medicine and Parasitology*, 91(1), 121–122.
60. Lindsay, S. W., Adiamah, J. H., Miller, J. E., Pleass, R. J., and Armstrong, J. R. M. (1993). Variation in attractiveness of human subjects to malaria mosquitoes (Diptera: Culicidae) in The Gambia. *Journal of Medical Entomology*, 30(2), 368–373.

61. Mukabana, W. R., Takken, W., Coe, R., and Knols, B. G. (2002). Host-specific cues cause differential attractiveness of Kenyan men to the African malaria vector *Anopheles gambiae*. *Malaria Journal*, 1(1), 17.
62. Hoel, D. F., Kline, D. L., Allan, S. A., and Grant, A. (2007). Evaluation of carbon dioxide, 1-octen-3-ol, and lactic acid as baits in mosquito magnet™ pro traps for *aedes albopictus* in north central Florida 1. *Journal of the American Mosquito Control Association*, 23(1), 11–17.
63. Henderson, J. P., Westwood, R., and Galloway, T. (2006). An assessment of the effectiveness of the Mosquito Magnet Pro model for suppression of nuisance mosquitoes. *Journal of the American Mosquito Control Association*, 22(3), 401–407.
64. Revay, E. E., Kline, D. L., Xue, R. D., Qualls, W. A., Bernier, U. R., Kravchenko, V. D., Ghattas, N., Pstygo, I., and Müller, G. C. (2013). Reduction of mosquito biting-pressure: spatial repellents or mosquito traps? A field comparison of seven commercially available products in Israel. *Acta Tropica*, 127(1), 63–68.
65. Xue, R. D., Qualls, W. A., Smith, M. L., Gaines, M. K., Weaver, J. H., and Debboun, M. (2012). Field evaluation of the OFF! Clip-on mosquito repellent (metofluthrin) against *Aedes albopictus* and *Aedes taeniorhynchus* (Diptera: Culicidae) in northeastern Florida. *Journal of Medical Entomology*, 49(3), 652–655.
66. Revay, E. E., Junnila, A., Xue, R. D., Kline, D. L., Bernier, U. R., Kravchenko, V. D., Qualls, W. A., and Müller, G. C. (2013). Evaluation of commercial products for personal protection against mosquitoes. *Acta Tropica*, 125(2), 226–230.
67. Coro, F., and Suarez, S. (2000). Review and history of electronic mosquito repellents. *Wing Beats*, 11(6).
68. Klun, J. A., Khrimian, A., Rowton, E., Kramer, M., and Debboun, M. (2006). Biting deterrent activity of a deet analog, two DEPA analogs, and SS220 applied topically to human volunteers compared with deet against three species of blood-feeding flies. *Journal of Medical Entomology*, 43(6), 1248–1251.

69. Becker, N., Zgomba, M., Petric, D., and Ludwig, M. (1995). Comparison of carbon dioxide, octenol and a host-odour as mosquito attractants in the Upper Rhine Valley, Germany. *Medical and Veterinary Entomology*, 9(4), 377–380.
70. WHO, Communicable diseases prevention and control, WHO pesticide evaluation scheme (WHOPES). Guidelines for safe and effective use of household insecticides products (2000), 23–29.
71. Elliot, M. (1987). The pyrethroids: Early discovery, recent advances and the future†. *Pesticide Science*, 27(4), 337–351.
72. <http://en.wikipedia.org/wiki/Pyrethroid>_accessed on April 20, 2013.
73. Khambay, B. P. (2002). Pyrethroid insecticides. *Pesticide Outlook*, 13(2), 49–54
74. Tomlin, C. D. S. (2003) The pesticide manual: A world compendium. *British Crop Protection Council/BCPC*, 305–306.
75. Gahukar, R. T. (1998). *Agrochemical guide to synthetic pesticides*. Agro-horticulture publishing house, Nagpur, 305–335.
76. WHO. IPCS, International programme on chemical safety. *Environmental health criterion 87: Allethrins, d-allethrin, bio-allethrin* (1989), 17–23.
77. WHO. IPCS, International programme on chemical safety. *Environmental health criterion 82-Cypermethrin* (1989), 23–30.
78. WHO. IPCS, International programme on chemical safety. *Environmental health criterion 97-Deltamethrin* (1990), 21–30.
79. Soderlund, D. M., Clark, J. M., Sheets, L. P., Mullin, L. S., Piccirillo, V. J., Sargent, D., Stevens, J. T., and Weiner, M. L. (2002). Mechanisms of pyrethroid neurotoxicity: implications for cumulative risk assessment. *Toxicology*, 171(1), 3–59.
80. Herzka, A. (1966). *International encyclopedia of pressurized packaging: Aerosols*. Pergamon Press, 508–531.
81. Maciver, D. R. (1963). Mosquito coils. Part I: General description of coils, their formulation and manufacture. *Pyrethrum post*, 7(2), 22–27.
82. Chadwick, P. R. (1975). The activity of some pyrethroids, DDT and lindane in smoke from coils for biting inhibition, knockdown and kill of mosquitoes (Diptera, Culicidae). *Bulletin of Entomological Research*, 65(1), 97–107.

83. Yap, H. H., and Chung, K. K. (1987). Laboratory bioassays of mosquito coil formulations against mosquitoes of public health importance in Malaysia. *Tropical Biomedicine*, 4, 13–1.
84. Hudson, J. E., and Esozed, S. (1971). The effects of smoke from mosquito coils on *Anopheles gambiae* Giles and *Mansonia uniformis* (Theo.) in verandah-trap huts at Magugu, Tanzania. *Bulletin of Entomological Research*, 61(2), 247–265.
85. Mosha, F. W., Njau, R. J. A., and Alfred, J. (1992). Efficacy of esbiothrin mosquito coils at community level in northern Tanzania. *Medical and Veterinary Entomology*, 6(1), 44–46.
86. Mosha, F. W., Njau, R. J. A., and Myamba, J. (1989). Biological efficacy of new formulations of mosquito coils and a critical review of test methods. *Pyrethrum Post*, 2, 47–52.
87. Yap, H. H., Tan, H. T., Yahaya, A. M., Baba, R., Loh, P. Y., and Chong, N. L. (1990). Field efficacy of mosquito coil formulations containing d-allethrin and d-transallethrin against indoor mosquitos especially *Culex quinquefasciatus* say. *The Southeast Asian Journal of Tropical Medicine and Public Health*, 21(4), 558–563.
88. Smith, A., Hudson, J. E., and Esozed, S. (1972). Trials with pyrethrum mosquito coils against *Anopheles gambiae* Giles, *Mansonia uniformis* Theo. and *Culex fatigans* Wied. entering verandah-trap huts. *Pyrethrum Post*.
89. Mosha, F. W., Njau, R. J. A., and Alfred, J. (1992). Efficacy of Esbiothrin mosquito coils at community level in northern Tanzania. *Medical and Veterinary Entomology*, 6(1), 44–46.
90. Mosha, F. W., Njau, R. J. A., and Myamba, J. (1989). Biological efficacy of new formulations of mosquito coils and a critical review of test methods. *Pyrethrum Post*.
91. Birley, M. H., Mutero, C. M., Turner, I. F., and Chadwick, P. R. (1987). The effectiveness of mosquito coils containing esbiothrin under laboratory and field conditions. *Annals of Tropical Medicine and Parasitology*, 81(2), 163–171.
92. K Katsuda, Y., Leemingsawat, S., Thongrunkiat, S., Komalamisara, N., Kanzaki, T., Watanabe, T., and Kahara, T. (2008). Control of mosquito vectors of tropical infectious diseases: (1) bio-efficacy of mosquito coils containing several

- pyrethroids and a synergist. *Southeast Asian J Trop Med Public Health*. Jan; 39(1):48-54.
93. Amalraj, D. D., Sivagnaname, N., Boopathidoss, P. S., and Das, P. K. (1996). Bio-efficacy of mosquito mat, coil and dispenser formulations containing allethrin group of synthetic pyrethroids against mosquito vectors. *The Journal of Communicable Diseases*, 28(2), 85–93.
94. Matsuo, N., Ujihara, K., Shono, Y., Iwasaki, T., Sugano, M., Yoshiyama, T., and Uwagawa, S. (2005). Discovery and development of a novel pyrethroid insecticide ‘Metofluthrin (SumiOne®, Eminence®)’. *Sumitomo Kagaku*, 2, 4–16.
95. Ujihara, K., Matsuo, N., Mori, T., Shono, Y., and Iwasaki, T. (2008). Metofluthrin: novel pyrethroid insecticide and innovative mosquito control agent. *Journal of Pesticide Science*, 33(2), 178–179.
96. Rapley, L. P., Russell, R. C., Montgomery, B. L., and Ritchie, S. A. (2009). The effects of sustained release metofluthrin on the biting, movement, and mortality of *Aedes aegypti* in a domestic setting. *The American Journal of Tropical Medicine and Hygiene*, 81(1), 94–99.
97. Lucas, J. R., Shono, Y., Iwasaki, T., Ishiwatari, T., Spero, N., and Benzon, G. (2007). US laboratory and field trials of metofluthrin (Sumione®) emanators for reducing mosquito biting outdoors. *Journal of the American Mosquito Control Association*, 23(1), 47–54.
98. Kawada, H., Yen, N. T., Hoa, N. T., Sang, T. M., Van Dan, N., and Takagi, M. (2005). Field evaluation of spatial repellency of metofluthrin impregnated plastic strips against mosquitoes in Hai Phong City, Vietnam. *The American Journal of Tropical Medicine and Hygiene*, 73(2), 350–353.
99. Kawada, H., Maekawa, Y., and Takagi, M. (2005). Field trial of the spatial repellency of metofluthrin-impregnated plastic strip against mosquitoes in shelters without walls (Beruga) in Lombok, Indonesia. *Journal of Vector Ecology*, 30(2), 181–185.
100. Kawada, H., Iwasaki, T., Le Loan, L., Tien, T. K., Mai, N. T. N., Shono, Y., Katayama, Y., and Takagi, M. (2006). Field evaluation of spatial repellency of metofluthrin-impregnated latticework plastic strips against *Aedes aegypti* (L.) and

- analysis of environmental factors affecting its efficacy in My Tho City, Tien Giang, Vietnam. *The American Journal of Tropical Medicine and Hygiene*, 75(6), 1153–1157.
101. Argueta, T. B. O., Kawada, H., and Takagi, M. (2004). Spatial repellency of metofluthrin-impregnated multilayer paper strip against *Aedes albopictus* under outdoor conditions, Nagasaki, Japan, *Medical Entomology and Zoology*. 55, 211–216.
102. Kawada, H., Temu, E. A., Minjas, J. N., Matsumoto, O., Iwasaki, T., and Takagi, M. (2008). Field evaluation of spatial repellency of metofluthrin-impregnated plastic strips against *Anopheles gambiae* complex in Bagamoyo, Coastal Tanzania. *Journal of the American Mosquito Control Association*, 24(3), 404-409.
103. Lucas, J. R., Shono, Y., Iwasaki, T., Ishiwatari, T., Spero, N., and Benzon, G. (2007). US laboratory and field trials of metofluthrin (Sumione®) emanators for reducing mosquito biting outdoors 1. *Journal of the American Mosquito Control Association*, 23(1), 47–54.
104. Rapley, L. P., Russell, R. C., Montgomery, B. L., and Ritchie, S. A. (2009). The effects of sustained release metofluthrin on the biting, movement, and mortality of *Aedes aegypti* in a domestic setting. *The American Journal of Tropical Medicine and Hygiene*, 81(1), 94–99.
105. Lee, D. K. (2007). Lethal and repellent effects of transfluthrin and metofluthrin used in portable blowers for personal protection against *Ochlerotatus togoi* and *Aedes albopictus* (Diptera: Culicidae). *Entomological Research*, 37(3), 173–179.
106. Lukwa, N., and Chiwade, T. (2008). Lack of insecticidal effect of mosquito coils containing either metofluthrin or esbiothrin on *Anopheles gambiae* sensu lato mosquitoes. *Tropical Biomedicine*, 25(9).
107. Achee, N. L., Sardelis, M. R., Dusfour, I., Chauhan, K. R., and Grieco, J. P. (2009). Characterization of spatial repellent, contact irritant, and toxicant chemical actions of standard vector control compounds 1. *Journal of the American Mosquito Control Association*, 25(2), 156–167.
108. Schmidt, C. W. (2005). Outsmarting olfaction: the next generation of mosquito repellents. *Environmental Health Perspectives*, 113(7), A468.

109. Ujihara, K., Mori, T., and Matsuo, N. (2012). Recent advances of pyrethroids for household use in Pyrethroids (pp. 31–48). Springer Berlin Heidelberg.
110. Moore, S. J., Davies, C. R., Hill, N., and Cameron, M. M. (2007). Are mosquitoes diverted from repellent-using individuals to non-users? Results of a field study in Bolivia. *Tropical Medicine & International Health*, 12(4), 532–539.
111. World Health Organisation. (1981). The use of impregnated bed nets and other materials for vector borne disease control, *Division of vector biology and control*, 18–80.
112. World Health Organisation. (1990). International programme on chemical safety. *Environmental health criterion 94-permethrin*, 18–24.
113. Deguchi, Y., Yamada, T., Hirose, Y., Nagahori, H., Kushida, M., Sumida, K. and Okuno, Y. (2009). Mode of action analysis for the synthetic pyrethroid metofluthrin-induced rat liver tumors: evidence for hepatic CYP2B induction and hepatocyte proliferation. *Toxicological Sciences*, kfp006.
114. United States, Environment pesticide agency, Office of prevention, pesticides and toxic substances, Fact sheet on Metofluthrin, September, 2006. Accessed on April, 2014
http://www.epa.gov/opp00001/chem_search/reg_actions/registration/fs_PC-109709_01-Sep-06.pdf
115. Langer, R., and Peppas, N. (1983). Chemical and physical structure of polymers as carriers for controlled release of bioactive agents: a review. *Journal of Macromolecular Science-Reviews in Macromolecular Chemistry and Physics*, 23(1), 61–126.
116. Small, P. A. (1947). Diffusion of Plasticisers from polyvinyl chloride, *Journal of the Society of Chemical Industry*, 66 (1), 17–19.
117. Schultz, H. A., and Webb, A. B. (1969). Laboratory bioassay of pesticide-impregnated rubber as a mosquito larvicide. *Mosquito News*, 29(1), 38–41.
118. Cussler E. L. (2009). Diffusion mass transfer in fluid system, Cambridge Series in Chemical Engineering, 2nd edition, 30–150.

119. Kolhapure, N. H., and Venkatesh, K. V. (1997). An unsaturated flow of moisture in porous hygroscopic media at low moisture contents. *Chemical Engineering Science*, 52(19), 3383–3392.
120. Collins, R. L., and Doglia, S. (1973). Concentration of pesticides slowly released by diffusion. *Weed Science*, 343–349.
121. Canellas, E., Aznar, M., Nerín, C., and Mercea, P. (2010). Partition and diffusion of volatile compounds from acrylic adhesives used for food packaging multilayers manufacturing. *Journal of Materials Chemistry*, 20(24), 5100–5109.
122. Department of pesticide regulation, Department of the California Environmental Protection Agency. Fumigant transport modeling using hydrus: 2. Comparison of model simulations to analytical solutions of Fick's second law of diffusion by department of pesticide regulation, august 2007 accessed on http://www.cdpr.ca.gov/docs/emon/pubs/ehapreps/analysis_memos/2077_segaw_a.pdf
123. Zhang, L. Z., and Niu, J. L. (2003). Mass transfer of volatile organic compounds from painting material in a standard field and laboratory emission cell. *International Journal of Heat and Mass Transfer*, 46(13), 2415–2423.
124. Directive 98/8/EC concerning the placing of biocidal products on the market. Assessment report-Metofluthrin by European Commission-Directorate General Environment accessed on <http://www.bfafh.de/inst4/45/pdf/treatart.pdf> on April 27, 2014.
125. Xiaoli, W., Youshun, L., Yifei, J., and Tiechun, C. (2009). Analytical Method for Metofluthrin TC by GC. *Pesticide Science and Administration*, 9, 023.
126. S. Skoog, D., West, D., Holler, F. L., and Crouch, S. (2013). Fundamentals of Analytical Chemistry, Publishers: Holt, Rinehart & Winston, 1979, 7th edition , 686–700.
127. Barnard, D. R., Bernier, U. R., Xue, R. D., and Debboun, M. (2007). Standard methods for testing mosquito repellents. Insect repellents: principles, methods, and uses/edited by Mustapha Debboun, Stephen P. Frances, Daniel Strickman.
128. Ishiwatari, T., Sugano, M., Lucas, J. R., and Shono, Y. (2009). Biological efficacy of metofluthrin, a new pyrethroid insecticide, highly effective against

- mosquitoes. In ACS symposium series (vol. 1014, pp. 161–169). Oxford University Press.
129. Ritchie, S. A., and Devine, G. J. (2013). Confusion, knock-down and kill of *Aedes aegypti* using metofluthrin in domestic settings: a powerful tool to prevent dengue transmission? *Parasites & Vectors*, 6(1), 1–9.
130. Yap H.H, Lim M.P. (1996). Vector control unit, efficacy and sub-lethal effects of mosquito coils on *Aedes aegypti* & *Culex quiquefasciatus*. *Proceedings of second International conference on urban pesticides*. Editor K.B.Wildey (1996)
131. Bliss, C. I. (1934). The method of probits—a correction. *Science*, 79(2053), 409–410.
132. Thistle, H. W. (1996). Atmospheric stability and the dispersion of pesticides. *Journal of the American Mosquito Control Association*, 12(2 Pt 2), 359–363.
133. Bayer Cropscience, EP 2377395, A 1, Non-woven fabric containing insecticide, October 19, 2011.
134. United States Patent 005236703A: polymeric substrates containing povidone iodine as a control release biologically active, Virex Inc, July 20,1989.
135. Marer, P. J. (2000). *The safe and effective use of pesticides* (vol. 1). UCANR Publications.
136. Maxim Technologies, Nonwoven paving fabric study, Industrial fabrics association International geo textiles Division; December 1997, 1–7.
137. Anand, S. C., Swarbrick, G., and Russell, S. J. (2007). Handbook of Nonwovens. *the textile institute, Woodhead Publishing ISBN-10, 1-84569*.
138. Bartels, V. (Ed.). (2011). *Handbook of medical textiles*. Elsevier.
139. PDL staff and William Andrew. (2008). Handbook of plastics : A practical guide , Plastic design Library publishers, 2nd edition, 2008, 203–265.
140. Holik, H. (Ed.). (2006). *Handbook of paper and board*. John Wiley & Sons.
141. Carmody, O., Frost, R., Xi, Y., and Kokot, S. (2008). Selected adsorbent materials for oil-spill cleanup. *Journal of Thermal Analysis and Calorimetry*, 91(3), 809–816.
142. Willard, H. H., Merritt, L., and Dean, J. A. (1965). Instrumental methods of analysis. In *Instrumental methods of analysis*. Van Nostrand Reinhold.

143. Boppana, R., Kulkarni, R. V., Setty, C. M., and Kalyane, N. V. (2010). Carboxymethylcellulose–aluminium hydrogel microbeads for prolonged release of simvastatin. *Acta Pharmaceutica Scientia*, 52, 137–143.
144. Sunitha, A., and Kumar, S. (2010). Study on the effect of polymers on the release rate of drug from ciprofloxacin hydrochloride microspheres. *Journal of Pharmaceutical Cosmetology*, 1, 1–8.
145. Chialva, F., Gabri, G., Liddle, P. A. P., and Ulian, F. (1982). Qualitative evaluation of aromatic herbs by direct head space (GC) 2 analysis. Applications of the method and comparison with the traditional analysis of essential oils. In *Aromatic Plants* (pp. 183–195). Springer Netherlands.
146. Kanervo, J. (2003). *Kinetic analysis of temperature-programmed reactions*. Helsinki University of Technology.
147. Wzorek, B., Mochalski, P., Śliwka, I., and Amann, A. (2010). Application of GC-MS with a SPME and thermal desorption technique for determination of dimethylamine and trimethylamine in gaseous samples for medical diagnostic purposes. *Journal of Breath Research*, 4(2), 026002.
148. Walton, K. S., and Snurr, R. Q. (2007). Applicability of the BET method for determining surface areas of microporous metal-organic frameworks. *Journal of the American Chemical Society*, 129(27), 8552–8556.
149. Tan, Y. H., Davis, J. A., Fujikawa, K., Ganesh, N. V., Demchenko, A. V., and Stine, K. J. (2012). Surface area and pore size characteristics of nanoporous gold subjected to thermal, mechanical, or surface modification studied using gas adsorption isotherms, cyclic voltammetry, thermogravimetric analysis, and scanning electron microscopy. *Journal of Materials Chemistry*, 22(14), 6733–6745.
150. Carmody, O., Frost, R., Xi, Y., and Kokot, S. (2007). Surface characterisation of selected sorbent materials for common hydrocarbon fuels. *Surface Science*, 601(9), 2066–2076.
151. Skovmand, O., and Bosselmann, R. (2011). Strength of bed nets as function of denier, knitting pattern, texturizing and polymer. *Malaria Journal*, 10(1), 87.

152. Abell, A. B., Willis, K. L., and Lange, D. A. (1999). Mercury intrusion porosimetry and image analysis of cement-based materials. *Journal of Colloid and Interface Science*, 211(1), 39–44.
153. Rutledge, G. C., Lowery, J. L., and Pai, C. L. (2009). Characterization by mercury porosimetry of nonwoven fiber media with deformation. *Journal of engineered fibers and fabrics*. Volume 4, Issue -03,1-12
154. Rios, P. F., Dodiuk, H., Kenig, S., McCarthy, S., and Dotan, A. (2007). The effect of polymer surface on the wetting and adhesion of liquid systems. *Journal of Adhesion Science and Technology*, 21(3, 4), 227–241.
155. Mittal, K. L. (Ed.). (2006). *Contact angle, wettability and adhesion* (vol. 4). CRC Press.
156. Mark, R. E., and Borch, J. (Eds.). (2002). *Handbook of physical testing of paper* (vol. 1). CRC Press.
157. Olek, J., Cohen, M. D., and Lobo, C. (1990). Determination of surface area of portland cement and silica fume by mercury intrusion porosimetry. *American Concrete Institute Materials Journal*, 87(5), 473–478.
158. Manfred, S. (2008). Polymer surfaces and interfaces characterization, modification and applications.
159. Sibilial, J. P. (Ed.). (1996). *A guide to materials characterization and chemical analysis*. John Wiley & Sons.
160. Dhoot, G., Auras, R., Rubino, M., Dolan, K., and Soto-Valdez, H. (2009). Determination of eugenol diffusion through LLDPE using FTIR-ATR flow cell and HPLC techniques. *Polymer*, 50(6), 1470–1482.
161. Pavia, D. L., Lampman, G. M., Kriz, G. S., and Vyvyan, J. R. (2007). *Introduction to Spectroscopy*, Cengage Learning India Pvt. Ltd, New Delhi.
162. Rivera, D., and Harris, J. M. (2001). In situ ATR-FT-IR kinetic studies of molecular transport and surface binding in thin sol-gel films: reactions of chlorosilane reagents in porous silica materials. *Analytical Chemistry*, 73(3), 411–423.
163. Foster, M., Furse, M., and Passno, D. (2002). An FTIR study of water thin films on magnesium oxide. *Surface Science*, 502, 102–108.

164. Liu, M., Wu, P., Ding, Y., Chen, G., and Li, S. (2002). Two-dimensional (2D) ATR-FTIR spectroscopic study on water diffusion in cured epoxy resins. *Macromolecules*, 35(14), 5500–5507.
165. Shen, X., and Chen, Z. (2010, September). Fractal diffusion of VOCs in dry porous building materials. In *Building Simulation* (vol. 3, No. 3, pp. 225–231). Tsinghua Press.
166. Asakura, T., and Ando, I. (Eds.). (1998). *Solid state NMR of polymers* (vol. 84). Elsevier.
167. Kobayashi, T., Babu, P. K., Chung, J. H., Oldfield, E., and Wieckowski, A. (2007). Coverage dependence of CO surface diffusion on Pt nanoparticles: an EC-NMR study. *The Journal of Physical Chemistry C*, 111(19), 7078–7083.
168. Deng, F., Hu, J., Xiong, J., and Du, Y. (1993). Solid-state NMR studies of ^1H spin diffusion in adsorbed organic molecules. *Solid state nuclear magnetic resonance*, 2(3), 97–103.
169. Hoffmann, H. C., Debowski, M., Müller, P., Paasch, S., Senkovska, I., Kaskel, S., and Brunner, E. (2012). Solid-State NMR Spectroscopy of Metal–Organic Framework Compounds (MOFs). *Materials*, 5(12), 2537–2572.
170. Kuhn, A., Sreeraj, P., Pöttgen, R., Wiemhöfer, H. D., Wilkening, M., and Heitjans, P. (2011). Li ion diffusion in the anode material $\text{Li}_{12}\text{Si}_7$: Ultrafast quasi-1D diffusion and two distinct fast 3D jump processes separately revealed by ^7Li NMR relaxometry. *Journal of the American Chemical Society*, 133(29), 11018–11021.
171. Wilkening, M., and Heitjans, P. (2012). From micro to macro: access to long-range Li^+ diffusion parameters in solids via microscopic $^6, ^7\text{Li}$ spin-alignment echo NMR spectroscopy. *ChemPhysChem*, 13(1), 53–65.
172. Gegner, J. (2006). Concentration-and temperature-dependent diffusion coefficient of carbon in FCC iron mathematically derived from literature data. 4th Int Conf Mathematical Modeling and Computer Simulation of Materials Technologies. Ariel, College of Judea and Samaria.
173. Ghosh, T. K., and Bhattacharyya, B. C. (2010). Relation between volumetric mass transfer coefficient and power input per unit volume for converging–

- diverging tube airlift fermenter. *International Journal of Chemical Reactor Engineering*, 8(1)
174. Bird, R. B., Stewart, W. E., and Lightfoot, E. N. (2007). *Transport phenomena*. John Wiley & Sons.
175. Matsuda, A., Yamamoto, K., and Yamasaki, S. (2006). U.S. Patent Application 11/332,733.
176. Balakrishnan, K., Bowman, G. R., Junus, R., Kemmis, B. G., Ridley, P. S., and Thompson, I. A. (2004). U.S. Patent Application 10/578,282.
177. Argueta, T. B. O., Kawada, H., Shimabukuro, K., Kubota, S., Shono, Y., Tsushima, K., and Takagi, M. (2004). Comparative insecticidal efficacy of a new pyrethroid, metofluthrin, against colonies of Asian *Culex quinquefasciatus* and *Culex pipiens pallens*. *The Japan Society of Medical Entomology & Zoology*, 55(4), 289–294.
178. Netrabukkana, R., Lourvanij, K., and Rorrer, G. L. (1996). Diffusion of glucose and glucitol in microporous and mesoporous silicate/aluminosilicate catalysts. *Industrial & Engineering Chemistry Research*, 35(2), 458–464.
179. Vicente, A. A., Dluhý, M., Ferreira, E. C., Mota, M., and Teixeira, J. A. (1998). Mass transfer properties of glucose and O₂ in *Saccharomyces cerevisiae* flocs. *Biochemical Engineering Journal*, 2(1), 35–43.
180. Ternan, M. (1987). The diffusion of liquids in pores. *The Canadian Journal of Chemical Engineering*, 65(2), 244–249.
181. Anderson, J. L., and Quinn, J. A. (1974). Restricted transport in small pores: a model for steric exclusion and hindered particle motion. *Biophysical Journal*, 14(2), 130–150.
182. Jaynes, D. B., and Rogowski, A. S. (1983). Applicability of Fick's law to gas diffusion. *Soil Science Society of America Journal*, 47(3), 425–430.
183. Webb, S. W., and Pruess, K. (2003). The use of Fick's law for modeling trace gas diffusion in porous media. *Transport in Porous Media*, 51(3), 327–341.

List of Publications:

1. Debojit Chakrabarty, Reena Bibals and Rajdip Bandopadhyay, Evaluation and comparison of relative release rates of a volatile synthetic pyrethroid impregnated within different substrates using chromatographic and thermo analytical measurements, Pesticide research Journal, June 2015.
2. Debojit Chakrabarty, Reena Bibals and Rajdip Bandopadhyay. Insights into factors influencing the release of synthetic pyrethroid loaded on polymeric substrates, Accepted by Journal of Insect science.

List of Patents:

1. Indian Patent Application No.: 0821/MUM/2012 dated March 26, 2012 in the name of GODREJ CONSUMER PRODUCTS LIMITED .Entitled AIR FRESHENER DISPENSING DEVICE FOR USE IN CARS OR OTHER VEHICLES.
2. Indian Patent Application Nos: 1685/MUM/2007. AN EFFICACIOUS WATER WASH RESISTANT MULTIINSECT KILLER SOLUTION.

Specific contributions

I am indebted to the following selfless people who helped me with lots of inputs in the area of instrumental analysis and modeling.

For all the modeling work: Prof. Rajdip Bandyopadhyaya, Associate Professor, (Colloids and Nano materials Lab. Chemical Engineering Department at IIT, Bombay.) Mr. Vikas Gayasen & Mr. Amol P Avhad Chemical Engineering, IIT Bombay.

For Thermal & IR studies :Dr. Jitendra Kelkar , Mr. Amit Joshi, , Mr. Dheeraj Handique & Mr. R. Girijan, Shimadzu Analytical (India) Pvt. Ltd ,Andheri (E) Mumbai .

For the BET studies :Dr. Deepa Khushalani (TIFR) Associate Professor, Materials Chemistry, Dept. of Chemical Sciences, Tata Institute of Fundamental Research (TIFR), Mumbai.

For the NMR studies: Dr. PR Rajamohan (NCL), Scientist, Central NMR Facility, NCL, Pune.

For the XRD & Surface FTIR: Prof .Kannan .S & Mr. P. Koilraj, Central Salt & Marine Chemicals Research Institute, Bhavnagar, Gujarat.

For Mercury Intrusion Porositmetry: Mr. Kannan Iyer, Environmental Geo-technology Lab, Indian Institute of Technology, Bombay, & Sachindra Pal, S P Pal, Regional Manager, Quanta chrome Instrument, Mumbai

For Thermal desorption studies: Ashutosh Namdeo, Chemical Engg., IIT Bombay.

For contact angle measurements: Sonali Kulkarni, Chemical Engg., IIT Bombay.

For SEM studies: Dr Phil Waterfield and Ms Jane Brown, Unilever Research & Development Laboratories, Port Sunlight, Bebington, Wirral, United Kingdom.

Brief Biography

Dr Debojit Chakrabarty earned his PhD Degree in Organometallic Chemistry from the Indian Institute of Technology, Bombay in 1991 working under the supervision of Prof Pradeep Mathur in the area of ‘Synthesis of Chalcogen bridged Transition Metal Non Metal Carbonyl Cluster Compounds’. Subsequently, he spent time between 1992-1994 working in the research laboratories of Prof Mercuri Kanatzidis at the Chemistry Department and Centre for Fundamental Materials Research at Michigan State University in the area of ‘Solid State Syntheses of Chalcogenide Based Materials’ as a Post-doctoral researcher.

He then joined Unilever Research India where he spent twelve years working on platform projects within Unilever Home and Personal Care Category, more specifically in Oral Care, Personal Wash and Skin Lightening Categories. Dr Chakrabarty was responsible for leading few Unilever – Industry scientific partnership programmes, notably a project on trying to understand structuring behaviour of surfactants in soap bars and liquids employing Solid State NMR Methods. In 2006, he moved over to Head Household Insecticides and Air Care Research at Godrej Sara Lee Limited, in addition to heading the Quality Assurance function of the organization as well. Currently, Dr Chakrabarty currently heads the Personal Care Category at Godrej Consumer Products Ltd (GCPL) comprising Air Care, Hair Care and Personal Wash / Laundry sub categories, whilst, also being responsible for the International Innovation Project Portfolio within GCPL International business. He has had several international publications and patents to his credit during his 19 years of professional association in Industry, and, continues to work together with academia on scientifically relevant projects.

Brief Biography of Reena Bibals:

Reena Bibals has completed her Master of Science. (M.Sc.-Analytical Chemistry) from University Department of Chemistry, University of Mumbai in the year 1994. She has been working with Godrej Consumer products R&D Centre, since 1994 and perusing her Ph.D. from BITS Pilani since 2009. She works on new product development in consumer goods and has filed patents. She has more than 21 years of Industrial research experience.